



Experimental and Numerical Investigation of Solar Photovoltaic Panel Using Back Side Water Cooling Chamber

A Thesis

Submitted to the Council of the Erbil Technical Engineering College at Erbil Polytechnic University in Partial Fulfillment of the Requirements for the Degree of Master of Science in Mechanical and Energy Engineering.

By:

Ilaf Nawzad Rasool

B.Sc. in Refrigeration and Air-Conditioning Engineering Techniques. 2014

Supervised by:


Assist. Prof. Dr. Ranj Sirwan Abdullah

ERBIL KURDISTAN

March 2023

DECLARATION

I declare that the Master Thesis entitled **Experimental and Numerical Investigation of Solar Photovoltaic Panel Using Back Side Water Cooling Chamber** is my own original work, and hereby I certify that unless stated, all work contained within this thesis is my own independent research and has not been submitted for the award of any other degree at any institution, except where due acknowledgement is made in the text.


Signature: 

Student name: Ilaf Nawzad Rasool

Date: 25-4-2023

LINGUISTIC REVIEW

I confirm that I have reviewed the thesis titled **Experimental and Numerical Investigation of Solar Photovoltaic Panel Using Back Side Water Cooling Chamber** and Testing from the English linguistic point of view, and I can confirm that it is free of grammatical and spelling errors.

Signature: 

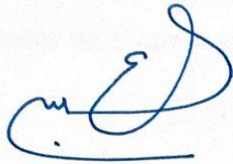
Reviewer name: Jack C Wynker

Date:

SUPERVISOR CERTIFICATE

This thesis has been written under my supervision and has been submitted for the award of the degree of Master of Science in Mechanical and Energy Engineering with my approval as a supervisor.

Signature:



Name: Assist. Prof. Dr. Ranj Sirwan Abdullah

Date: 25-4-2023

I confirm that all requirements have been fulfilled.

Signature:



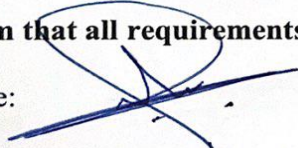
Name: Assist. Prof. Dr. Ahmed Mohammed Adham

Head of the Department of Technical Mechanical and Energy Engineering

Date: 25/4/2023

I confirm that all requirements have been fulfilled.

Signature:



Name: Mr. Byad Abdulqader Ahmed

Postgraduate Office

Date: 26-4-2023



EXAMINING COMMITTEE CERTIFICATION

We certify that we have read this thesis: **Experimental and Numerical Investigation of Solar Photovoltaic Panel Using Back Side Water Cooling Chamber** and as an examining committee, examined the student (Ilaf Nawzad Rasool) in its content and what related to it. We approve that it meets the standards of a thesis in terms of scope and quality for the degree of Master in Mechanical Engineering.

Signature:



Name: Assist. Prof. Dr. Ahmed M. Adham

Member

Date: 11/4/2023

Signature:



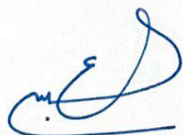
Name: Assist. Prof. Dr. Ayad Y. Abdullah

Member

16-4-2023

Date:

Signature:



Name: Assist. Prof. Dr. Ranj S. Abdullah

Member & Supervisor

Date: 12/4/2023

Signature:



Name: Assist. Prof. Dr. Rizgar B. Weli

Chairman

Date: 12/4/2023

Signature:



Name: Prof. Dr. Ayad Z. Saber Agha

Dean of Erbil Technical Engineering College

Date:

25-04-2023

DEDICATION

This dissertation is for my family. Thank you for giving me the support I need to reach my dreams and finish my dissertation. I am grateful to have them all.

To my beloved husband (Muhammad) who has been a constant source of support and encouragement during my studies. I am truly thankful for having you in my life.

To my sisters and brother, whose support, understanding, and belief in me made me proud of the work that I have produced.

To my great treasure, my daughters (Dania and Delan)

ACKNOWLEDGMENT

First, I would like to express my endless appreciation to Almighty Allah and be very grateful for whatever He gave me throughout my research. Nevertheless, peace be upon our messenger, leader, and guide Mohammed, and very grateful for his treasure of advice and guidance he left for us.

I would like to express my deep gratitude to my supervisor, Asst. Prof. Dr. Ranj Sirwan Abdullah, for his valuable help and encouragement during the project. His advice, careful inspection, academic guidance, and scientific approach have helped me a lot to finish this thesis.

I'd also like to thank my husband (Muhammad), and my daughters (Daina and Delan), as well as my siblings and the rest of my family, for always their supporting my project and cheering me on during this study. Thank you, especially, to my mother; her prayers for me have kept me going this far.

I would like to thank Dr. Ahmed, Head of the Department of Technical Mechanical and Energy Engineering, who was very helpful. I would also like to thank Dr. Hemin, head of the Research Center, who was helpful during the experimental study.

Finally, I'd like to express my gratitude and appreciation to all of my colleagues and friends, especially (Miss Sally and Miss Esra), for their assistance throughout my research and for the information they provided that was useful to me. Your understanding of my situation was one of the major sources of my success.

ABSTRACT

One of the biggest problems in the world that we live in nowadays is the environmental pollution caused by an overconsumption of energy. When fossil fuels are burned to generate energy, it emits CO₂, which is a leading cause of air pollution. Solar energy has the potential to replace fossil fuels as an alternative source of renewable energy. A photovoltaic solar system is one type of solar system that can convert the sun's light into electrical energy. One of the issues with PV panel is the high temperature of PV cells, especially in summer season when the ambient temperature can rise up to 50°C. As the temperature of solar modules increases, both the output power and the efficiency of PV panel decrease. To improve overall performance while extending the solar module's lifespan, this study proposes lowering photovoltaic cell temperature by using water cooling chamber installed at the back side of the PV panel. The proposed solar panel was developed and designed through both experimental study and ANSYS Fluent simulation. The photovoltaic module that was designed has a water-cooling chamber for the purpose of providing cooling under the condition of Erbil city. The rear side of the photovoltaic panel is cooled using water cooling chamber. The water-cooling chamber can absorb heat dissipation from the photovoltaic panel. The proposed cooling system for the solar panel is a closed cycle, and the cooling water is in contact with the back of the PV panel at different flow rates. According to experimental setup, the maximum water flow rate of 3.5 l/min gives the optimal heat transfer rate. Finally, results demonstrated an improvement in electrical efficiency by the following percentages: 10.42%, 11.87%, 13.77%, 18.09%, and 19.72% when the water volume flow rates of 1.5, 2, 2.5, 3, and 3.5 l/min, respectively, were applied. Meanwhile, the thermal efficiency of the PV system is 49.7% with a water flow rate of 1.5 l/min. and, the

thermal efficiency recorded 79.2% when the system operated at a flow rate of 3.5 l/min.

Table of Contents

DECLARATION	Error! Bookmark not defined.
LINGUISTIC REVIEW	II
SUPERVISOR CERTIFICATE.....	Error! Bookmark not defined.
EXAMINING COMMITTEE CERTIFICATION	IV
DEDICATION	V
AKNOWLEDGMENT	VI
ABSTRACT	VII
LIST OF FIGURES	v
LIST OF TABLES	ix
LIST OF ABBREVIATIONS.....	x
LIST OF SYMBOLS	x
GREEK SYMBOLS	xi
CHAPTER ONE	1
INTRODUCTION	1
1.1 The Background.....	1
1.2 Photovoltaic Solar Panel.....	3
1.2.1 Monocrystalline Silicon.....	4
1.2.2 Solar Cell Operation Principle	5
1.2.3 A photovoltaic module's characteristics	6
1.2.4 The relation between temperature and efficiency of PV panel.....	7
1.3 Problem Statement.....	8
1.4 The Objectives	9
1.5 Research Methodology Stages.....	10
1.6 Thesis outline.....	11
CHAPTER TWO	13

LITERATURE REVIEW	13
2.1 Introduction.....	13
2.2 Photovoltaic Panel Models	15
2.3 Photovoltage Cooling Methods.	15
2.3.1 Spray Water Cooling Technology	16
2.3.2 Air Cooling Method	20
2.3.3 Heat Exchanger Cooling System.....	22
2.3.4 Water Cooling Chamber of The Back Side of PV Panels.....	24
2.3.5 Alternative Method to Cool the Photovoltaic Panel.....	28
2.4 Photovoltaic Cooling Techniques Using Computational Fluid Dynamics .	32
2.5 Summary	34
CHAPTER THREE.....	35
MATHEMATICAL MODELLING	35
3.1 Introduction.....	35
3.2 Electrical Energy	35
3.3 Thermal Efficiency	36
3.4 Solar Angles and Monthly Solar Radiation.....	37
3.5 Modeling Simulation	39
3.5.1 The Governing Equation and Boundary Conditions	39
3.6 Process for Simulating.....	41
3.6.1 Geometry	41
3.6.2 Mesh	42
3.6.3 Setup	43
3.6.4 Solution.....	50
3.6.5 Result	54

CHAPTER FOUR.....	56
EXPERIMENTAL WORK.....	56
4.1. Introduction.....	56
4.2. Photovoltaic With the Cooling System	56
4.2.1 Solar Photovoltaic Module	59
3.2.2 Water Cooling Chamber System.....	59
4.2.3. Water Softener and Water Tank Supply.....	60
4.2.4. Water Flow Meter.....	61
4.2.5 Water pump	62
4.2.6 The Temperatures of The System	63
4.2.7 Current Sensor	64
4.2.8 Voltage Sensor.....	65
4.2.9 Data Logger	66
4.2.10 Solar Power Meter.....	66
4.2.11 MPPT Solar Charge Controller	67
4.2.12 Procedure of The Experiment.....	68
4.3 Equipment's Calibration and Uncertainty.....	69
4.3.1 Calibration of Volume Flow Rate	69
4.3.2 Calibration K-Type Thermocouple	70
4.3.3 Calibration of The Solar Power Meter	71
4.3.4 Uncertainty	71
CHAPTER FIVE.....	73
RESULTS AND DISCUSSION.....	73
5.1 Introduction.....	73

5.2 Solar Radiation	73
5.2 Experimental Result.....	74
5.2.1 Ambient Temperature and Solar Radiation.....	75
5.2.2 Photovoltaic Panel's Temperature.....	78
5.2.3 Performance Analysis.....	84
5.2.4 A Comparative Study of The Results.....	88
5.3 Simulation Results	89
5.3.1 Verification of Simulation Results with The Experimental Setup.....	89
5.3.2 Test for Mesh Independence	91
5.3.3. Thermal Analysis.....	92
5.3.4 Performance Analysis.....	103
CHAPTER SIX	105
CONCLUSION, RECOMMENDATIONS.....	105
6.1 Introduction.....	105
6.2 Conclusion	106
6.3 Recommendation	107
REFERENCES.....	R1
APPENDIX A.....	A1
Monthly Solar Radiation.....	A1
APPENDIX B	A4
UNCERTAINTY AND CALIBRATION ANALYSIS	A4
APPENDIX C	A7
ANSYS RESULTS	A7

LIST OF FIGURES

Figure 1. 1	Direct solar irradiation maps from around the world (Wang and Lu, 2016).	2
Figure 1. 2	Structure of monocrystalline and polycrystalline silicon (Hidayanti, 2020)	4
Figure 1. 3	The schematics of n-type and p-type semiconductors (Kalogirou, 2013).	5
Figure 1. 4	The schematics of the p-n junction (Kalogirou, 2013).	6
Figure 2. 1	Chart of literature review	14
Figure 2. 2	Illustrates various cooling methods (Sharaf et al., 2022).	16
Figure 2. 3	Schematic diagram of PV panel (Govardhanan et al., 2020).	18
Figure 2. 4	Schematic diagram of PV with water spray coolant (Hadipour et al., 2021).	19
Figure 2. 5	Both sides of the PV panel (Agyekum et al., 2021).	20
Figure 2. 6	A fan is installed on the Photovoltaic module's back side (Amelia et al., 2016).	21
Figure 2. 7	Design and experimental study of converging channel (Baloch et al., 2015).	25
Figure 2. 8	Illustrates the rear side of the water module construction (Gomaa et al., 2020).	27
Figure 2. 9	Illustrates a different design on the rear side (Muslim et al., 2020).	28
Figure 2. 10	The construction cooling system (Rakino et al., 2019).	31
Figure 2. 11	Schematic Diagram of PV Panel Cooling System (Agyekum et al., 2021a).	31
Figure 2. 12	Diagram of the PVT system (Nasrin et al., 2019).	32

Figure 3. 1	Illustrate beta angle (Morad et al., 2018).	37
Figure 3. 2	The dialog box of Fluid Flow (Fluent).	41
Figure 3. 3	The geometry of the photovoltaic panel.	42
Figure 3. 4	The mesh of the PV panel.	43
Figure 3. 5	Fluent Launcher	44
Figure 3. 6	Radiation Model	45
Figure 3. 7	Solar Calculator	45
Figure 3. 8	Defining a fluid in Fluent.	46
Figure 3. 9	Defining a Solid in Fluent.	47
Figure 3. 10	Define cell zone condition.	48
Figure 3. 11	Inlet boundary condition.	49
Figure 3. 12	Outlet boundary condition.	49
Figure 3. 13	The boundary condition of glass.	50
Figure 3. 14	Illustrate the task of the solution method.	51
Figure 3. 15	Modifying Fluent's solution monitoring.	52
Figure 3. 16	Solution initialization.	52
Figure 3. 17	Run calculation.	53
Figure 3. 18	Scaled residuals.	54
Figure 3. 19	Display result.	55
Figure 4. 1	Photovoltaic panels system components	57
Figure 4. 2	A schematic diagram of the cooled PV panel.	58
Figure 4. 3	A schematic diagram of the rear side PV panel.	60
Figure 4. 4	Water softener and water tank supply.	61
Figure 4. 5	Schematic diagram of water flow rate YF-s201 type.	61
Figure 4. 6	Water flow rate YF-s201 type.	62
Figure 4. 7	Water pump.	62
Figure 4. 8	k-type temperature sensor with MAX6675 modular.	64

Figure 4. 9	Illustrate the DHT sensor diagram connects to Arduino.....	64
Figure 4. 10	ACS712 Current Sensor	65
Figure 4. 11	SEN32 REV1.1 voltage sensor.	65
Figure 4. 12	Illustrate DBTU1300 solar power meter.	67
Figure 4. 13	Circuit diagram of the MPPT solar charge controller.	67
Figure 4. 14	Illustrate MAXMA solar charge controller.	68
Figure 4. 15	Display LCD digital.	69
Figure 4. 16	Calibrating between calculation flow rate and reading flow rate.	70
Figure 4. 17	Calibration between reading by K-type thermocouple and thermometer.	71
Figure 5. 1	Average monthly solar radiation	74
Figure 5. 2	Average daily ambient temperature (July and August).....	76
Figure 5. 3	Average daily solar radiation (July and August).....	77
Figure 5. 4	Total Solar radiation during the day (July 4 th)	77
Figure 5. 5	Total Solar radiation during the day (August 16 th)	78
Figure 5. 6	The surface temperature of the PV panel and the ambient temperature on (July 4 th).	79
Figure 5. 7	The surface temperature of the PV panel with and without cooling on (July 4 th).	80
Figure 5. 8	The surface temperatures of both PV panels on (July 3 rd).	80
Figure 5. 9	The temperature of the collector's backside at different water volume flow rates.....	81
Figure 5. 10	The temperature difference between out and in of the water.....	82
Figure 5. 11	Heat transfer rate of the cooling system and total solar irradiation. .	83
Figure 5. 12	Thermal efficiency at difference volume flow rate.....	83
Figure 5. 13	Relation between solar radiation with power and voltage.	84
Figure 5. 14	Electrical power generated by a PV panel (July 4 th)	85

Figure 5. 15	Rate of power at a different water flow rate for July	86
Figure 5. 16	PV panel electrical efficiency during the day on (July 4 th).....	87
Figure 5. 17	PV panel electrical efficiency during the day on (August 16 th).....	87
Figure 5. 18	The comparison between the current investigation and the earlier suggested designs for water cooling.	89
Figure 5. 19	Surface temperature at difference solar irradiation at flow rate (2 l/min).	91
Figure 5. 20	Outlet water temperature at difference solar irradiation at flow rate (2 l/min).	91
Figure 5. 21	Glass surface temperature without water cooling.	93
Figure 5. 22	Panel surface temperature at solar irradiance (1000 W/m ²).....	94
Figure 5. 23	Panel surface temperature at inlet water temperature (20°C)	95
Figure 5. 24	Panel surface temperature at inlet water temperature (25°C)	95
Figure 5. 25	Panel surface temperature at inlet water temperature (30°C)	96
Figure 5. 26	Water outlet Temperature at solar irradiance (1000 W/m ²).....	97
Figure 5. 27	Outlet water temperature at inlet water temperature (20°C).....	98
Figure 5. 28	Outlet water temperature at inlet water temperature (25°C).....	98
Figure 5. 29	Outlet water temperature at inlet water temperature (30°C).....	99
Figure 5. 30	Heat transfer rate at solar irradiance (1000 W/m ²)	100
Figure 5. 31	Heat transfer rate at inlet water temperature (20°C)	101
Figure 5. 32	Heat transfer rate at inlet water temperature (25°C)	101
Figure 5. 33	Heat transfer rate at inlet water temperature (30°C)	102
Figure 5. 34	Thermal efficiency at solar irradiance (1000 W/m ²).....	102
Figure 5. 35	Electrical efficiency at solar irradiance (1000 W/m ²).....	103
Figure 5. 36	Electrical efficiency with cooling and without cooling.	104
Figure B. 1	Calibration the K-type thermocouple.....	A5
Figure B. 2	Calibration of the DBTU1300 solar power meter	A6

Figure B. 3	Calibration of the volume flow rate	A6
Figure C. 1	Surface of PV panel temperature	A7
Figure C. 2	Surface of PV panel temperature	A8
Figure C. 3	Surface of PV panel temperature	A8

LIST OF TABLES

Table 3. 1	The thickness of the PV panel (Syafiqah et al., 2017b)	42
Table 3. 2	The properties of each material (Syafiqah et al., 2017b)	46
Table 4. 1	Mechanical data at standard test conditions @ (1000 W/m ² , 25 °C, 1.5 m/s).....	59
Table 4. 2	Details of the SUPER SHAEMGIE water pump.	63
Table 4. 3	Details of the solar power meter	66
Table 4. 4	Calibration of DBTU1300 solar power meter	71
Table 4. 5	Uncertainty equipment results	72
Table 5. 1	Monthly tilt angle.....	75
Table 5. 2	Experimental data	92
Table 5. 3	Test for mesh independence.	92
Table B. 1	Example to determine the uncertainty of water volume flow rate.....	A4

LIST OF ABBREVIATIONS

CFD	Computational Fluid Dynamics
CIGS	Copper Indium Gallium Selenide
CdTe	Cadmium Telluride
DHT	Digital Humidity Temperature
EVA	Ethylene Vinyl Acetate
MPPT	Maximum Power Point Tracking
PCM	Phase Change Material
PV	Photovoltaic
PV/T	Photovoltaic thermal
STC	Standard Test Condition

LIST OF SYMBOLS

A	Area of PV panel	m^2
C_p	Specific heat of water	J/kg. K
FF	Fill Factor	-
G	Solar radiation	W/m^2
G_{sc}	Solar constant	W/m^2
\bar{H}_d	Diffused radiation	$kW\ hr./\ m^2$
\bar{H}_b	Beam radiation	$kW\ hr./\ m^2$
\bar{H}_T	Incident radiation	$kW\ hr./\ m^2$
\bar{H}	Horizontal radiation	$kW\ hr./\ m^2$
\bar{H}_T	Incident radiation	$kW\ hr./\ m^2$
I_{mpp}	Maximum power current	Amp
I_{sc}	Short circuit current	Amp
k	Thermal conductivity	$W/m.K$
m	Mass flow rate of water	kg/s
N	number of readings	-
n	year's n^{th} day	-
P_{mp}	Maximum Power output	W
P	pressure	N/m^2
Q	Heat transfer rate of water	W
\bar{R}_b	Geometric factor	-
Re	Reynolds number	-

T_p	Temperature of the panel	°C
T_{amb}	Temperature of ambient	°C
T_f	Temperature of water	°C
T_g	Temperature of glass	°C
T_o	Standard temperature condition	°C
T_{in}	Inlet water temperature	°C
T_{out}	Outlet water temperature	°C
T_{sc}	Temperature of solar cell	°C
T_{td}	Temperature of tedlar	°C
u	velocity component at X-axis	m/s
U_{ga}	Heat transfer coefficient from glass to ambient	W/m ² .K
U_t	Heat transfer coefficient from inside PV layers	W/m ² .K
v	velocity component at Y-axis	m/s
V_{mpp}	Maximum power voltage	V
V_{oc}	Open circuit voltage	V
V_{in}	inlet water velocity	m/s
w	velocity component at Z-axis	m/s
\bar{x}	the average value of all of the readings taken for the X variable	-
x_i	i th measurement value	-

GREEK SYMBOLS

α_g	Absorptivity of glass	-
α_{sc}	Absorptivity of PV	-
α_{td}	Absorptivity of tedlar	-
τ_g	Glass transmittivity	-
ε_g	Glass emissivity	-
η_o	Standard cell efficiency	%
ρ	Density	kg/m ³
ρ_g	Ground reflectance	-
ω	Hour angle	°
ω_s	Sunset hour angle	°
ω_s'	Sunset hour angle for the tilted surface	°
θ	Incidence angle	°
ϕ	latitude	°
β	Tilt angle	°

δ	Declination angle	$^{\circ}$
β	Photovoltaic efficiency temperature coefficient	%
ρ_f	density of water	kg/m^3
μ_f	dynamic viscosity	kg/m.s
ν_f	kinematic viscosity	m^2/s

CHAPTER ONE

INTRODUCTION

1.1 The Background

The residential sector consumes a significant amount of overall energy, accounting for nearly one-third of global energy consumption. Today, the energy sectors divided into two types: non-renewable and renewable.

Non-renewable sources of energy pollute the environment and have limited resources. Non-renewable resources, like coal, fossil fuel oil, natural gas, etc., can always be taken out from the earth, but it will run out over time. Most of the power generation comes from the combustion of fossil fuels. Fossil fuels could generate high amounts of energy from a single source. Also release CO₂, which is the most significant cause of air pollution. This has aided in the rate of global warming. In addition, they might cause problems for people's health (Patel and Beik, 2021, AHMED et al., 2020). While renewable energy sources may consider as an alternative for using the traditional source of energy (fossil fuel).

A renewable resource has a natural resource that doesn't affect on the environment. Renewable sources are abundant in nature and are environment friendly. The most common kinds of renewable energy are as follows: Solar energy, geothermal energy, wind energy, biomass energy, and the hydropower energy.

Solar energy is considered as the most ancient source. An instrument that converts the solar radiation into thermal energy or electrical energy is called a solar collector. A photovoltaic solar panel is one kind of solar collector.

Figure 1.1 illustrates that the brown places have plenty of solar energy resources, while in the light-colored places' solar energy is not suitable for photovoltaic systems. The world's best areas for total solar intensity and periods of sunlight include North Africa, the Middle East, Mexico, and the United States southwest; Europe's south; Africa; South America; and China's western regions (Wang and Lu, 2016). Therefore, Iraq and our region is considered as a suitable region to install photovoltaic panels for utilizing the solar energy.

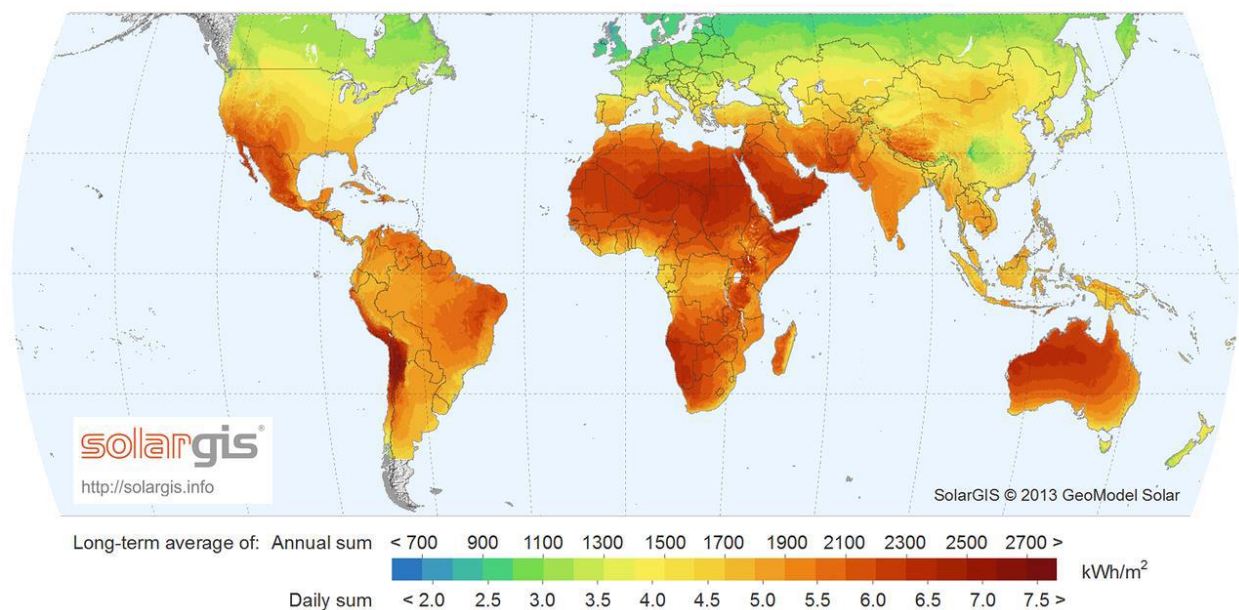


Figure 1. 1 Direct solar irradiation maps from around the world (Wang and Lu, 2016).

Due to rapid growth in the infrastructure of Erbil city, the need for of electrical power has increased dramatically (Ministry of electricity). Therefore, finding alternative sources of energy has become a crucial factor. The sun and the solar radiation can provide the planet with even more energy than it is required or used.

The most significant advantage of solar energy is that it is considered as one of the renewable energy resources which protect the environment from the effect of greenhouse gases. Meanwhile, the disadvantages of solar energy are the high initial costs of installing panels, the solar collectors are dependent on sunlight and don't work at night, and the problem of efficiency with increasing of PV panel temperature.

1.2 Photovoltaic Solar Panel

Solar photovoltaic systems use sunlight to generate electricity. Solar panels refer to smaller groups of solar cells. The first solar collectors in the world were found by Horace-Benedict in the 18th century (Smets et al., 2015). In 1839, Becquerel found the photovoltaic effect in selenium. First-generation cells were the first photovoltaic cells generated using silicon in 1954, with an efficiency of 6% (Sharaf et al., 2022). The converting efficiency of the "new" silicon cells, which were produced in 1958, was 11%. The efficiency of PV has now grown to around 15% (Kalogirou, 2013). The efficiency of the photovoltaic solar system varies based on the type of PV cell (Shirahata et al., 2017).

The cell is divided into four generations of solar cells. Cells from the first generation have been made of crystalline silicon, which includes materials like monocrystalline silicon and polycrystalline silicon, as shown in Figure 1.2. Monocrystalline solar panels have solar cells made of thinly sliced pure crystal of silicon while polycrystalline solar panels have solar cells made from several fragments of silicon melted together. This technology for making monocrystalline solar cells became the most efficient compared to polycrystalline solar cells (Sugianto, 2020).

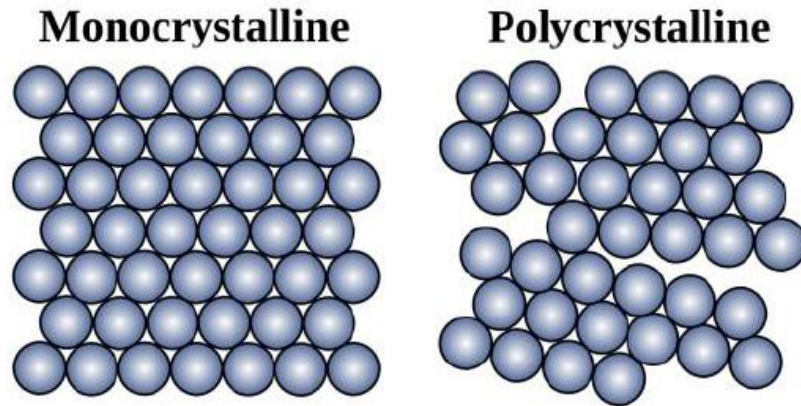


Figure 1. 2 Structure of monocrystalline and polycrystalline silicon (Hidayanti, 2020)

Second-generation solar cells have been thin-film cells like amorphous silicon, CIGS, and CdTe cell (Arun and Res, 2019). The third generation of solar cells (SCs) uses semiconducting organic macromolecules, inorganic nanoparticles, or hybrids. Three kinds of promising third-generation SCs are polymers: fullerene, hybrid polymers, and perovskite (Yan and Saunders, 2014). The term "4G solar cell technology" is also used to describe the fourth generation of solar cell technology. Inorganic and organic materials are combined to create this technology (Sharaf et al., 2022). PV systems are dependable and popular because they have a minimum life cycle cost (Bahaidarah et al., 2016). The performance of silicon PV material is the primary determinant of conversion efficiency and the starting cost for a solar panel. Furthermore, the average PV module guarantee is 20 years, with 1% degradation expected each year (Leary, 2019).

1.2.1 Monocrystalline Silicon

Monocrystalline silicon, also called single-crystalline silicon, is a crystalline solid in which the crystalline structure is continuous and unbroken with no bounds over the entire bulk, all the way to the edges. In contrast, polycrystalline silicon, which is

frequently referred to as simply "polysilicon," is a substance made up of several tiny crystalline particles with random orientations. The polycrystalline silicon has a shorter charge-carrier lifespan than monocrystalline silicon (Smets et al., 2015). Meanwhile, the monocrystalline panel can absorb more energy compared to other types, and more electricity is generated.

1.2.2 Solar Cell Operation Principle

The photovoltaic effect is what turns sunlight into direct-current electricity in the solar cell, which is a solid-state semiconductor p-n junction device. Each cell consists of two layers of silicon. The top layer is a mix of silicon and an n-type semiconductor element like phosphorus that has electrons that are easily freed. Meanwhile, the bottom layer contains a p-type semiconductor element with free electron positions. When the layers meet, free electrons from the n-type fill the empty spaces in the p-type, creating a barrier that stops more electrons from moving in this direction. Electrons and holes can move more freely in both n- and p-type semiconductors. The energy required to get an electron across a p-n junction in silicon is 1.11 eV. This varies based on the type of semiconductor material (Kalogirou, 2013).

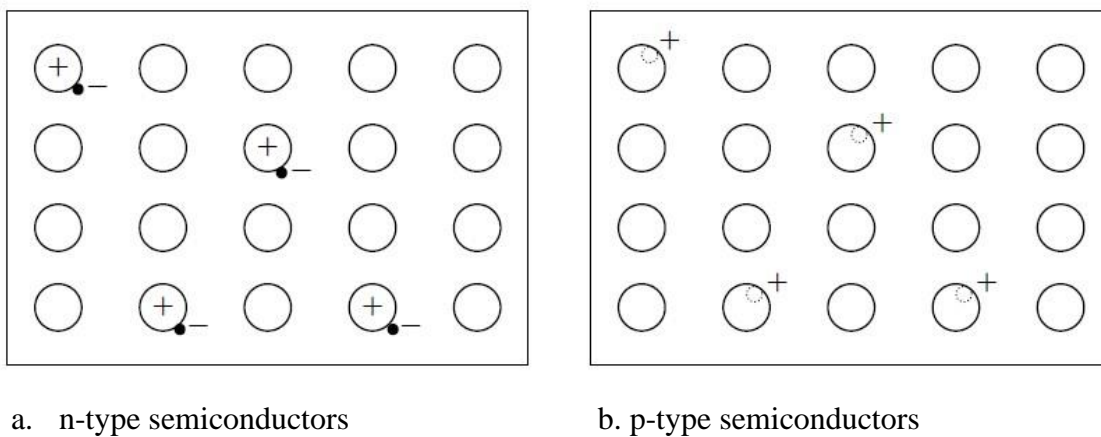


Figure 1. 3 The schematics of n-type and p-type semiconductors (Kalogirou, 2013).

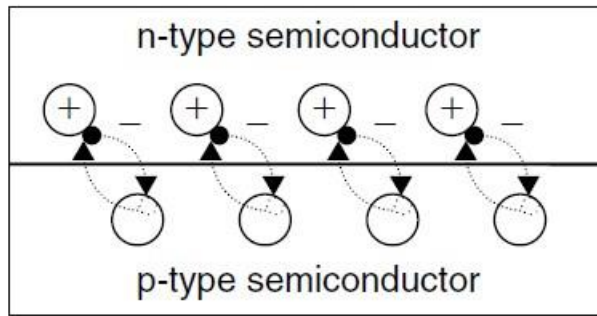


Figure 1. 4 The schematics of the p-n junction (Kalogirou, 2013).

1.2.3 A photovoltaic module's characteristics

A photovoltaic generator is made up of numerous solar cells that are electrically connected. The way a photovoltaic module acts electrically under solar radiation and temperature conditions is called its characteristic VI. These are the characteristics:

- Standard Test Conditions (STC)

The performance of the different panels can be compared using a set of criteria called "Standard Test Conditions." with 25°C cell temperature, 1000 W/m² irradiance, and 1.5 m/s air speed (Precup et al., 2019, p. 212).

- Maximum power (P_{mp})

When the voltage and current are produced, a maximum amount of power is produced under specified operating conditions. It is known as the point of maximum power.

- Short circuit current (I_{sc})

This is the current flowing through an external circuit when the photovoltaic cell's electrodes are short-circuited. Both the incident photon flux density and the incident sun's range affect how much current flows through the short circuit.

- Open circuit voltage (V_{oc})

The open circuit voltage is the highest voltage the solar panel can produce when there is no load on it. The open circuit voltage for silicon solar cells is approximately 700mV (Aribisala, 2013).

- Fill factor (FF)

The product $I_{mp} * V_{mp}$, which gives the maximum power delivered to the load, is smaller than the product $I_{sc} * V_{oc}$. FF is frequently used to quantify the characteristic curve's shape. The fill factor is a useful parameter that changes from one solar cell to another and usually has a value between 0.7 and 0.8 for several kinds of crystalline semiconductor cells.

1.2.4 The relation between temperature and efficiency of PV panel.

The photovoltaic panel technology uses semiconductors to produce electricity directly from the solar radiation. About 19–21% of solar radiation will be transformed directly into electricity, while the remainder is transformed into heat (Sainthiya et al., 2020). As a result, the absorbed heat raised the temperature of the solar cells, and the efficiency of the PV panel will decline. The efficiency of the solar panel decreases by 0.5% for every 1°C increase in the panel surface temperature (Agyekum et al., 2021). The PV panels are designed to work in nominal conditions, which include a temperature of 25°C and 1000 W/m² of solar radiation. The summer

ambient temperature in Erbil may reach up to 50°C. To obtain higher efficiency, it is important to find ways to keep PV panels cool, especially during conditions of high radiation. The cooling system is the best way to decrease the PV cell's temperature, while the solar panel's performance can be expected based on electrical efficiency. The electrical efficiency is determined by the proportion of maximum power output to the solar radiation incident on the photovoltaic module region. Efficiency is dependent on the cell's material (Calise et al., 2019, Bayod-Rújula, 2019).

1.3 Problem Statement

A photovoltaic panel system is considered as one type of solar energy systems. The use of photovoltaic systems for generating electricity has constantly increased due to a variety of factors:

1. Depletion of readily available fossil fuels and the limitation of this source.
2. Climate change is becoming a serious threat to all life in the world.

All these reasons have resulted in significant growth in renewable energy investments. In addition, Erbil has a severe electricity supply problem of up to 16,000 MW during the summer season (Ministry of electricity). The photovoltaic panels have a sensitivity to surface temperature. Furthermore, the efficiency of PV cells is reduced by the higher surface temperature. Every 1°C increase in the surface temperature of the PV panel results in a 0.5% drop in efficiency (Agyekum et al., 2021). The photovoltaic cells cannot convert all solar energy into electrical energy when the surface panel temperature increases. In this study, a PV cooling system has been developed and studied to demonstrate the effectiveness of that system on the

overall efficiency of the PV panel. A cooling system with a water chamber attached to the backside of the PV panel is installed to absorb the heat dissipation from the PV panel. The use of water fluid can extract more heat from a solar panel compared to air, especially at high ambient temperature and operation condition. As water has a higher specific heat compare to air, it can absorb more heat from the PV panel.

1.4 The Objectives

The main objective of the research is to investigate and conclude the best efficiency of the photovoltaic panel solar system. This will demonstrate the viability of using water cooling method to decrease the temperature of photovoltaic modules. In this study, variable water flow rate had been investigated to determine the power production and performance for both the PV with a cooling system and the PV without cooling system during the three hot months of the summer season. The following points have been addressed:

1. Developing, designing, and fabricating an experimental prototype of the solar PV modules with a water-cooling chamber, and then compared this prototype with a module without cooling system.
2. Apply ANSYS simulation software to study the thermal performance of the developed PV panel in a different operation condition.
3. Calculate theoretically and experimentally, the power output and efficiency for both PV modules.

1.5 Research Methodology Stages

The following are the basic progression of this research:

- A comprehensive review of all the previous research regarding the Photovoltaic panel with cooling to find the gaps which are needed to be studied. This will support the selection of a proper topic in terms of its scope and problems.
- Determine and find the main factors that influence the cell's temperature as well as the amount of electricity that can produced (define the problem statement then find the best contribution for enhancing the PV panel performance.
- The PV water cooling system was developed and installed at the Erbil Research Center, then experimental tests were conducted, and data was collected.
- A Computational Fluid Dynamics (CFD) software (ANSYS simulation program) was used to determine the thermal performance of the PV panel at through the use of different parameters. To validate the ANSYS simulation program results with experimental results.

1.6 Thesis outline

There are six primary chapters to this study, which are summarized below:

Chapter one provides some basic background for the study, laying out the scope of the issue and the motivation for doing this study. In addition to the study's purpose, the study's objective has also been mentioned.

In Chapter two, there is a thorough literature review on solar photovoltaic technology. This includes information on the different types of PV cells and different ways to improve the performance of PV panels. In addition, this chapter describes the different methods of cooling technology.

The third chapter shows the mathematical modeling, which includes calculations for electrical efficiency, thermal efficiency, PV angles, and monthly solar radiation. Furthermore, the ANSYS Fluent software has also been described so that the fundamentals of the simulation process can be comprehended in greater depth.

In chapter four described the experimental setup for the PV solar system. The PV panel with water cooling chamber has been designed and developed. A prototype model and all components are identified briefly.

In chapter five, we discuss our findings from both theoretical and experimental research on PV water cooling systems. Also, demonstrate the verification of

simulation results with the experimental data is demonstrated. Furthermore, the results show that ANSYS was used to model the water cooling system for the PV panels.

In chapter six, all the important findings and results from the other chapters are summarized. The purpose of this chapter is to provide the reader with a general understanding of the thesis' achievements.

CHAPTER TWO

LITERATURE REVIEW

2.1 Introduction

This chapter describes previous studies in the field of photovoltage systems. Those studies deal with the challenges of photovoltaic efficiency. It demonstrates the previous studies regarding the cooling of photovoltaic panels using different technologies. A comprehensive review about each of the parts of PV systems have been stated as shown in Figure 2.1

In this chapter the two methods of study (numerically and experimentally) for monocrystalline and polycrystalline silicon PV panels were discussed and reviewed. Those review studies demonstrated the various types of coolants involving water, air, and nanofluids. In addition, this chapter will highlight the results and the outcome the previous studies that used a variety of PV cooling methods, such as spray, fan, heat exchanger, and cooling chamber. The cooling chamber model is considered in this study, and therefore, various studies in this field are reviewed including front, back, and both sides.

The goal of this review is to find the gaps which need to be modified to produce a high-performance PV and to determine the best type of cooling for it.

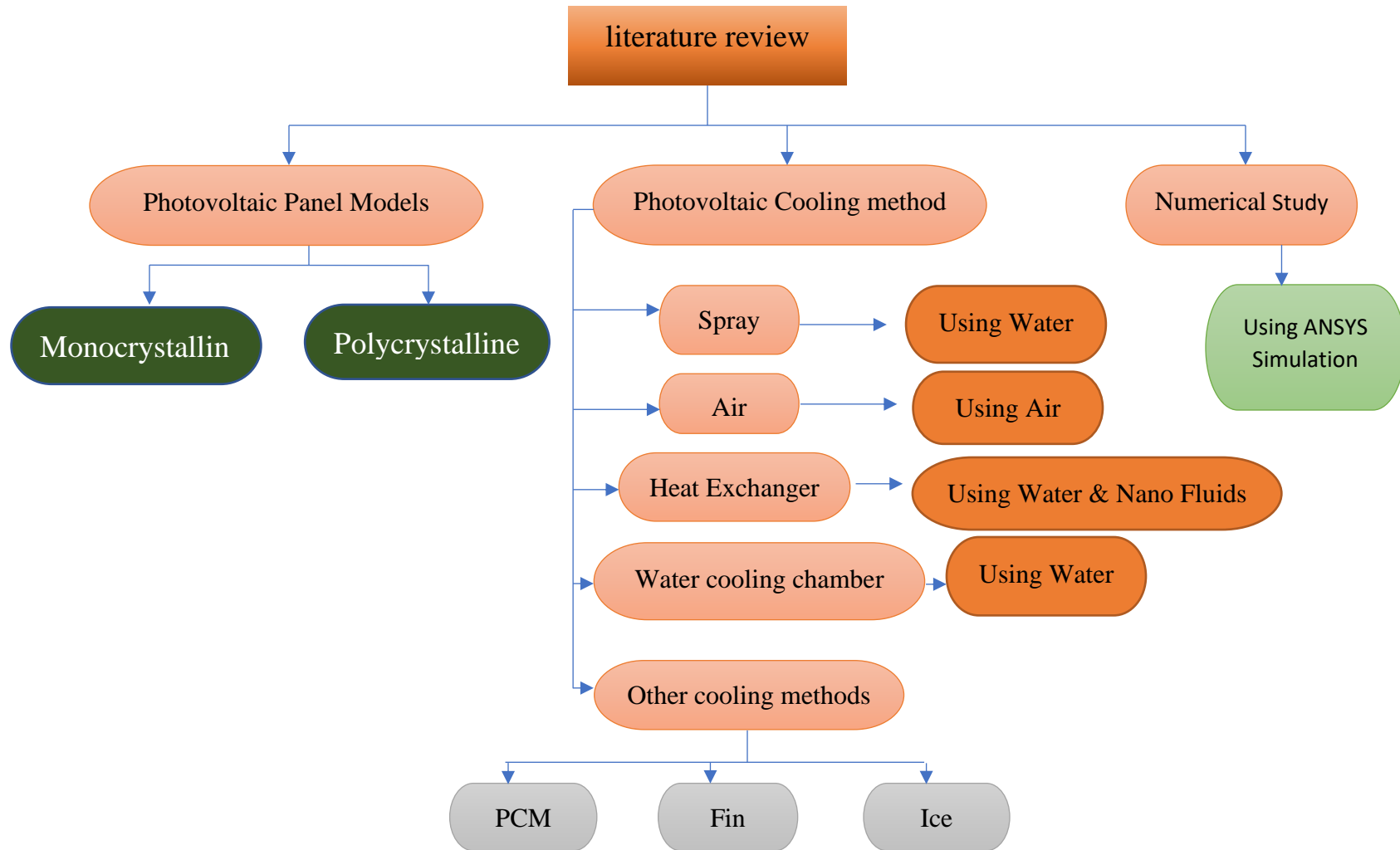


Figure 2. 1 Chart of literature review

2.2 Photovoltaic Panel Models

The solar system, particularly the photovoltaic system, is in high demand. As a result, a lot of research has been conducted to model the photovoltaic system and predict its efficiency.

(Jumrusprasert et al., 2009), performed experiments to compare the yearly performance of monocrystalline and polycrystalline solar panels in the same environment. The results show that the efficiencies for monocrystalline and polycrystalline were 6.8% and 5.7%, respectively.

Single-crystalline silicon was cell-based technology, including monocrystalline-silicon or polycrystalline-silicon, since silicon solar cells were also the most cost-effective and widely used PV devices (Xu et al., 2015, Hjerrild et al., 2016,).

(Hidayanti, 2020), investigated experimentally the solar cell efficiency for monocrystalline and polycrystalline silicon. The results stated that for monocrystalline silicon, the efficiency was 9.22% and for polycrystalline silicon, it was 7.94%.

Another experimental study by Ayadi et al. (2022) used two types of PV panels (monocrystalline and polycrystalline). The results showed the monocrystalline was more efficient than the polycrystalline.

2.3 Photovoltage Cooling Methods.

The cooling system is one method used to decrease cell temperature to increase the efficiency of the photovoltaic model. This section demonstrates all types of cooling systems.

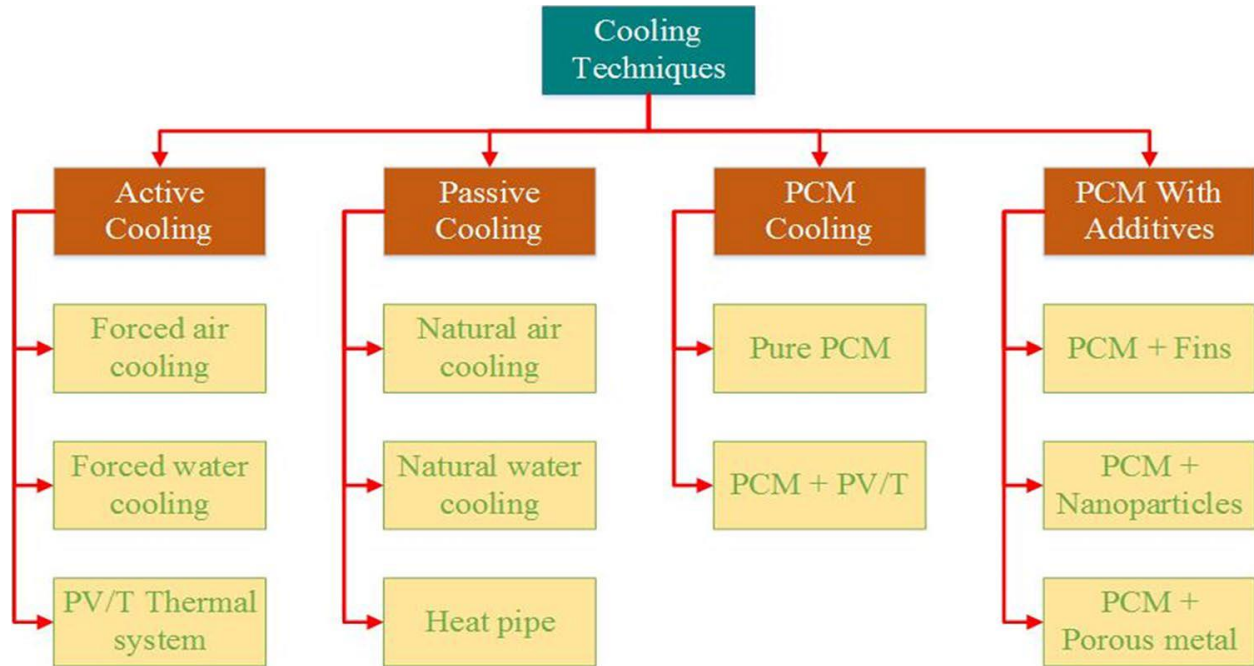


Figure 2. 2 Illustrates various cooling methods (Sharaf et al., 2022).

2.3.1 Spray Water Cooling Technology

Spray water cooling is used to decrease cell temperature. (Hachicha et al., 2015) In this study an experimental model has been implemented to improve PV panels by using spray water directly applied to the front, back, and combination sides. The results showed that the back cooling can reduce the temperature of the photovoltaic panel cell by 1.7%, the front cooling can decrease temperature by 11.3%, and the combined side cooling can decrease temperature by 18.3%. It showed the power of the photovoltaic cooling was enhanced by 2.3%, 3.6%, and 5.5% for back, front, and combination front–back cooling modules, respectively.

(Irwan et al., 2015) studied experimentally a prototype PV panel. Spray water was used on the front side of the PV panel at different solar radiation. The results showed that cell temperatures decreased to 5°C, 7.7°C, 13.2°C, and 23.1°C for solar radiation

at 413, 620, 821, and 1016 W/m², respectively, while increasing the power output of a water-cooled photovoltaic panel by 9–22%.

(Jailany et al., 2016) conducted an experimental study of the cooled photovoltaic panel through two different methods. First, the water is sprayed directly on the top surface of the PV panel, while the second option was natural air cooling. The results of this study showed that the temperature effect of air-cooling was 39.83°C, while using water was 30.78°C. The average power was 17.49W for cooling with air and 19.22W for cooling with water.

(Ali and Celik, 2017) conducted an experimental study in indoor conditions using two techniques. First, a photovoltaic cell was cooled by spraying water on the front side at two different flow rates: 1 & 2 g/min. In a second method, air cooling on the backside was used. The result obtained raised the efficiency of solar panels by 9.51% for air cooling, while by water cooling the efficiency was 9.72% using 1 g/min and 9.86% using 2 g/min. The power output increased by 2.4% for air cooling, and 4.7% for water at 1 g/min and 6.3% for water at 2 g/min.

(Bevilacqua et al., 2020) in this experimental study used three different cooling systems. First the PV cooling by two wide-cone water spray nozzles on the back surface is used. Second, the PV is similar to first PV with the addition of a metallic panel attached to the back of it. Third, the PV panel cooled by air forced convection at the rear side. The temperature results have been first PV is 36.9°C, second PV is 40.4°C and third PV is 50.3°C. For electrical power, second PV has recorded a maximum power of 27.8W and first PV 17.9W.

(Govardhanan et al., 2020) used water flow over the surface of the PV panel as an experiment. During the study, they examined the effect of the water-cooling system at different flow rates on the photovoltaic panel. The results showed that when using a high mass flow rate of 5.3 kg/min, the power output was 23 watts. Also, the temperature of the solar module drops by 30%, while its efficiency rises by 14%.

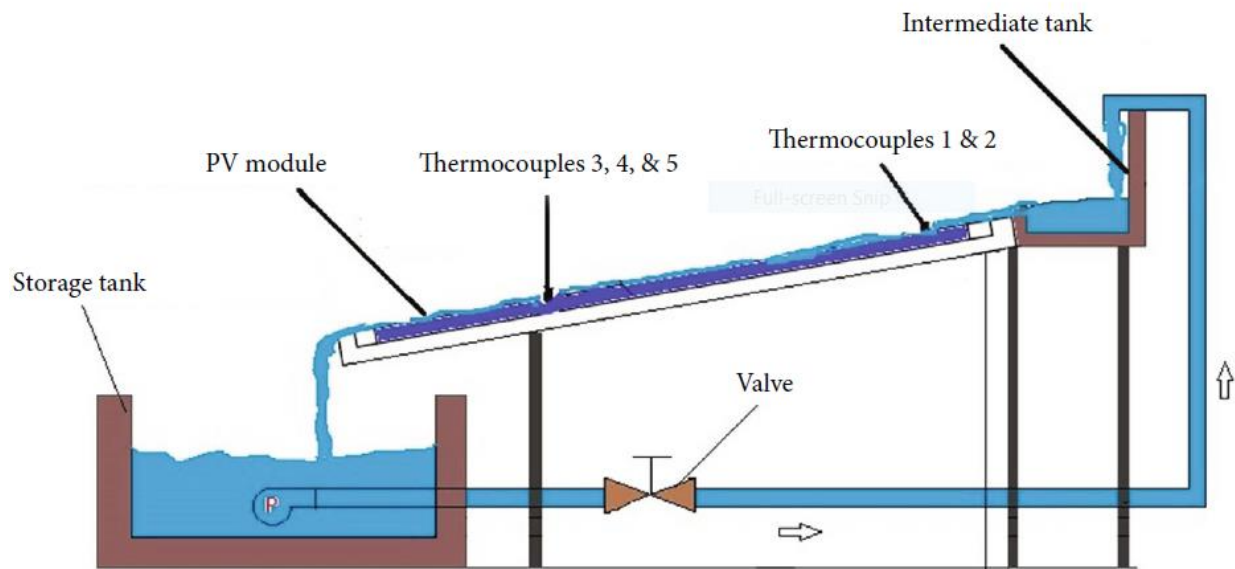


Figure 2. 3 Schematic diagram of PV panel (Govardhanan et al., 2020).

(Hadipour et al., 2021) introduced an experimental study of different technical spray-water cooling system. The first PV system used spray water at steady flow with a 1.24 l/min volume flow rate, and the second PV system used pulsed-spray water cooling with a 0.12 l/min and 0.52 l/min volume flow rate. The result obtained was that the cell temperature decreased to 24.8°C for steady flow, 26.5°C, and 25.7°C for pulsed-spray rates of 0.12 l/min and 0.52 l/min, respectively. The output power was 72 W for steady flow, 67 W for pulsed-spray with 0.54 l/min, and 68W for pulsed-spray with 0.12 l/min, compared to 54W for the uncooled photovoltaic

panel. Therefore, the efficiency of the panel rises to 12.1%, 11.6%, and 11.5% for steady flow, pulsed spray with 0.54 l/min and 0.12 l/min, respectively.

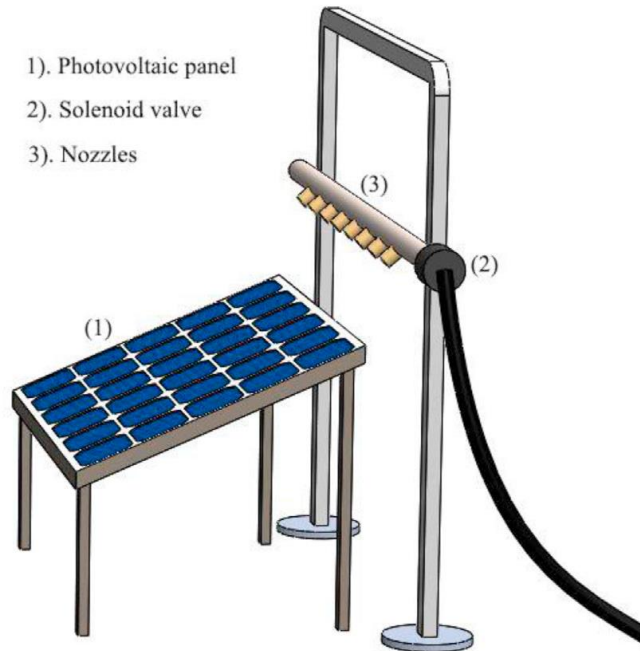
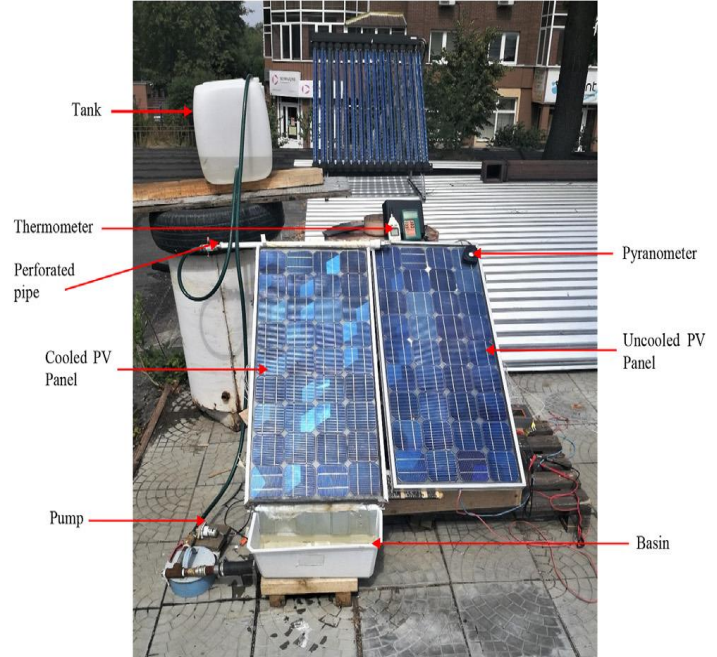


Figure 2. 4 Schematic diagram of PV with water spray coolant (Hadipour et al., 2021).

(Agyekum et al., 2021) studied experimentally the cooling process of the photovoltaic panel from both sides (front and back). In this study, the rear part of the panel was cooled by adding wetted cotton, while the front side of the panel was cooled by spraying water over the photovoltaic cells. The results showed that the cooled panel had an average temperature of 35.72°C and a power of 13.03W with a 14.36% efficiency, while the uncooled PV panel had an average temperature of 59.27°C and a power of 10.0W with a 12.83% efficiency.



a. Back side with cotton and covered by aluminum.



b. Front side with spray coolant

Figure 2. 5 Both sides of the PV panel (Agyekum et al., 2021).

2.3.2 Air Cooling Method

(Mazón-Hernández et al., 2013) conducted an experimental study using an air-cooling system for both natural and forced convection. The result showed the electrical power of a PV system cooled by forced air is 3–5% greater than that of a PV system cooled by natural convection.

(Amelia et al., 2016) experimentally analyzed the performance of air cooling (forced convection) with the use of a DC fan for air cooling and increased the number of fans from one to four. The result obtained that the cell temperature dropped to 53.64°C and 39.86°C when cooled by one and four units of DC, respectively, while the cell temperature was 59.88°C for non-cooling systems. As a consequence, as the number of fans increases, the temperature of the PV panels decreases.

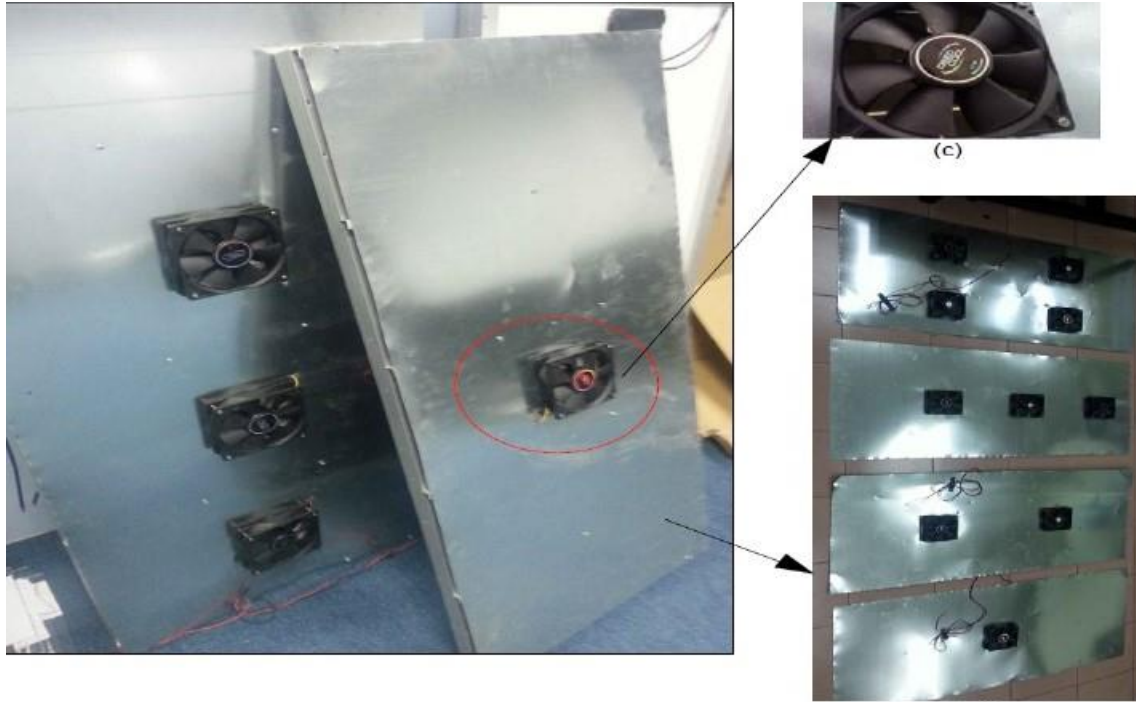


Figure 2. 6 A fan is installed on the Photovoltaic module's back side (Amelia et al., 2016).

The use of a backside convective cooling technique on solar panels has been studied experimentally and numerically (Nižetić et al., 2016). Consequently, electrical efficiency increased from 2.5 to 4.5%.

(Ahmad et al., 2021) used experimental and theoretical waste air from the air-conditioning system was used to create a rear cooling system. Results indicate that when compared to the reference panel, the average temperature was reduced by 32.03% compare to noncooled PV panel, while electrical efficiency increased by on average of 0.97%.

Experimentally, researchers (Sultan et al., 2021) introduced two methods of cooling: air cooling and water cooling. For the air cooling, a DC fan was used in the back of the PV module. The result of air cooling is that the cell temperature, power output, and efficiency are 55.8°C, 9.44W, and 8.32 %, respectively. Meanwhile the

water cooling method used different methods. First, two aluminum blocks with two openings for exchanging and transferring water were installed on the rear side of the photovoltaic panel. Second, sprayed water-cooling technique was implemented on the front side of the PV panel. The result of the water-cooling system showed cell temperature of 63.4°C, 9.08W power output, and 8.01% efficiency for the first case, and 51.9°C, 9.71W, and 8.56%, respectively, for the second case. Meanwhile, the cell temperature, power output, and efficiency for the non-cooling system recorded 71.5°C, 8.57W, and 7.56%, respectively.

2.3.3 Heat Exchanger Cooling System

(Rahman et al., 2015) cooled the surface temperature of photovoltaic panels by using a heat exchanger on the 7 copper pipes attached on the rear side. In the lab experiment, the PV panel without cooling at 1000 W/m² solar radiation, the power output dropped to 29.42W and the temperature of the cell rose to 88.10°C. The results showed that when the PV panel is cooled by a water heat exchanger at 1000 W/m², the cell temperature is reduced to 65.75°C, the power output is increased to 37.46W, and the efficiency of the model is increased to 5.73%.

(Hussein et al., 2017) developed a cooling technique using water and nanofluid on the backside of the photovoltaic panel. They studied numerically and experimentally; the copper pipes were connected to the PV panel's model from back side by using different fluid. In the first case using water cooling system with volume flow rates of 1, 1.5, and 2 l/min. was used. Results showed that when the flow rate increases, the electrical efficiency of the PV panel also increases. The optimal electricity efficiency of 6.5% and thermal efficiency of 60% are attained when the flow rate is set to 2 l/min. In the second case of the study, a Zn-water nanofluid was made by mixing the particles with 1.5 liters of ionized water in five ratios (0.1, 0.2,

0.3, 0.4, and 0.5%). Results show that ratios of 0.3% is the best for Zn-water nanofluid cooling in photovoltaics. Also, the electrical efficiency rises to 7.8%.

(Abu-Rahmeh, 2017) experimentally investigated three different techniques for cooling systems for PV cells. The first model was cooled by water, and the second model was cooled by a TiO_2 nanofluid. Both modules circulate inside the copper tube affixed to the module's rear surface. The third PV module was cooled by 24 vertically rectangular aluminum fins affixed to the module's rear surface. Thus, the temperatures recorded at noon are 44°C , 42.5°C , and 52°C for the first, second, and third modules of PV, respectively, compared to a non-cooled system, which is 54°C . The maximum results in electricity values at noon have been 15.3W, 15.7W, 15.1W, and 14.9W for the first, second, third, and noncooled modules of PV, respectively.

(Kumar and Dubey, 2018) experimentally studied the performance of a photovoltaic panel that was water-cooled by using seven pipes from the aluminum heat exchanger on the backside. It was observed that the temperature at the rear of the module has been lowered from 38 to 35.5°C , and electrical efficiency is rising.

(Abass et al., 2019) studied experimentally a photovoltaic panel cooled by water. The system was cooled by using a collector made of copper tubes that was attached to the rear of the PV panel. The result demonstrated that the temperature was reduced by 11.25%. In addition, the current, power output, and voltage increased by 10.68%, 4.87%, and 8.43%, respectively.

(Hossain et al., 2019) studied experimentally a modified photovoltaic panel using cooling system. The electrical efficiency of the polycrystalline photovoltaic panel increased up to 10.46% by using water cooling on their backside. The copper pipes

in this experiment were connected with an aluminum absorber sheet at the back side of the PV panel, with a water flow rate of 0.5 to 4 l/min. The results showed that using 2 l/min gives the best thermal efficiency, while using 0.5 l/min gives the highest water outlet temperature.

2.3.4 Water Cooling Chamber of The Back Side of PV Panels

Chamber technology is one of the methods that is used for the cooling system on the rear side of the photovoltaic solar cell. In this method, the water directly contacts the backside of the PV panel. In this part, the previous studies on this field were presented to find the new gap in model.

(Bahaidarah et al., 2013) experimentally and numerically studied water cooling at the backside of the PV panel. The results indicated that the cell temperature dropped from 43°C to 26°C, the power increased from 170W to 200W, and the electrical efficiency improved by 9%.

(Mehrotra et al., 2014) studied experimentally a new design of photovoltaic panel. The photovoltage panel was placed in a plastic box full of water. Results showed that the output voltage, the power output, and the electrical efficiency increased by 9.98%, 5.34%, and 17.8% respectively, compare to the non-cooled system.

(Baloch et al., 2015) conducted experimental and numerical research on the converging channel with a 1.8 l/min water flow rate. Results showed that the cell temperature was reduced to 45.2°C and the power output rose to 16.2W, compared to the non-cooling system's cell temperature of 71°C and power output of 11.9W.

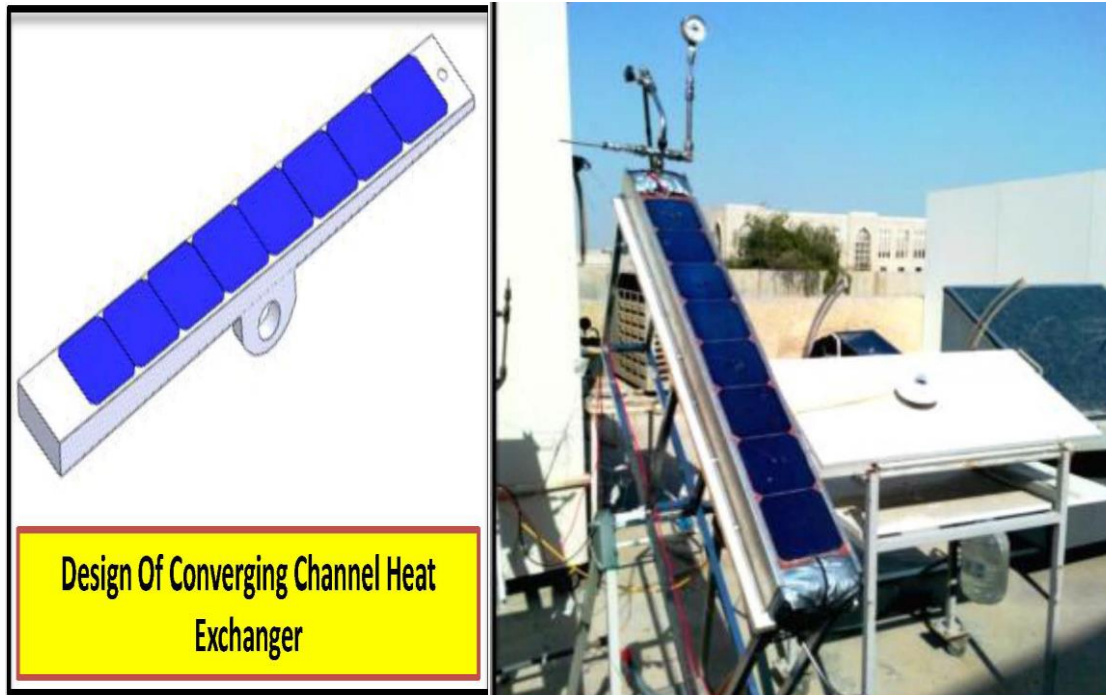


Figure 2. 7 Design and experimental study of converging channel (Baloch et al., 2015).

Another study by (Bashir et al., 2018) investigated experimentally the performance of two different PV modules (monocrystalline c-Si and polycrystalline p-Si) during the peaks of July and August. The water flowed at flow rate of 0.02 kg/sec and made direct contact with the PV modules on the back side. The average temperature of a monocrystalline and polycrystalline module was shown to be reduced by 13.6% and 7%, respectively. For monocrystalline modules, the efficiency of the electricity increased by 13%, and for polycrystalline modules, it increased by 6.2%.

(Fakouriyan et al., 2019) developed a new method for improving solar cell performance through experimental and theoretical test of water cooling system by using container made of aluminum attached to the backside of the PV panel. The results showed an improvement in the power performance of the PV panel from

60.5W changed to 67.5W, while the cell temperature of 60°C changed to 44°C, and the electrical efficiency of 11% changed to 12 %.

(Mohammed et al., 2019) studied experimental water cooling using acrylic glass, which has been used to create water-glazing chambers. The acrylic glass was installed on the photovoltaic modules' back and top so the concept of water chamber was made. The temperatures of the PV panel on the rear side with cooling and non-cooling systems are 50°C and 78°C, respectively, and the peak power and electrical efficiency of the photovoltaic module obtained are 12.69% and 14.20%, respectively.

(Sainthiya et al., 2020) conducted experimental research on the water-cooling method at the back, front, and combined surfaces of photovoltaic panel. The result showed that the average cell temperature of the back surface without and with water cooling was 66.72°C and 39.75°C, respectively. The power output was 16.5W with water cooling on the back side and 17.4W with a combined surface, while the power output without cooling was 16.2W.

(Gomaa et al., 2020) conducted an experimental and theoretical investigation on the rear side of PV panel. The developed model was designed to cool the PV panel by using two different modules. In the first model, the water channel includes 15 baffles of galvanized steel that attached to the rear side of the photovoltaic panel, while in the second model, the rectangular aluminum fins used to make a heat sink and are attached to the rear side of the photovoltaic panel. According to results, the power output at noon of non-cooling, water cooling, and fin cooling was 207W, 220W, and 218W, respectively. Additionally, the water cooling and fin cooling both reduced the rear side temperature by 30% and 3.5%, respectively.

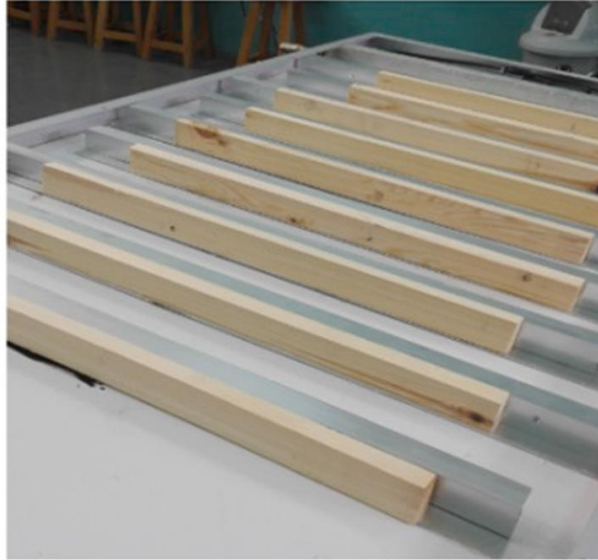


Figure 2. 8 Illustrates the rear side of the water module construction (Gomaa et al., 2020).

(Muslim et al., 2020) illustrated an experimental prototype design technique for increasing overall electrical efficiency in photovoltaic systems by using a water cooling chamber that is fixed to the rear side of the photovoltaic panel. Cooling fluid has been used in two different directions (up-flow and down-flow), with variant flow rate (1-4 l/min). In addition, the author implemented three different designs for the backside of the PV cell: first case with six passes and an angle of 60° , second-case included six passes with an angle of 30° , and the third-case five passes with an angle of 0° . According to the findings the electrical efficiency when using a 4 l/min water volume flow rate increased by 17% for the first case, 15.3% for the second case, and 13.6% for the third case compared to the non-cooling system. Also, the temperature reduction in the first case for up flow and down flow is 32.9% and 32%, respectively.

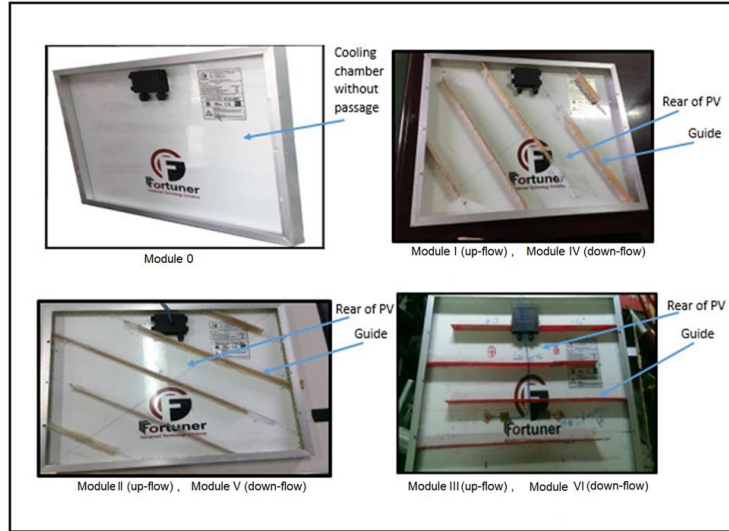


Figure 2. 9 Illustrates a different design on the rear side (Muslim et al., 2020).

2.3.5 Alternative Method to Cool the Photovoltaic Panel.

(Indartono et al., 2015) experimentally demonstrated the effectiveness of using PCM that was attached to the rear side of the PV module with different thicknesses (0.508 cm, 0.762 cm, and 1.016 cm). The results of their experiment show that increasing the thickness of PCM leads to a lower temperature on the panel, which results in a rise in both the panel's efficiency and its output power. When a 1.016-cm PCM was used, the average power output increased by 23.8%, and the average electrical efficiency rose by 29.3%. This suggests that using a thicker PCM is more effective in improving the performance of photovoltaic panels.

In an experimental investigation by (Ebrahimi et al., 2015), natural vaporization was developed to cool a photovoltaic solar cell on the backside with different mass flow rates. The design flow rates were 1.6, 3, and 5 g/min, which reduced the temperature to 48.3, 44.8, and 39.3°C, compared to the non-cooled temperature of 55.4°C. The power output increased to 3.367W, 3.528W, and 3.698W, compared to the non-cooled rate of 3.00W.

(Sharma et al., 2015) studied a method of cooling PV panel through developing a method in which a 2-pass reverse flow absorber collector was used with a flow rate of 0.01 kg/s. According to their study's findings, the efficiency of the PV module was enhanced by 4.59% and the temperature of the cell decrease to 30.62°C.

Further, Peng et al. (2017) established a new methodology of using ice to cool down an indoor solar panel. In this experiment, ice was equally scattered across the backside of the photovoltaic panels, which enhanced the efficiency of the photovoltaic panel by 47%.

(Hasan et al., 2017) developed a way to cool photovoltaic panels through vaporization concept. This method of water cooling involves evaporation on the back side of the panel. Different water flow rates were used (0.54, 0.702, 1.32, 1.9, 2.25, and 2.4 l/hr.). The best effect was seen at a flow rate of 1.9 l/hr. While the power output was 9.3W and 11W for uncooled and water cooling, the PV panel efficiency recorded 9.15% and 11.84% for uncooled and water cooling, respectively.

(Hasan et al., 2017a) demonstrated experimentally a cooling method for the PV panels by using nozzles on the rear side with different fluids. The fluids were basic water, and nanofluids (SiO_2 , TiO_2 , and SiC). The system contained 36 nozzles that injected fluid directly into the rear's photovoltaic panel with variable flow rates ranged from (0.05 to 0.16 kg/s.) They found that the output power of PV panels increased by 62.5%, 57%, 55%, and 50% for cooling with (SiC , TiO_2 , SiO_2) nanofluids, and water, respectively. Furthermore, cooling PV with SiC nanofluids increases electrical and thermal efficiency by 12.75% and 85%, respectively.

(Mohammed et al., 2018) developed water-cooling technique for the front side of a photovoltaic cell based on water flow double glazing with two axis tracking. According to their experiment results, a 44% decrease in PV cells' temperature led to a 36.6% increase in inefficiency.

(Rakino et al., 2019) designed a new method to conduct experiment that used a water and heat sink cooling system on the rear side of the panel. Their results indicated that the temperature on the panel with cooling by water, heat sink, and combined cooling (water and heat sink) is 51.17°C , 51.83°C , and 46.58°C , respectively, and without cooling it is 53.33°C . The power output for a non-cooling system is 18.82W; the power output is 25.68W with a heat sink, 23.91W with water, and 27.80W with combined cooling.



a) Reference PV panel



b) Water cooling system



c) Heat sink system

Figure 2. 10 The construction cooling system (Rakino et al., 2019).

(Agyekum et al., 2021a) developed and designed a new technology experimentally, in which the panel was cooled using aluminum fins, which were used to create a heat sink. An ultrasonic humidifier was employed to provide a humid environment on the PV module's backside. 1.5 liters of water was consumed during the test. The results indicated the average temperature for the cooling system is 35.74°C compared to 50.35°C for the non-cooling system. Also, the power that a cooling system generates is 12.23 watts, compared to a non-cooling system's 10.8 watts.

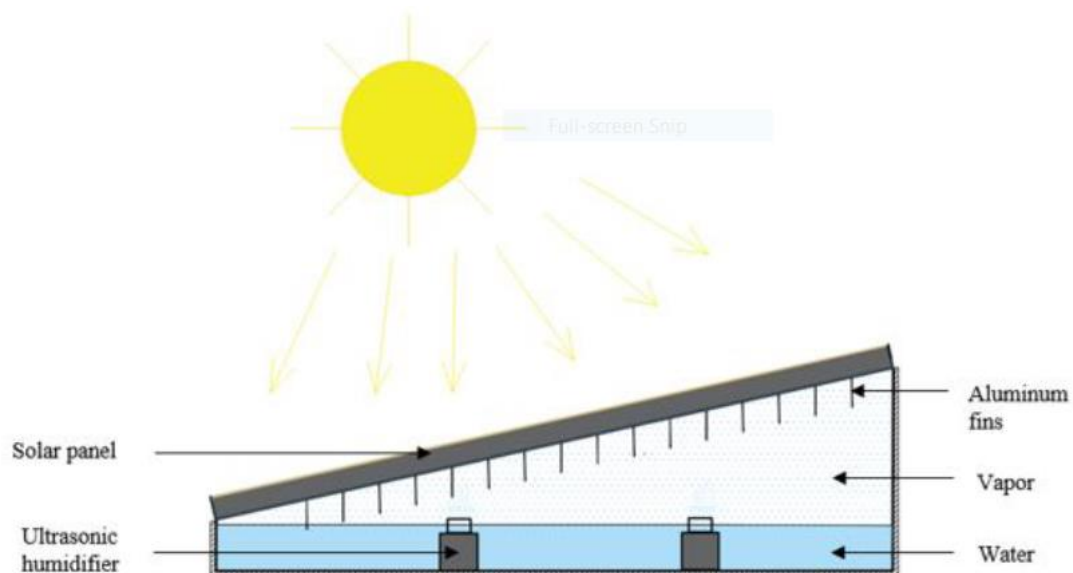


Figure 2. 11 Schematic Diagram of PV Panel Cooling System (Agyekum et al., 2021a).

2.4 Photovoltaic Cooling Techniques Using Computational Fluid Dynamics

Different studies in this field had been investigated theoretically and verified later experimentally. For example, (Michael et al., 2015) researched the effect of an air cooled system with different flow rates on the photovoltaic model using the ANSYS Fluent software. Another study by (Nasrin et al., 2019) presented a numerical and simulation analysis that compared what would happen if different fluids were used. In their study 16 baffles made of aluminum were used and attached to the rear side. The electrical efficiency of water, water/ Cu, water/Ag, and water/Al nanofluids increased to 12.35%, 12.5%, 12.51%, and 12.48%, respectively. The results of the experiments and simulations showed a very good combination between the two methods. Generally using cooling-based system to the PV panels will increase both the efficiency and the power output from the panels.

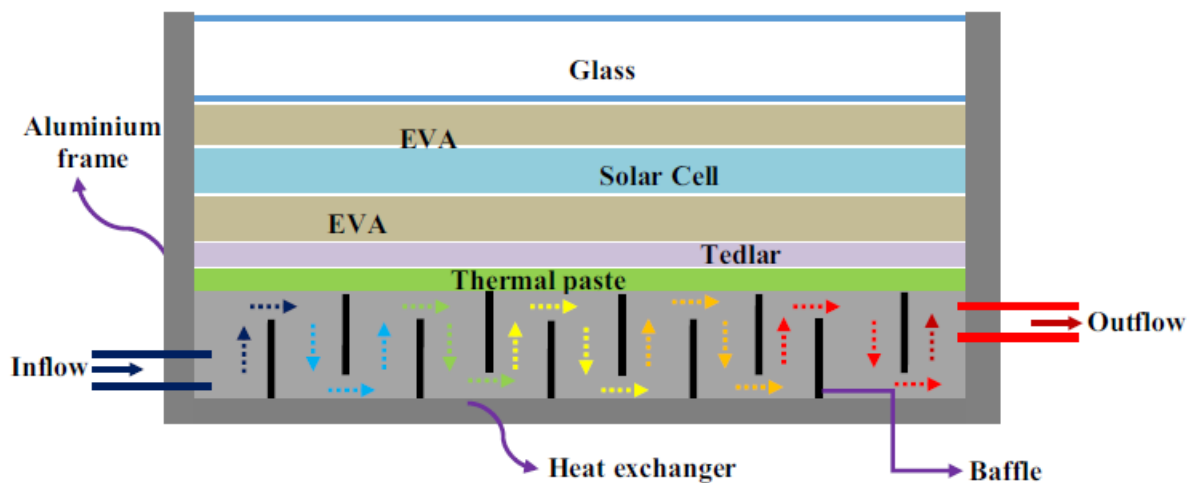


Figure 2. 12 Diagram of the PVT system (Nasrin et al., 2019).

(Misha et al., 2020) presented numerical and experimental study, design for water cooling photovoltaic using dual copper tube at the rear side for different volume flow

rates. ANSYS 19.2 was used for numerical analysis based on CFD. Based on the results, the electrical efficiency was 10.31%, 11.17 %, and 11.71% when 2, 4, and 6 l/min were used, respectively. Furthermore, when using 2, 4, and 6 l/min, the temperature difference between a non-cooled and a water-cooled PV panel was 5.1°C, 7.6°C, and 7.9°C, respectively.

(Chin et al., 2020) investigated the cold plate, which was made up of several channels connected to the back side of the PV panel, both experimentally and numerically (ANSYS). They found that the difference in temperature and power output between uncooled PV and cooled PV is 21.2°C and 8.5 watts, respectively.

(Baranwal and Singhal, 2021) conducted a numerical simulation. ANSYS software for different heat fluxes and different flow rates was used. A spiral water collector is used for cooling the PV model. Based on the findings of this investigation, the temperatures of the cooling system decrease with the decrease in the solar irradiance. Also, the temperature of the PV panel decreased with using cooling system.

The ANSYS program was used in the (Gomaa et al., 2022) study for the water-cooling system on the back side of PV panel. The model was designed as heat exchanger with thicknesses of 3 mm and 15 mm. It had been found that as the cooling fluid flow rate increased, the average solar cell temperature decreased for both thicknesses. In addition, for every 0.5 l/min rise in cooling flow rate, the average cell temperature for 15 mm and 3 mm was reduced by 1.34°C and 3.06°C, respectively. The outlet water temperature is 32.4°C and 38.9°C for 15 mm and 3 mm, respectively.

2.5 Summary

This chapter provided and reviewed the previous studies in the field of cooling photovoltaic panel. All the studies showed an improvement in the PV panel, thorough analysis of the evolution of photovoltaic cooling systems. The researchers demonstrated the overall performance of the photovoltaic panel by using different types of cooling systems. In this study, it is crucial to use alternative fluids and resources to cool the solar panels with minimum fluid flow rate and less water consumption. Additionally, the water-based cooling systems were considered more efficient because it can remove more heat from the PV panel than air-based cooling systems. When the fluid is in direct contact with the side of the PV panel, it can absorb more heat from the panel. Using acrylic glass to make the chamber, the water has direct contact with the rear side. In this study, a water cooling chamber is developed to cool the rear side of the PV panel by adopting a simple design of cooling chamber and using different designs of baffles inside the chamber to increase heat transfer rate. Further, the monocrystalline PV panel type has better efficiency than polycrystalline. This study will improve the photovoltaic panels by installing a system that will cool-down with water and use monocrystalline silicon.

CHAPTER THREE

MATHEMATICAL MODELLING

3.1 Introduction

This chapter outlines the research techniques used to calculate and improve PV performance. it is divided into two parts: In the first part, there are mathematical models that use a water chamber cooling system to figure out the electrical and thermal efficiency of PV module. The second part, which includes numerical simulations by ANSYS-fluent 2019 R2, will demonstrate the geometry, assumptions, and boundary conditions of the model.

3.2 Electrical Energy

The solar panel's performance can be expected based on its electrical efficiency. The electrical efficiency is determined by the proportion of maximum power output to the incident solar radiation on the surface area of the photovoltaic panel (Elminshawy et al., 2019).

$$\text{Electrical efficiency} = \frac{P_{mp}}{G \cdot A} \quad (3.1)$$

P_{mp} is maximum power output (W), G is the Global solar irradiance (W/m^2), A is an area of PV panel (m^2),

The maximum electrical power of a photovoltaic solar system can be expressed by this equation (Syafiqah et al., 2017)

$$P_{mp} = V_{mp} * I_{mp} = FF * V_{oc} * I_{sc} \quad (3.2)$$

FF (fill factor) measures the performance of a solar cell.

However, the electrical efficiency can be calculated based on the temperature of the PV panels, which is done mostly using CFD simulation (Ruoping et al., 2020).

$$\eta_{pv} = \eta_o * [1 - \beta * (T_p - T_o)] \quad (3.3)$$

β is the photovoltaic efficiency temperature coefficient, and it is equal to -0.45% per degree Celsius for mono-crystalline silicon (Dash et al., 2015, Hashim and Abbood, 2016,).

η_o is standard cell efficiency at 1000 W/m² irradiance with 25°C cell temperature, and 1.5 m/s air speed, T_p is the temperature of the panel, T_o is the standard temperature condition is 25°C.

3.3 Thermal Efficiency

The heat generated by the PV panel can be absorbed by the water flow inside the cooling chamber. The thermal efficiency is defined as the heat gain of the water to the solar radiation incident on the photovoltaic module region, as shown in the equation below (Elminshawy et al., 2019)

$$\text{Thermal efficiency} = \frac{Q}{G * A} \quad (3.4)$$

$$Q = \dot{m} * c_p * (T_{out} - T_{in}) \quad (3.5)$$

\dot{m} is the mass flow rate of water (kg/s), C_p is the specific heat of water (4182 J/kg.K), T_{in} inlet water temperature (°C), T_{out} outlet water temperature (°C).

3.4 Solar Angles and Monthly Solar Radiation

The solar angle and monthly solar radiation can be determined by using the following equations (Duffie and Beckman, 1980)

Slope angle (β)

The photovoltaic cells, need to be set up at an angle of beta degrees to collect the maximum solar energy from the sun.

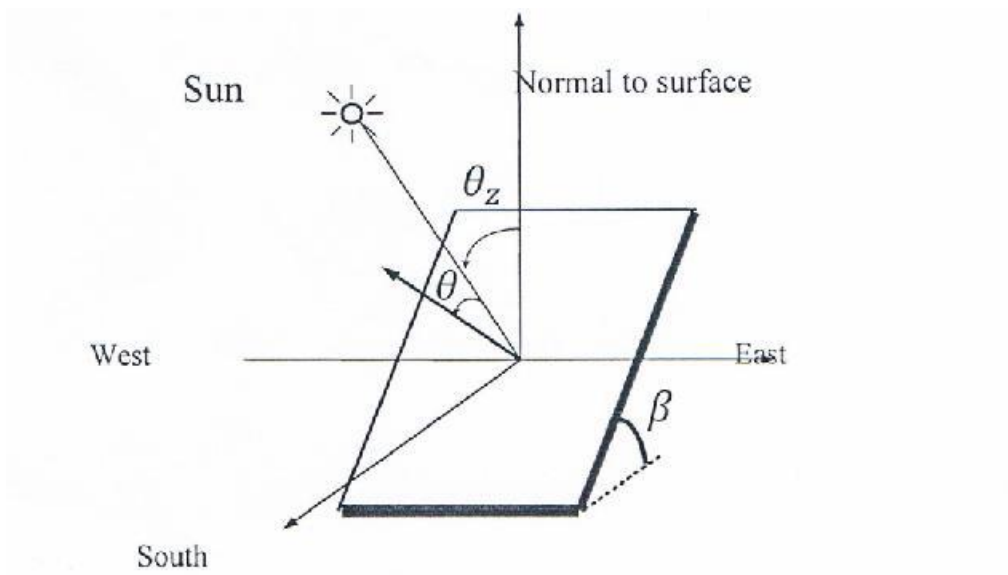


Figure 3. 1 Illustrate beta angle (Morad et al., 2018).

$$\beta = |\phi - \delta| \quad (3.6)$$

where δ is the declination, and determined by

$$\delta = 23.42 * \sin \frac{360 * (284 + n)}{365} \quad (3.7)$$

where n represents the year's nth day. For instance, January 3rd n = 3.

ϕ Latitude is the angular location north or south of the equator.

while Erbil's latitude (ϕ) is = 36.19°

- Incident radiation (\bar{H}_T)

$$\bar{H}_T = \bar{H}_b * \bar{R}_b + \bar{H}_d \left(\frac{1+\cos\beta}{2} \right) + \bar{H} \rho_g \left(\frac{1-\cos\beta}{2} \right) \quad (3.8)$$

- Diffused irradiance (\bar{H}_b)

$$\bar{H}_b = \bar{H} - \bar{H}_d \quad (3.9)$$

$$\frac{\bar{H}_d}{\bar{H}} = 1.311 - 3.022 \bar{K}_T + 3.427 \bar{K}_T^2 - 1.821 \bar{K}_T^3 \quad (3.10)$$

- Horizontal irradiance (\bar{H})

$$\bar{K}_T = \frac{\bar{H}}{\bar{H}_0} \quad (3.11)$$

$$\bar{H}_0 = \frac{24*3600}{\pi} * G_{sc} * \left(1 + 0.033 * \cos \frac{360 n}{365} \right) * \left(\cos\phi \cos\delta \sin w_s + \frac{\pi w_s}{180} \sin\phi \sin\delta \right) \quad (3.12)$$

$$\cos w_s = -\tan\phi * \tan\delta \quad (3.13)$$

$$\bar{R}_b = \frac{\cos(\phi-\beta)\cos\delta \sin\omega_s + \left(\frac{\pi}{180}\right) \omega_s \sin(\phi-\beta) \sin\delta}{\cos\phi\cos\delta \sin\omega_s + \left(\frac{\pi}{180}\right) \omega_s \sin\phi \sin\delta} \quad (3.14)$$

$$\omega_s = \cos^{-1} (-\tan(\phi - \beta) \tan\delta) \quad (3.15)$$

The Reynolds number is used to determine whether the flow is laminar or turbulent.

$$Re = \frac{v_{in} \rho_f l}{\mu_f} = \frac{v_{in} l}{\nu_f} \quad (3.16)$$

where v_{in} inlet water velocity (m/s), ρ_f density of water (kg/m³), l length of the PV panel (m), μ_f dynamic viscosity (kg/m. s), ν_f kinematic viscosity (m²/s).

3.5 Modeling Simulation

ANSYS is a part of engineering simulation software created by John Swanson in 1970. This program is utilized for the numerical solution of a variety of mechanical issues. Some of these issues are thermal, fluid, electromagnetic, etc. ANSYS Workbench, which serves as a bridge between them, was used to access the various programs that are part of ANSYS.

ANSYS Fluent is a part of the software in the ANSYS suite that is used to perform computational fluid dynamics (CFD) analysis. In this study, the PV model with cooling has been investigated, and the proposed simulations show how the cooling system affects the photovoltaic module. The proposed model of the PV with cooling systems using the CFD simulation technique is considered a heat absorber for the solar cell. In ANSYS-fluent, the fluid's flow is determined by the heat transfer rate calculations, which result in a temperature distribution profile. Simulations have been done on personal computers with AMD Ryzen 7 5800H with Radeon Graphics 3.20 GHz processors and 16 GB of RAM.

3.5.1 The Governing Equation and Boundary Conditions

For this simulation, we used the governing equation and boundary conditions listed below (Nasrin et al., 2018).

For the glass:

$$-\left(\frac{k}{\rho C_p}\right)_g \left(\frac{\partial^2 T_g}{\partial x^2} + \frac{\partial^2 T_g}{\partial y^2} + \frac{\partial^2 T_g}{\partial z^2}\right) = \alpha_g G - U_{ga} (T_g - T_{amb}) - \epsilon_g \sigma (T_g^4 - T_s^4) - U_t (T_g - T_{sc}) \quad (3.17)$$

For the cell:

$$-\left(\frac{k}{\rho C_p}\right)_{sc} \left(\frac{\partial^2 T_{sc}}{\partial x^2} + \frac{\partial^2 T_{sc}}{\partial y^2} + \frac{\partial^2 T_{sc}}{\partial z^2}\right) = \alpha_{sc} \tau_g G - E_e - U_t (T_{sc} - T_{td}) - U_t (T_{sc} - T_g) \quad (3.18)$$

For the tedlar

$$-\left(\frac{k}{\rho C_p}\right)_{td} \left(\frac{\partial^2 T_{td}}{\partial x^2} + \frac{\partial^2 T_{td}}{\partial y^2} + \frac{\partial^2 T_{td}}{\partial z^2}\right) = -U_t (T_{sc} - T_{td}) - U_{td} (T_{td} - T_f) \quad (3.19)$$

For the fluid domain

$$\frac{\partial u}{\partial x} + \frac{\partial v}{\partial y} + \frac{\partial w}{\partial z} = 0 \quad (3.20)$$

$$\rho \left(u \frac{\partial u}{\partial x} + v \frac{\partial u}{\partial y} + w \frac{\partial u}{\partial z} \right) = -\frac{\partial p}{\partial x} + \mu_f \left(\frac{\partial^2 u}{\partial x^2} + \frac{\partial^2 u}{\partial y^2} + \frac{\partial^2 u}{\partial z^2} \right) \quad (3.21)$$

$$\rho \left(u \frac{\partial v}{\partial x} + v \frac{\partial v}{\partial y} + w \frac{\partial v}{\partial z} \right) = -\frac{\partial p}{\partial y} + \mu_f \left(\frac{\partial^2 v}{\partial x^2} + \frac{\partial^2 v}{\partial y^2} + \frac{\partial^2 v}{\partial z^2} \right) \quad (3.22)$$

$$\rho \left(u \frac{\partial w}{\partial x} + v \frac{\partial w}{\partial y} + w \frac{\partial w}{\partial z} \right) = -\frac{\partial p}{\partial z} + \mu_f \left(\frac{\partial^2 w}{\partial x^2} + \frac{\partial^2 w}{\partial y^2} + \frac{\partial^2 w}{\partial z^2} \right) \quad (3.23)$$

$$(\rho_f C_{p_f}) \left(u \frac{\partial T_f}{\partial x} + v \frac{\partial T_f}{\partial y} + w \frac{\partial T_f}{\partial z} \right) = k_f \left(\frac{\partial^2 T_f}{\partial x^2} + \frac{\partial^2 T_f}{\partial y^2} + \frac{\partial^2 T_f}{\partial z^2} \right) \quad (3.24)$$

where k_f is thermal conductivity of fluid, ρ_f density of fluid, C_{p_f} specific heat at constant pressure of fluid, μ_f dynamic viscosity of fluid. $\sigma = 5.670367 \times 10^{-8} \text{ W/m}^2 \text{ K}^4$ (Stefan-Boltzmann value), $T_s = 0.0552 T_{amb}^{1.5}$ is the sky temperature.

And the boundary conditions

1. For side surface of PVT: $-n \cdot (-k \nabla T) = 0$
2. For solid boundary of fluid domain: $u = v = w = 0$
3. For fluid-solid interface: $k_f \left(\frac{\partial T}{\partial n} \right)_f = k_{td} \left(\frac{\partial T}{\partial n} \right)_{td}$

4. For inlet $T = T_{in}, u = 0, v = V_{in}, w = 0$
5. For outlet $P = 0$

where n is the distance along x or y or z directions, acting normal to the surface.

3.6 Process for Simulating

ANSYS Workbench opens initially, then chose Fluid Flow (Fluent), which appears in the dialog box as shown in Figure 3.2. The overall steps in FLUENT numerical methods will be as follows: There are five major steps, (Geometry, Mesh, Setup, Solution, and Results).

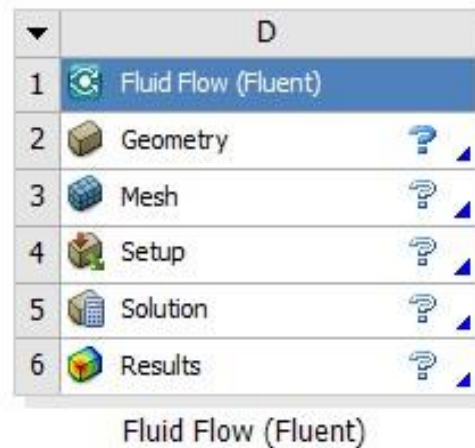


Figure 3. 2 The dialog box of Fluid Flow (Fluent).

3.6.1 Geometry

The geometry cell in the Fluid Flow (Fluent) starts to make a geometrical shape with ANSYS Design Modeler. The photovoltaic panel is designed with the length and width of 1.2 m and 0.67 m, respectively. The photovoltaic panel consists of 5 layers of Glass, Ethylene Vinyl Acetate (Eva 1), Silicon a sunlight-to-electricity conversion device, Eva 2, and Tedlar. The water-cooling chamber is connected to

the back side of the PV. The thickness of each part is shown in Table 3.1, while Figure 3.3 shows the geometry of the PV panel.

Table 3. 1 The thickness of the PV panel (Syafiqah et al., 2017b)

Materials	Thickness (mm)
Glass	3
Eva 1	3
Silicon	4
Eva 2	3
Tedlar	0.1
Water	15

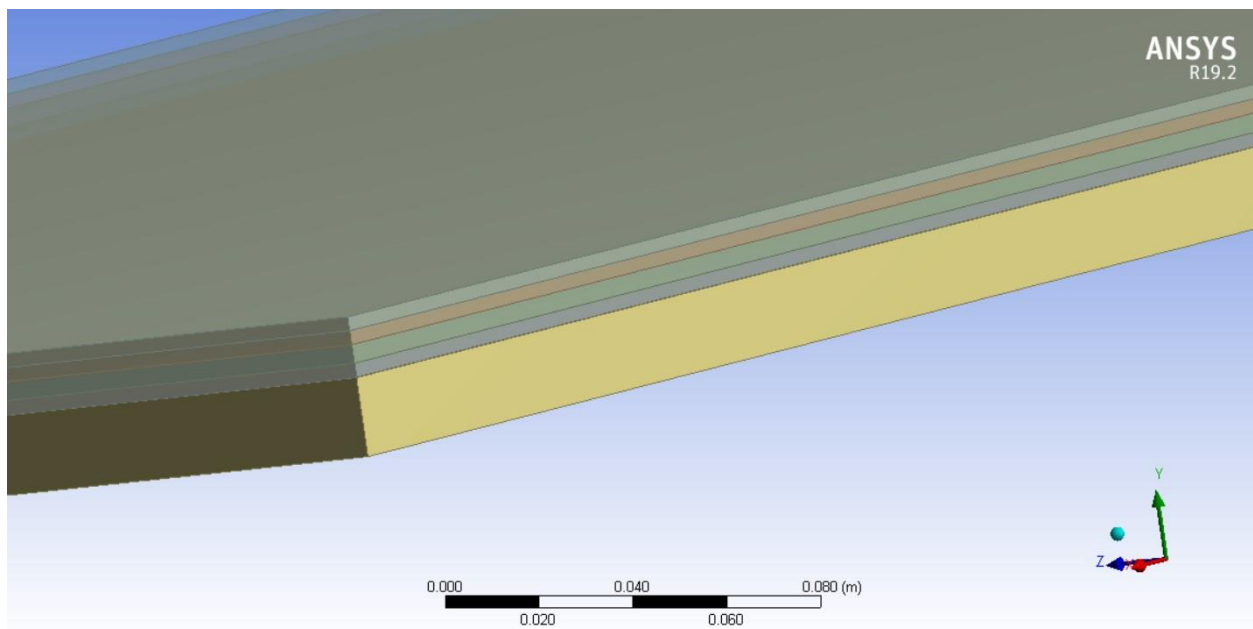


Figure 3. 3 The geometry of the photovoltaic panel.

3.6.2 Mesh

The mesh cell in the Fluid Flow (Fluent) is created. The intricate geometric shape object is divided into several cells with a specific number of nodes during the meshing process. In the mesh process selection, the default value for CFD in physics is chosen, while, the solver preference was fluent, and liner for the element order.

The best element size for the geometry is $4\text{e-}003\text{m}$ based on the test for mesh independence. In the quality of the mesh, the average skewness is 1.3113×10^{-10} , the average element quality is 0.876, and the average aspect ratio is 5.4. The nodes and elements are created to be 409360 and 364500, respectively. And according to (Raval et al., 2014), a skewness value near to zero means high and good meshing. Figure 3.4 shows the mesh of the PV panel. The next step in the meshing process is to identify the name of each part of the geometry.

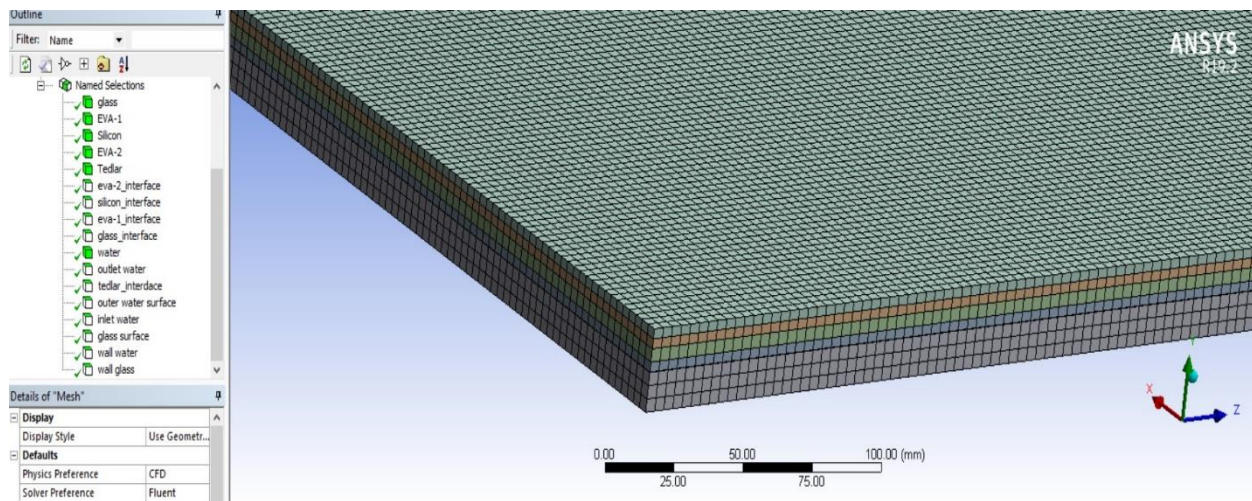


Figure 3. 4 The mesh of the PV panel.

3.6.3 Setup

The setup setting is very necessary for the simulation model since it includes the necessary input data. Figure 3.5 shows the dialog box for the setup. In the options, choose double precision, and in the processing options, choose parallel solver, then click OK.

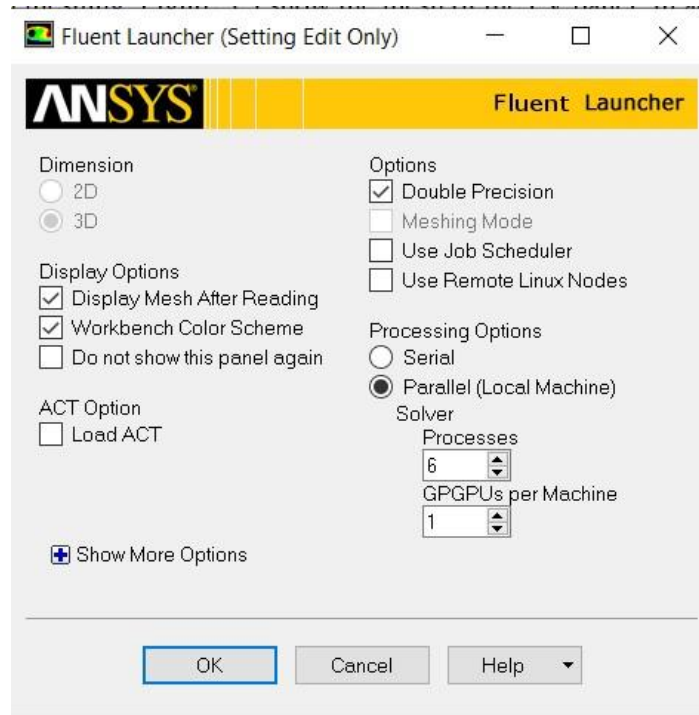
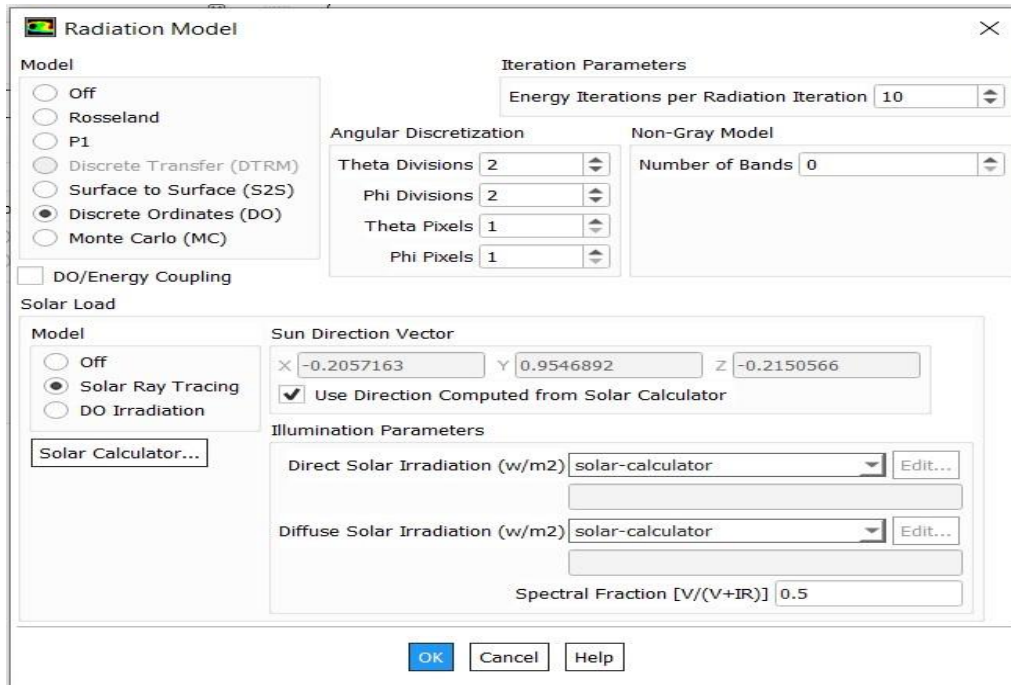


Figure 3. 5 Fluent Launcher

Under open setup, the models' tasks include multiphase, energy, viscous, radiation, heat exchanger, etc. The energy is activated and changed to "on." This allows calculations of heat transfer within the solar panel. While for the viscous setup, the laminar flow is chosen based on eq. (3.16). In the radiation section, select Discrete Ordinates (DO), and in the solar load, select solar ray tracing. After selecting solar ray tracing, in the Illumination Parameters, both Direct Solar Irradiation and Diffuse Solar Irradiation must be selected on the option "solar-calculator." In this dialog box, a global position, date and time, mesh orientation, and solar irradiation method are used. In the global position, the longitude and latitude of Erbil city are selected as 44° and 36.2° , and the time zone is +3. Figures 3.6 and 3.7 illustrate the Radiation Model and Solar Calculator, respectively.



Radiation Model

Model

- ☐ Off
- ☐ Rosseland
- ☐ P1
- ☐ Discrete Transfer (DTRM)
- ☐ Surface to Surface (S2S)
- ☒ Discrete Ordinates (DO)
- ☐ Monte Carlo (MC)

☐ DO/Energy Coupling

Iteration Parameters

Energy Iterations per Radiation Iteration: 10

Angular Discretization

Theta Divisions: 2
Phi Divisions: 2
Theta Pixels: 1
Phi Pixels: 1

Non-Gray Model

Number of Bands: 0

Solar Load

Model

- ☐ Off
- ☒ Solar Ray Tracing
- ☐ DO Irradiation

Sun Direction Vector

X: -0.2057163 Y: 0.9546892 Z: -0.2150566

☒ Use Direction Computed from Solar Calculator

Illumination Parameters

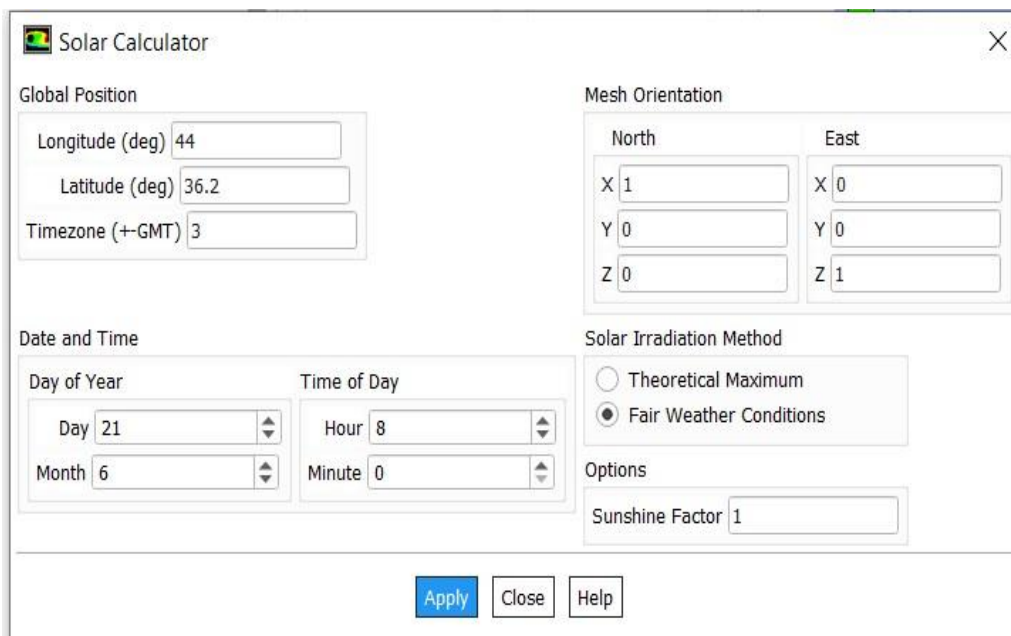
Direct Solar Irradiation (w/m2): solar-calculator Edit...

Diffuse Solar Irradiation (w/m2): solar-calculator Edit...

Spectral Fraction $[V/(V+IR)]$: 0.5

OK Cancel Help

Figure 3. 6 Radiation Model



Solar Calculator

Global Position

Longitude (deg): 44
Latitude (deg): 36.2
Timezone (+GMT): 3

Mesh Orientation

North		East	
X	1	X	0
Y	0	Y	0
Z	0	Z	1

Date and Time

Day of Year: Day 21 Month 6
Time of Day: Hour 8 Minute 0

Solar Irradiation Method

- ☐ Theoretical Maximum
- ☒ Fair Weather Conditions

Options

Sunshine Factor: 1

Apply Close Help

Figure 3. 7 Solar Calculator

The material specifications are required for each layer that is used in the geometry. In the material section, choose water for the fluid, and for solids, identify five solid

layers of the PV panel. The layers are glass, EVA1, silicon, EVA2, and tedlar. Table 3.2 showed the density, specific heat, and thermal conductivity of each layer and water. Figure 3.8 and Figure 3.9 display the definition of solid and fluid.

Table 3. 2 The properties of each material (Syafiqah et al., 2017b)

Materials	Density kg/m ³	Specific heat J/kg-K	Thermal Conductivity w/m-K
Glass	3000	500	0.98
EVA 1	960	2090	0.23
Silicon	2329	712	148
EVA 2	960	2090	0.23
Tedlar	1200	1250	0.36
Water	997	4180	0.59

Create/Edit Materials

Name: water-liquid

Material Type: fluid

Chemical Formula: h2o<|>

Fluent Fluid Materials: water-liquid (h2o<|>)

Mixture: none

Order Materials by: ☒ Name ☐ Chemical Formula

Fluent Database...
User-Defined Database...

Properties

Density (kg/m3): constant 997 [Edit...]

Cp (Specific Heat) (j/kg-k): constant 4180 [Edit...]

Thermal Conductivity (w/m-k): constant 0.59 [Edit...]

Viscosity (kg/m-s): constant 0.001003 [Edit...]

Change/Create Delete Close Help

Figure 3. 8 Defining a fluid in Fluent.

Create/Edit Materials

Name: glass

Material Type: solid

Chemical Formula: glass

Fluent Solid Materials: glass

Mixture: none

Order Materials by: ☒ Name ☐ Chemical Formula

Fluent Database...

User-Defined Database...

Properties

Density (kg/m3): constant (3000) [Edit...]

Cp (Specific Heat) (j/kg-k): constant (500) [Edit...]

Thermal Conductivity (w/m-k): constant (0.98) [Edit...]

Absorption Coefficient (1/m): constant (0) [Edit...]

Change/Create Delete Close Help

Figure 3. 9 Defining a Solid in Fluent.

Setting the cell zone conditions is necessary to differentiate between the solid and liquid domains. In this study, every boundary condition for each face of the geometry has been identified.

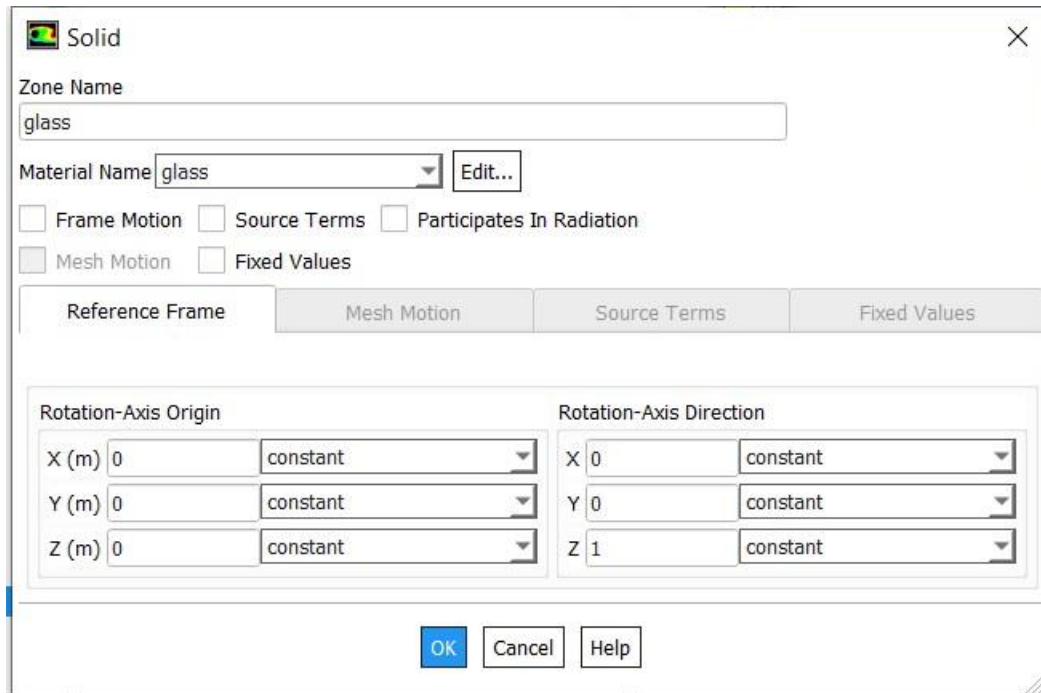
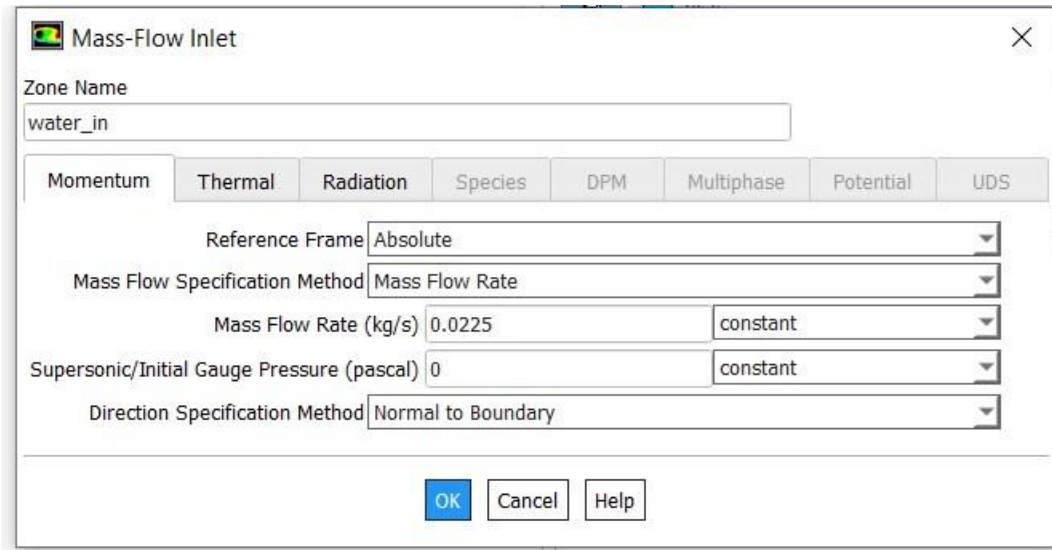


Figure 3. 10 Define cell zone condition.

Identify every boundary condition for each face of the geometry. For instance, the mass flow has been selected as the inlet face boundary condition. For the outlet, the pressure outlet is set to atmospheric pressure. The "Participates in Solar Ray Tracing" setting has been selected off for both the input and the output, as shown in Figures 3.11 and 3.12.



Mass-Flow Inlet

Zone Name
water_in

Momentum Thermal Radiation Species DPM Multiphase Potential UDS

Reference Frame Absolute

Mass Flow Specification Method Mass Flow Rate

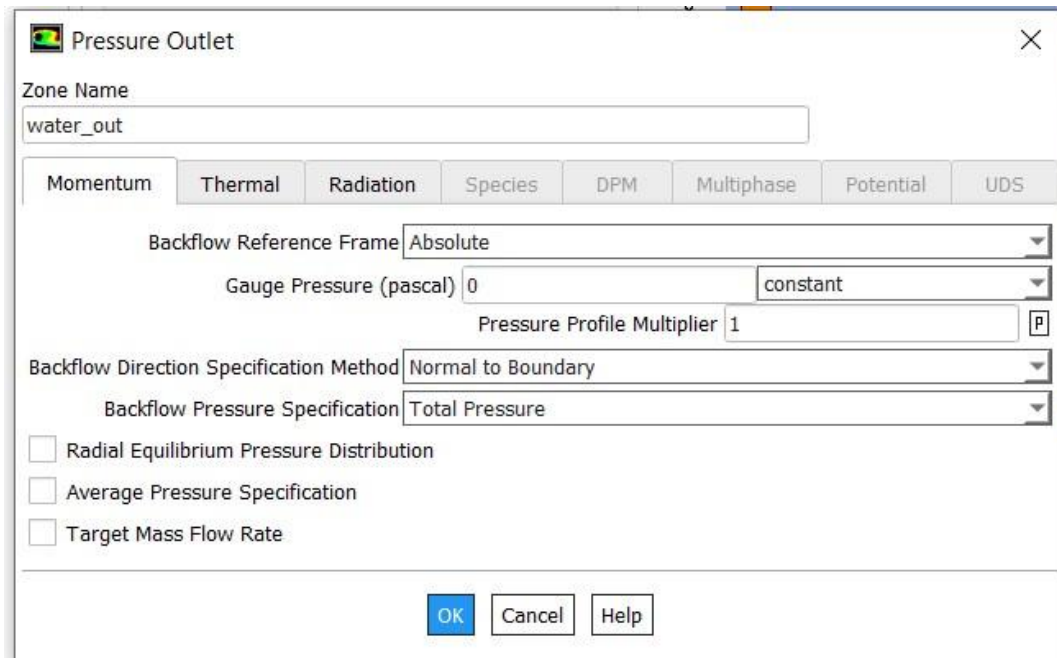
Mass Flow Rate (kg/s) 0.0225 constant

Supersonic/Initial Gauge Pressure (pascal) 0 constant

Direction Specification Method Normal to Boundary

OK Cancel Help

Figure 3. 11 Inlet boundary condition.



Pressure Outlet

Zone Name
water_out

Momentum Thermal Radiation Species DPM Multiphase Potential UDS

Backflow Reference Frame Absolute

Gauge Pressure (pascal) 0 constant

Pressure Profile Multiplier 1 P

Backflow Direction Specification Method Normal to Boundary

Backflow Pressure Specification Total Pressure

☐ Radial Equilibrium Pressure Distribution

☐ Average Pressure Specification

☐ Target Mass Flow Rate

OK Cancel Help

Figure 3. 12 Outlet boundary condition.

Mixed was chosen for both glass surfaces and wall-glass. Heat transfer coefficient is $10 \text{ W/m}^2 \cdot \text{K}$ (Baranwal and Singhal, 2021). Semi-transparent for glass surfaces, opaque for wall glass, as shown in Figure 3.13. Other layers are selected via System Coupling. Wall water and outer water surface select convection.

Wall
 ✕

Zone Name

Adjacent Cell Zone

Momentum Thermal Radiation Species DPM Multiphase UDS Wall Film Potential

Thermal Conditions

☐ Heat Flux
☐ Temperature
☐ Convection
☐ Radiation
☒ Mixed
☐ via System Coupling
☐ via Mapped Interface

Heat Transfer Coefficient (w/m2-k)

 Free Stream Temperature (c)

 External Emissivity

 External Radiation Temperature (c)

 Internal Emissivity

 Wall Thickness (m)

 Heat Generation Rate (w/m3)

☐ Shell Conduction

Material Name

Figure 3. 13 The boundary condition of glass.

3.6.4 Solution

In the solution, the method is selected. The SIMPLE algorithm is used, and in spatial discretization, least squares cell-based is selected. For the pressure, select second order; in both the momentum and energy select second order upwind; and in discrete ordinates select first order upwind.

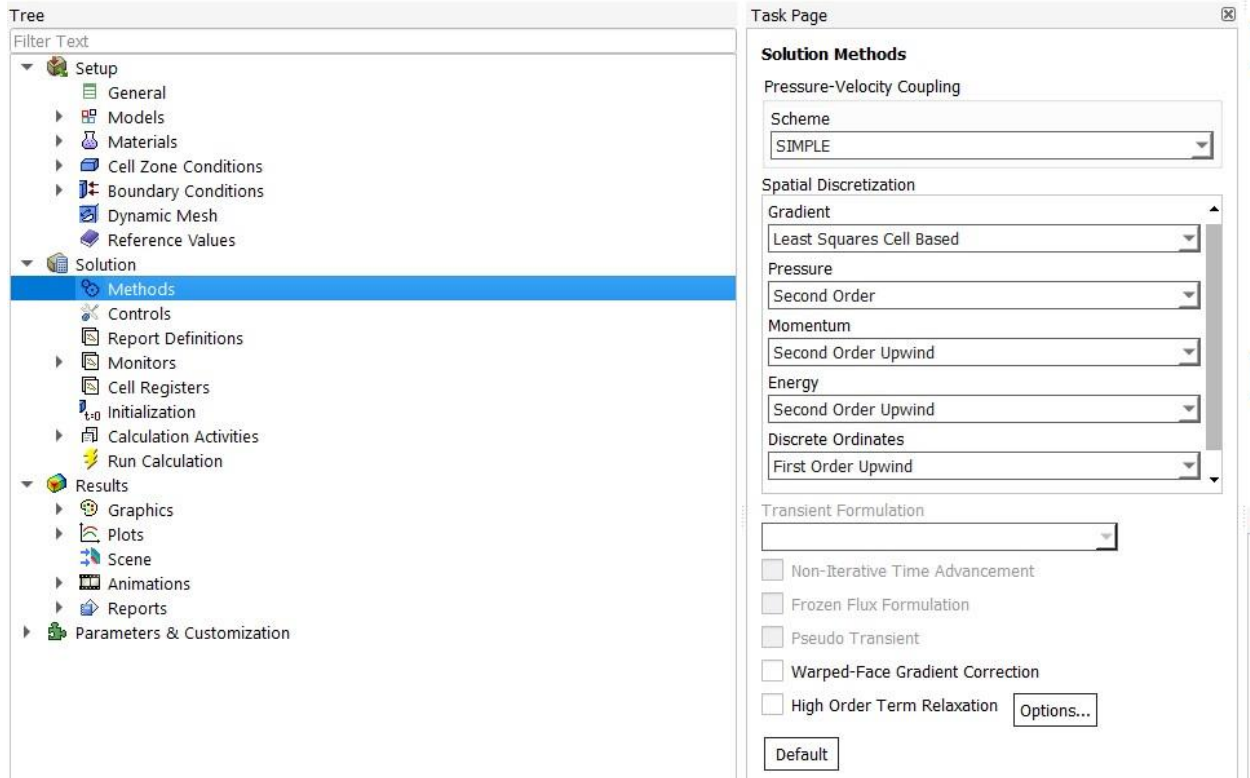


Figure 3. 14 Illustrate the task of the solution method.

Modify the monitoring view as necessary with terms for residuals, report files, report plots, and any necessary convergence conditions.

Setting the residual monitors of the continuity equation, the energy equation, and the do-intensity to 10^{-12} , and for the X, Y, and Z velocity equations to 10^{-10} . The analysis that needs to converge at the given range according to Figure 3.15.

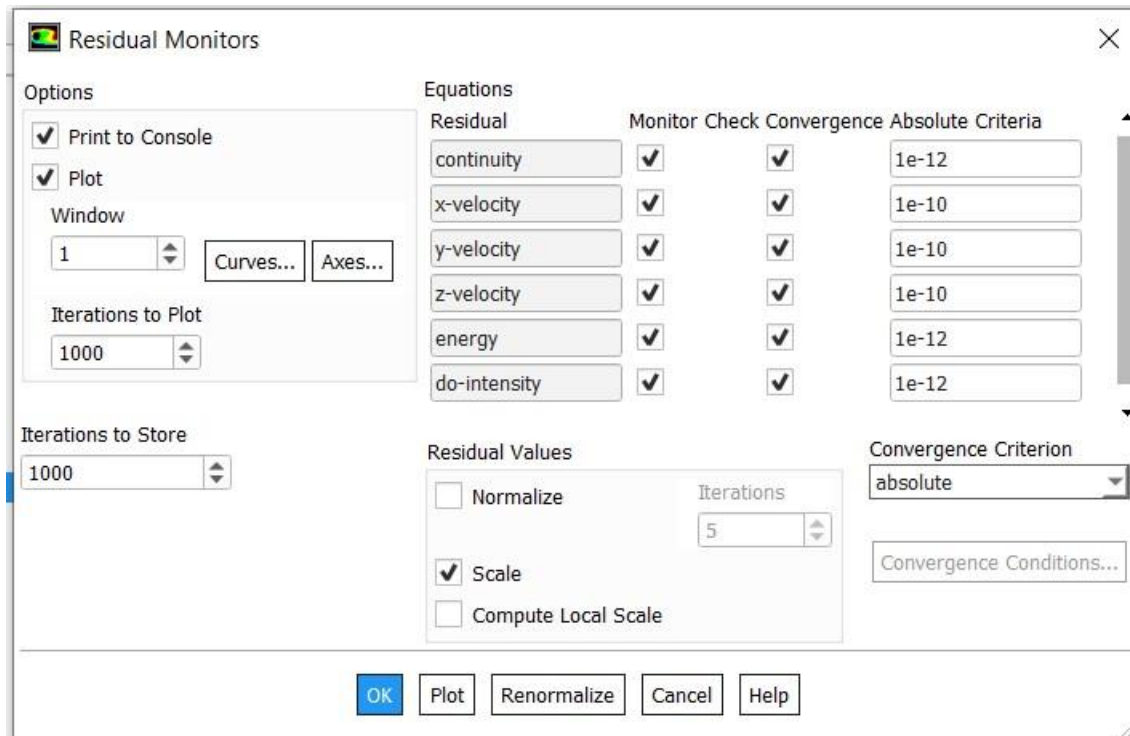


Figure 3. 15 Modifying Fluent's solution monitoring.

Then in the Solution initialization, two solution methods have been considered: hybrid initialization and standard initialization as shown in Figure 3.16.

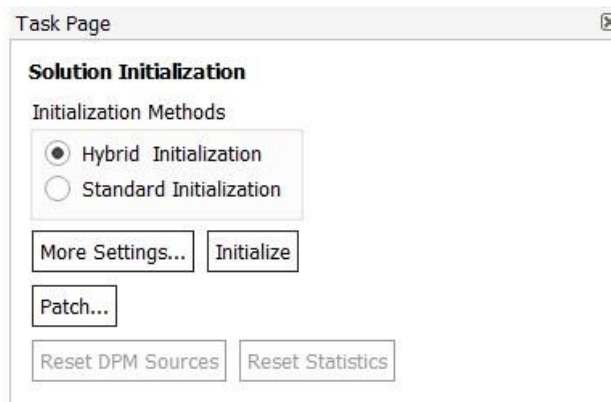


Figure 3. 16 Solution initialization.

The last step in the solution and calculation process is to enter the number of iterations needed to get to a solution. The two used parts of the run calculation part are illustrated in Figure 3.17.

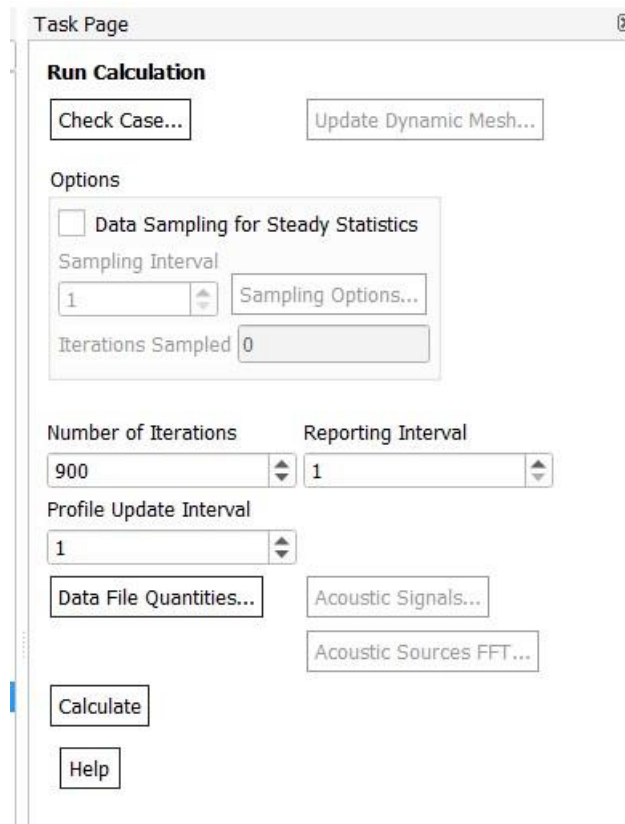


Figure 3. 17Run calculation.

While the trend remains constant and does not vary as the number of iterations increases, the solution is converged.

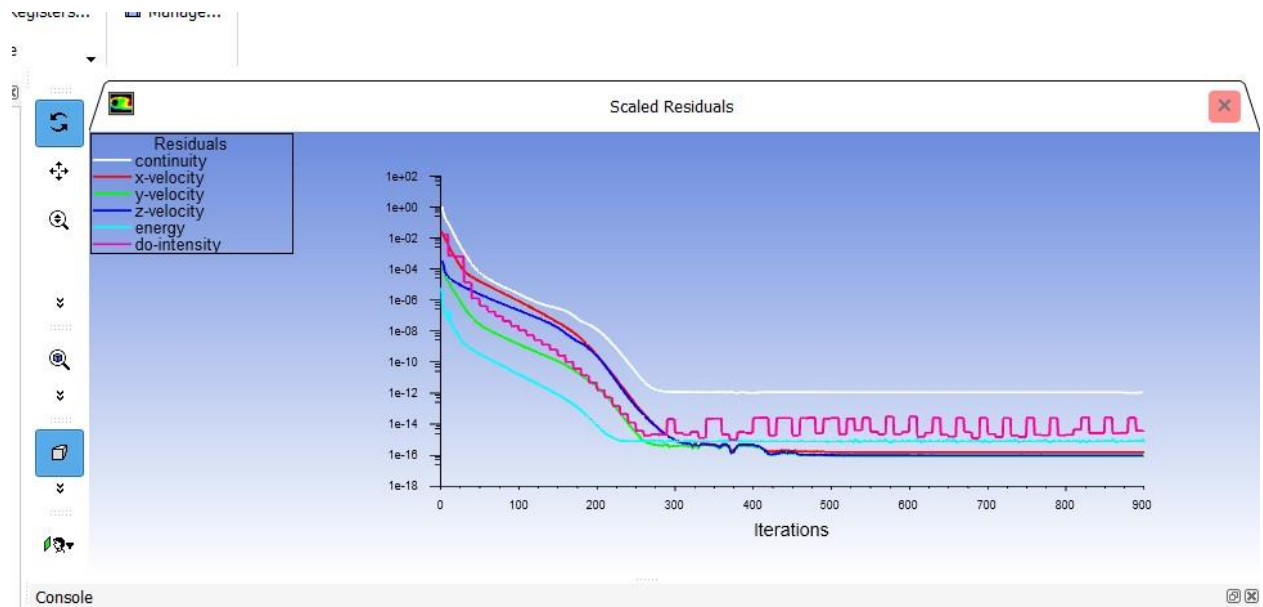


Figure 3. 18 scaled residuals.

3.6.5 Result

Figure 3.19 shows that displaying the results in the same part of the calculations includes the results section, which is made up of:

- Graphic
- Plots
- Animations
- Reports

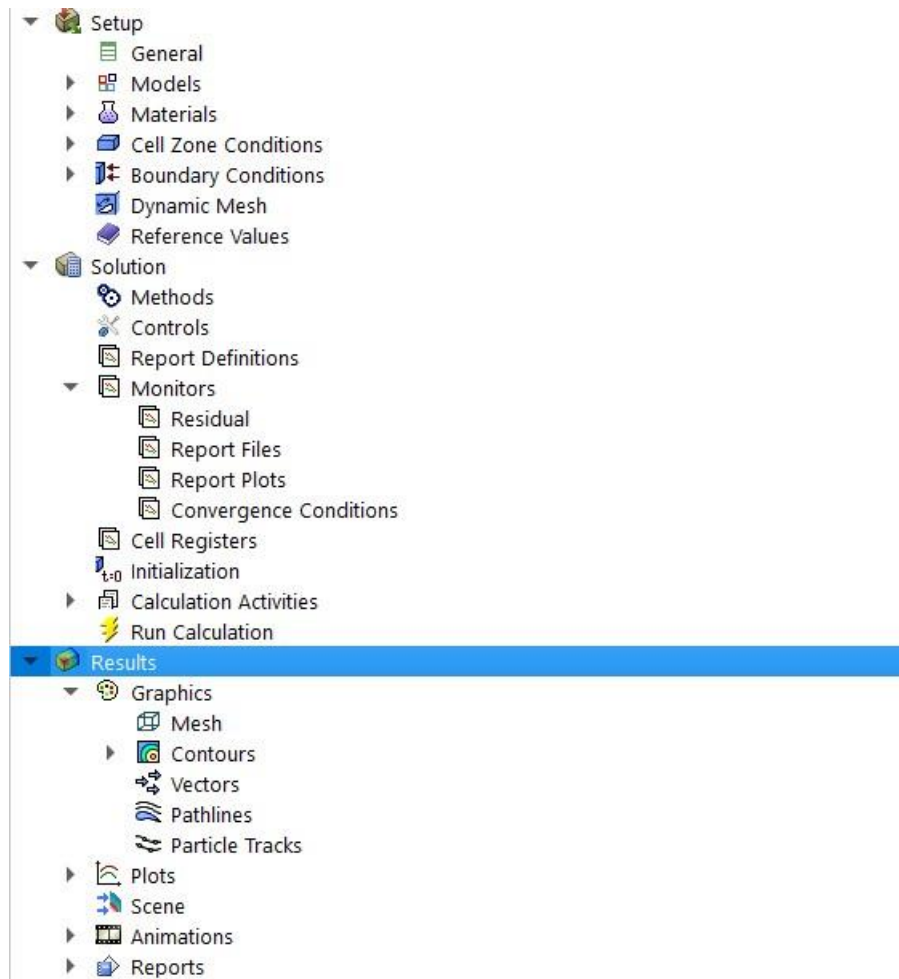


Figure 3. 19 display result

The above-mentioned processes are implemented in this study design model. In the following chapters, the different analyzed parameters, together with a discussion of the causes of the results will be demonstrated.

CHAPTER FOUR

EXPERIMENTAL WORK

4.1. Introduction

The ambient temperature is directly affected by the solar radiation, and this will be reflected on the overall temperature of PV panel, which resulted in a reduction in power output. In summer, Iraq's climate is hot and dry. In addition, to the reduction in the efficiency of the PV panel, this will affect its lifespan. Therefore, it is preferred to cool the PV panel systems to reduce the effect of heat and the high temperature. In this chapter a comprehensive overview of the experimental installation design and setup is described. The PV system is installed at the Research Center at Erbil Polytechnic University, Erbil, Iraq. The experimental study of the solar photovoltaic system was done under outdoor conditions during summer months of 2022.

4.2. Photovoltaic With the Cooling System

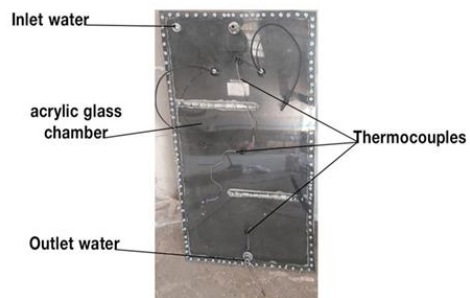
The cooling system uses water as an operating fluid to reduce the temperature of the PV panels. The PV module is the key component of the system, while the second part is an acrylic glass chamber. The third component in the PV system with cooling is a pump that circulates the cooling water. The fourth part is a data logger to record data. Finally, the fifth part is a solar power meter to measure solar radiation. Figure 4.1 shows an illustration of how the experiment was set up. Figure 4.2 illustrates the schematic plan of the developed prototype setup.



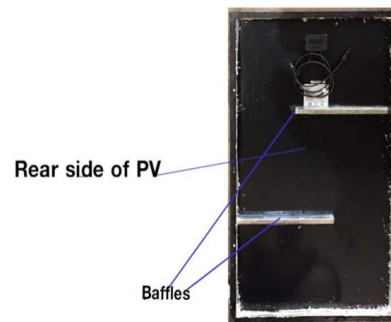
a. front side of the photovoltaic panel



b. back side of the photovoltaic panel



c. rear side of the PV panel with chamber



d. T back side of the design has baffles.

Figure 4. 1 Photovoltaic panels system components

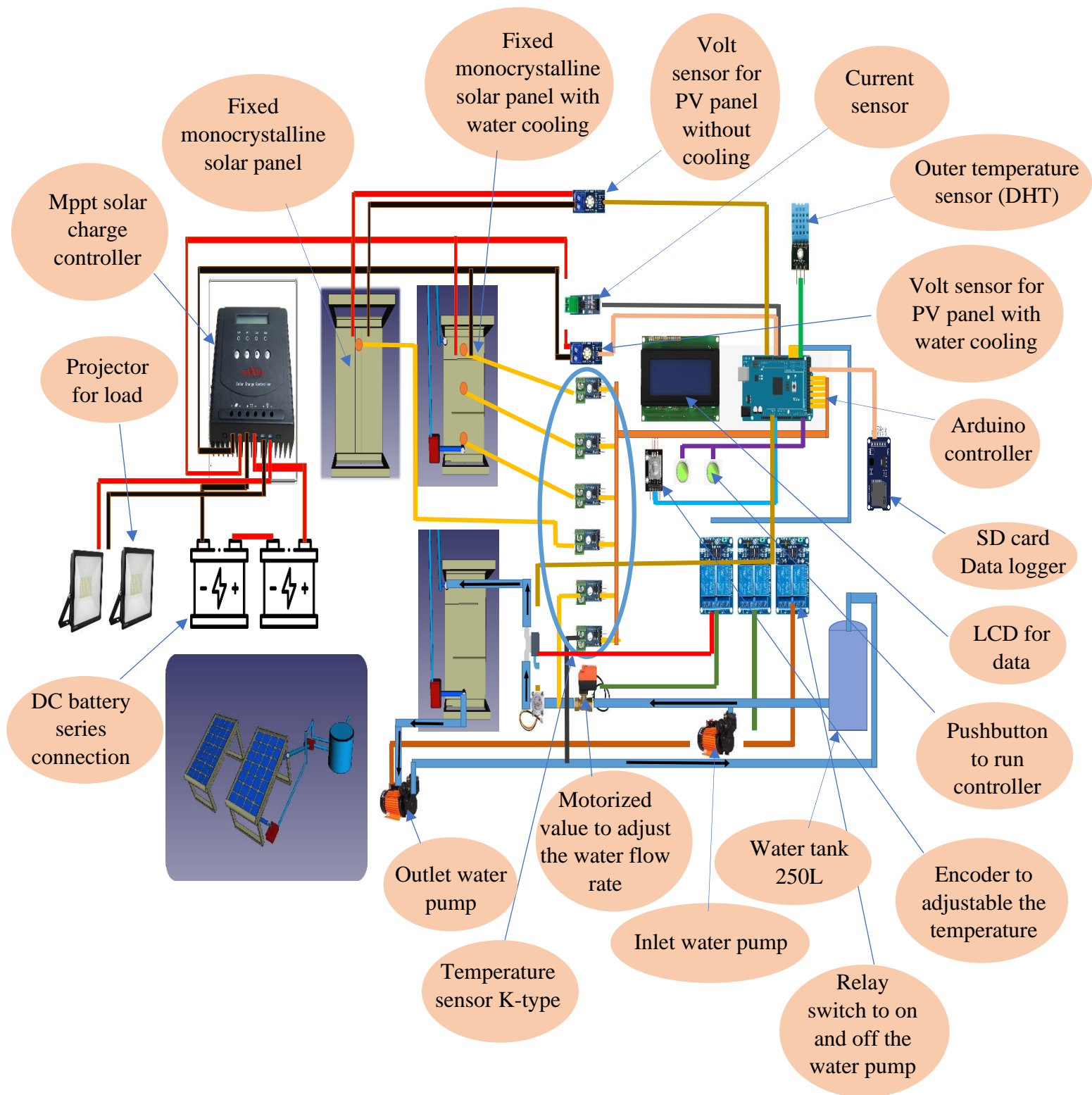


Figure 4. 2 A schematic diagram of the cooled PV panel.

4.2.1 Solar Photovoltaic Module

In this experiment, two monocrystalline PV panels were installed to produce electricity. Table 4-1 shows the technical information about the PV panels that were used in the study. The first PV panel is developed to be cooled by the water chamber cooling at the panel's back surface, while the second panel is used as a reference panel without any design modification.

Table 4. 1 Mechanical data at standard test conditions @ (1000 W/m², 25 °C, 1.5 m/s)

Cell type	Monocrystalline
Module dimension	1230* 670* 30 mm
Maximum power current	7.54 Amp
Maximum power voltage	22.55 V
Open circuit voltage (V_{oc})	26.65 V
Short circuit current (I_{sc})	8.05 Amp
Working temperature	-40 °C ~ +80 °C

3.2.2 Water Cooling Chamber System.

The proposed cooling system in this study is water cooling chamber which is designed to be attached the rear side of the photovoltaic panel. The cooling system fluid of the PV panel is a closed cycle, and the cooling fluid contacts the panel directly through the rear side of the PV panel.

The cooling chamber of the PV panel is made of acrylic glass 8 mm thick. When compared to window glass of equal thickness, acrylic glass is nearly 50% lighter and has higher transparency. The glass chambers were fixed to the rear side of the photovoltaic panel. The water chamber is designed to have a water inlet from the top of the PV panel and an outlet of the water from the middle bottom of the PV panel as shown in Figure 4.3. The developed chamber has been designed to have two paths of water flow through the baffles to increase the surface heat transfer between water

and Tedlar, the length of each baffle is 48 cm, as shown in Figure 4.1 c & d. The acrylic glass was fixed and attached to a PV frame by silicon.

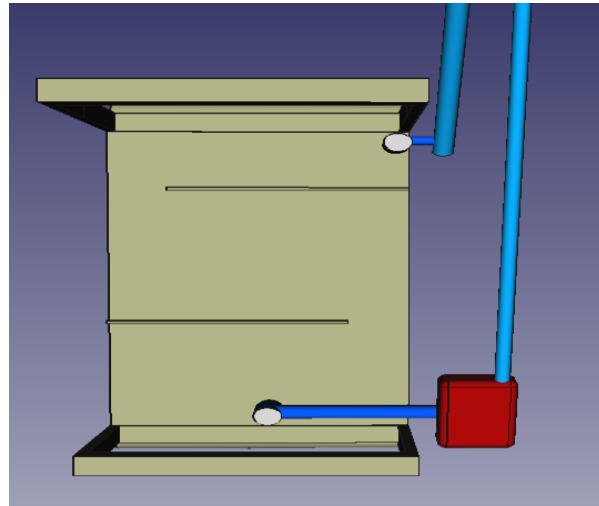


Figure 4. 3 A schematic diagram of the rear side PV panel.

4.2.3. Water Softener and Water Tank Supply

The hardness of water is solved by using softener system for the closed water cycle system. This is done using a technique known as "ion exchange." When calcium and magnesium build up, stains will accumulate, clog pipes, and slow the flow of water to pump and other equipment. Therefore, these stains affect will negatively the PV panel, reducing its efficiency and life span. A water softener is utilized, which is a device connected to the water supply tank. The amount of water that can be carried in the tank is 250 liters. The water softener and the water supply tank are illustrated in Figure 4.4.



Figure 4. 4 Water softener and water tank supply.

4.2.4. Water Flow Meter

The flow rate is measured by flow rate sensor model YF-s201. This sensor contains a pinwheel sensor that measures the amount of liquid passing through it. The operating range of the flow rate is from 1 to 30 liters per minute, while the temperature range of working fluid is between -25 and +80 °C.

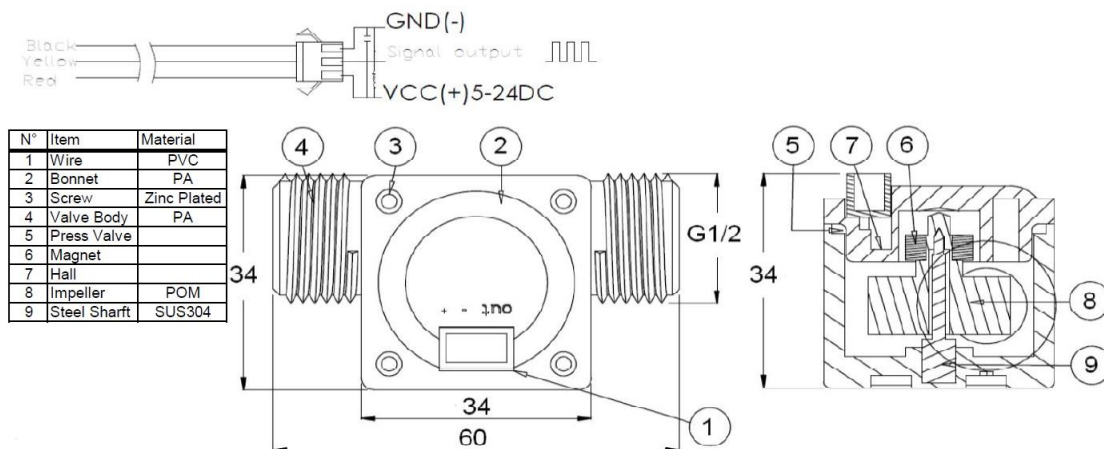


Figure 4. 5 schematic diagram water flow rate YF-s201 type.



Figure 4. 6 water flow rate YF-s201 type.

4.2.5 Water pump

One of the major parts of the photovoltaic/thermal system is the pump. In this study, closed loop water system is used to circulate the water through the cooling chamber using a SUPER SHAEMGIE water pump as shown in Figure 4.7. Table 4.2 shows the technical details of the water pump.



Figure 4. 7 Water pump.

Table 4. 2 Details of the SUPER SHAEMGIE water pump.

Parameters	Specification
Power supply	AC type
Voltage	220 V
Power	0.37 kW or 0.55 hp
Maximum Head	27 m
Maximum flow rate	30 l/min
Speed	2850 r/min

4.2.6 The Temperatures of The System

The temperature of the PV panels, inlet and outlet water, and ambient temperature are recorded by the data logger with a 7-channel temperature recorder. Utilize a Secure Digital (SD) card to save both the data and the time (year, month, day, minute, and second). K-type of thermocouples are used in this model. The temperature sensors connect to the MAX6675 modular and then connects to Arduino.

The technical specification of the connection is described as the following, a serial peripheral interface (SPI) is used to send the temperature reading from the module to the microcontroller. It has seven pins in total, two of which are used to attach the thermocouple positive and negative leads, three of which are used for the SPI interface, and two of which are used to connect power and ground.

The ambient temperature was measured by DHT (Digital Humidity Temperature) sensor and the temperature range between 0-50°C.

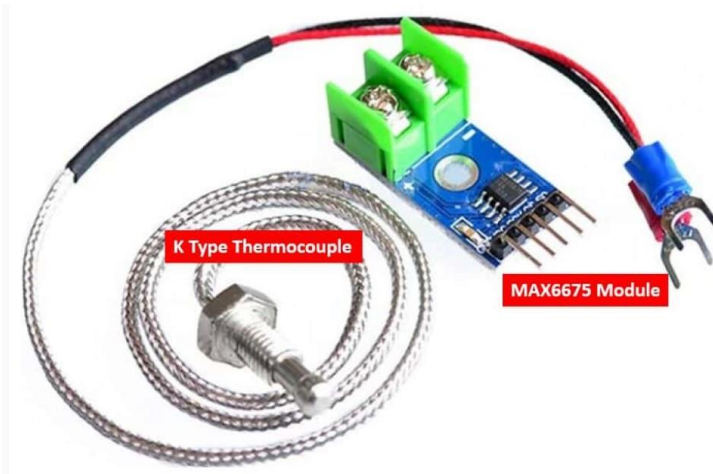


Figure 4. 8 k-type temperature sensor with MAX6675 modular.

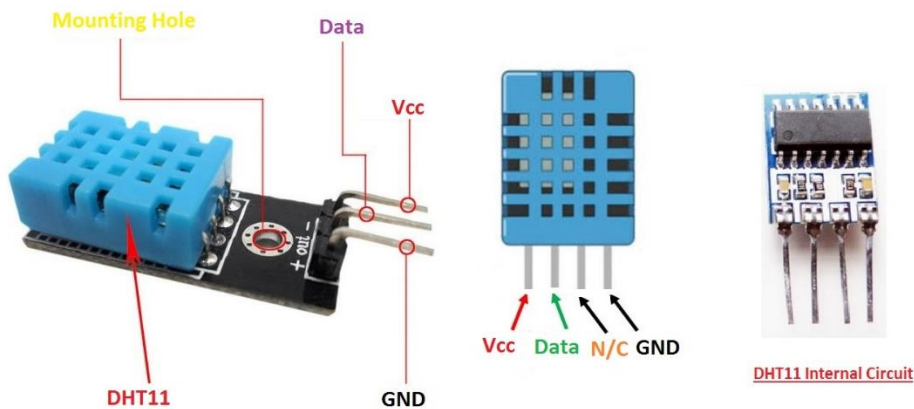


Figure 4. 9 Illustrate the DHT sensor diagram connects to Arduino.

4.2.7 Current Sensor

The ACS712 Current Sensor is used in this study to measure the flow of current. The sensor will be used to find out how much current is going through the conductor and figure out how much it is, without having an effect on the operation of the system. The sensor is made up of a linear Hall sensor. The Hall effect turns the magnetic field produced by the current passing through the sensor into a voltage

proportionate to the current. This lets the sensor produce a voltage that is related to the amount of current going through it.

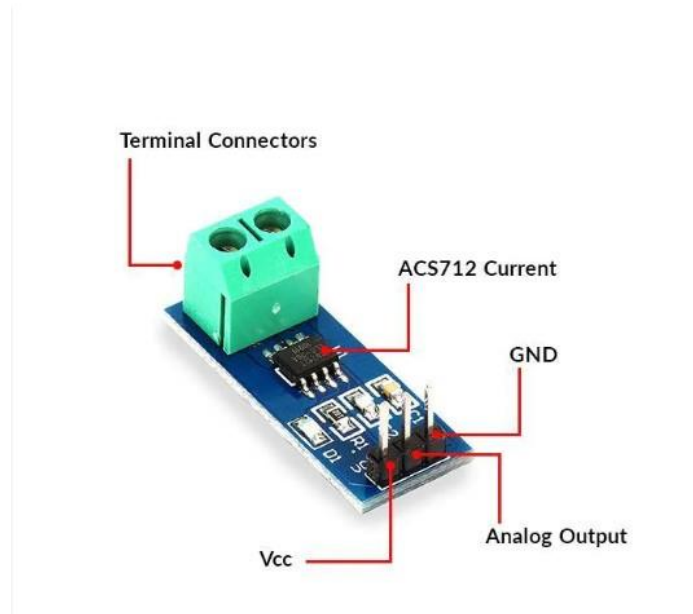


Figure 4. 10 ACS712 Current Sensor

4.2.8 Voltage Sensor

SEN32 REV1. 1 sensor model is perfect for measuring both AC and DC voltage. It measures voltages up to 50 volts AC or DC with high precision and consistency.

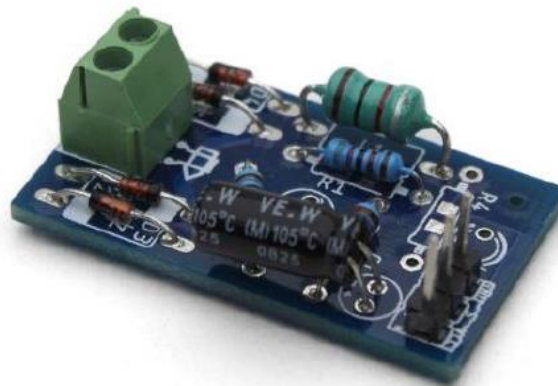


Figure 4. 11 SEN32 REV1.1 voltage sensor.

Both voltage and current are calibrated using comparison data collected with a multimeter.

4.2.9 Data Logger

The data logger is designed to have 7-channels for temperature sensors, 2-channels for voltage sensors, 2-channels power, and 1-channel for flow rate recorder that are saved data and time to an SD card (year, month, day, hour, minute). The size of the memory card is 32 GB. As mentioned above, the temperature sensors measured the temperature of the surface of the PV panels, the water in and out, and the ambient temperature. Meanwhile, the voltage, current and power are measured for both PV panels with cooling and without cooling. And finally, the water flow rate was measured and recorded based on the same data recorded (year, month, day, hour, minute).

4.2.10 Solar Power Meter.

The solar power meter (Pyranometer) is used to measure the amount of power that comes from the sun (beam, diffuse, and reflected). The DBTU1300 portable device is used to measure the intense solar radiation on the solar system. Solar power is shown on a digit LCD in W/m^2 or Btu/ft^2 depending on the unit of measurement.

Table 4. 3 Details of the solar power meter

Measuring range	0 - 2000 W/m^2
Precision in angles	<5% for angle <60°
Operating temperature and humidity	0 °C -50 °C, and 0% - 80% RH.



Figure 4. 12 Illustrate DBTU1300 solar power meter.

4.2.11 MPPT Solar Charge Controller

MPPT (Maximum Power Point Tracking) Solar charge controller is mostly a DC-DC converter that control the DC voltage from the solar panel and use it in the battery charger. The solar charge controller maintains optimum levels of voltage and current. PV systems and batteries are linked by MPPT. For this experiment, the kind of the MPPT solar charge controller is MAXMA. The circuit diagram of the MPPT solar charge controller is illustrated in Figure 4.13.

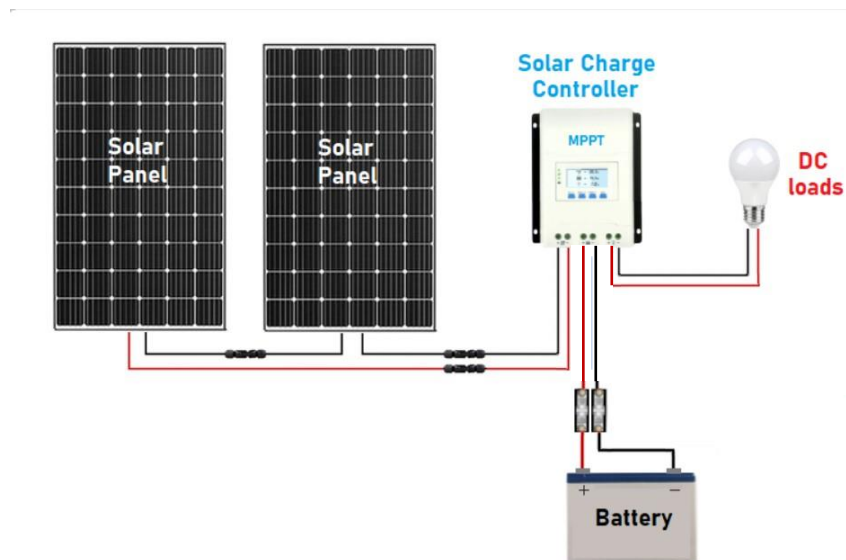


Figure 4. 13 circuit diagram of the MPPT solar charge controller.



Figure 4. 14 Illustrate MAXMA solar charge controller.

4.2.12 Procedure of The Experiment

The back-side water cooling with forced circulation method for cooling the PV collector is described as follows:

1. In the first step, Turn the power on, enabling the datalogger to function. Once that is done, both the input and output pumps will begin operating automatically. All the sensors are connected to a datalogger (Arduino device).
2. Adjust the water flow rate through water ball valve.
3. The solar power meter device start measuring the solar radiation based on the installed direction of the Panel. The data was taken every 15 min manually.
4. The LCD digital display shows and records the measured parameter such as temperatures of the environment, the non-cooled photovoltaic panel and the cooled photovoltaic panel in addition to the inlet and outlet temperature of the circulated water from the PV panel.
5. The power and the voltage are recorded using the LCD digital monitor. The data are measured for both panels.

6. All the data are recorded and measured in every five min intervals then the measuring data are saved to external hard drive.



Figure 4. 15 Display LCD digital.

4.3 Equipment's Calibration and Uncertainty.

Different instruments have been used to measure volume flow rate, solar radiation, water and ambient temperatures, voltage, and current of the PV panels. Different type of errors, may be considered either randomly or systematically. An uncertainty study has the potential to reduce random errors, while good calibration has the ability to remove systematic errors (Aldihani, 2017).

4.3.1 Calibration of Volume Flow Rate

A glass beaker and a stopwatch are used to calibrate the YF-s201 water flow meter. The stopwatch has been used to measure how long it took to fill the glass beaker

with water. Different flow rate readings from (1–6 l/min) had been obtained, and the flow rate was determined by using equation 4.1 (Moaveni, 2008). Calibrating the flow meter (YF-s201) is depicted in Figure 4.16.

$$\text{mass flow rate} = \frac{\text{collected volume (litter)}}{\text{time (min)}} \quad (4.1)$$

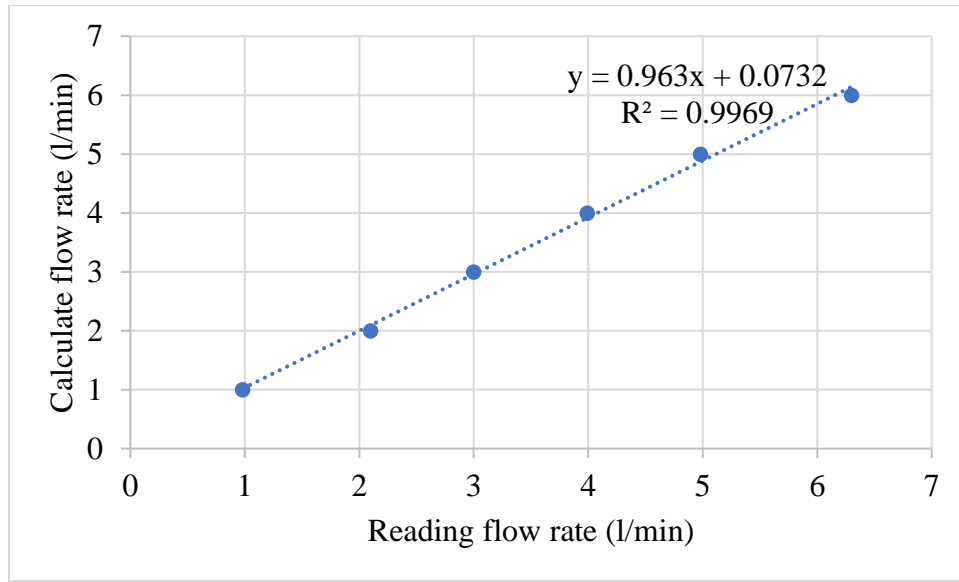


Figure 4. 16 Calibrating between calculation flow rate and reading flow rate.

4.3.2 Calibration K-Type Thermocouple

To obtain the most accurate temperature reading, the K-type thermocouple should be calibrated. The K-type thermocouple was calibrated by a comparison of the recorded values with the thermometer, first by putting it into ice water and recording a temperature of 0°C, and then by heating the water in the electric kettle to a range of 0 to 100°C and recording the temperature between this range. The relationship between a T-type thermocouple reading and a thermometer reading is demonstrated in Figure 4.17. The thermocouple calibration is presented in Appendix (B).

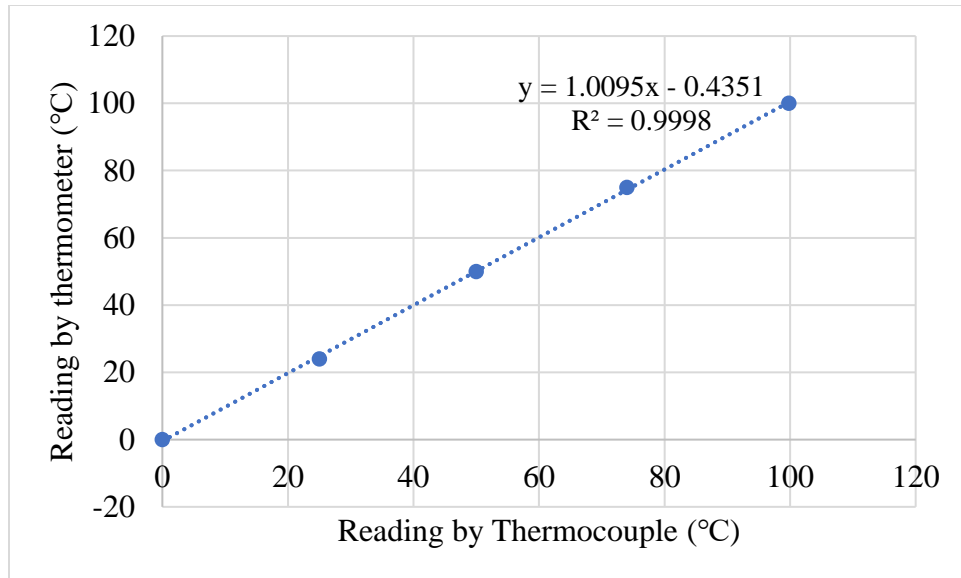


Figure 4. 17 Calibration between reading by K-type thermocouple and thermometer.

4.3.3 Calibration of The Solar Power Meter

The DBTU1300 solar power meter was calibrated with the SM206-SOLAR solar power meter. Both solar power meters were put in the same place, and the readings from each instrument were compared, as demonstrated in Table 4.4.

Table 4. 4 Calibration of DBTU1300 solar power meter

Reading by DBTU1300 solar power meter	Reading by SM206-SOLAR solar power meter
1069	1076
1075	1076
1073	1078

4.3.4 Uncertainty

The following equation can be used to estimate the level of uncertainty (Dieck and Sensor Handbook, 1999, and Bell, 2001 p.13).

$$\text{Uncertainty (u)} = \sqrt{\frac{\sum_{i=1}^n (x_i - \bar{x})^2}{N * (N-1)}} \quad (4.2)$$

where N is the number of readings, \bar{x} is the average value of all the readings taken for the X variable, the result of the ith measurement is represented by x_i .

Table 4.5 illustrates calculation of the uncertainty of all equipment used in the experiment.

Table 4. 5 Uncertainty equipment results

Instruments	Uncertainty
Flow meter	± 0.03
K type thermocouple	± 0.08
DHT sensor	± 0.08
Voltage	± 0.05
Power	± 0.09

CHAPTER FIVE

RESULTS AND DISCUSSION

5.1 Introduction

This chapter presents the findings from the analysis of experimental and numerical data obtained through Computational Fluid Dynamics (CFD). The first section focuses on the experimental results, which were collected during summer of 2022. The data collected provided insight into the impact of solar irradiance on both the temperature and performance of the PV system, both electrically and thermally. The prototype was installed at Erbil Polytechnic University's Research Center in Erbil-Iraq, located at latitude $36.191188^{\circ}\text{N}$ and longitude $44.009189^{\circ}\text{E}$. In the second section, the numerical model validation is presented first based on the experimental results of a photovoltaic panel. While, in the last section a comprehensive numerical study is analyzed to discover the effect of using water cooling chamber on the PV system.

5.2 Solar Radiation

Based on eqs. 3.6 to 3.15, we determine the average solar radiation for all months in Erbil city, as shown in figure 5.1. December's average solar radiation is $4.22 \text{ kWh/m}^2/\text{day}$, whereas June's average solar irradiation is $7.41 \text{ kWh/m}^2/\text{day}$. The average solar irradiation is seen as being at a low level during the winter months and at a high level during the summer months. The reason for collecting all the data

during the summer months was that Erbil recorded the highest solar radiation and high ambient temperature.

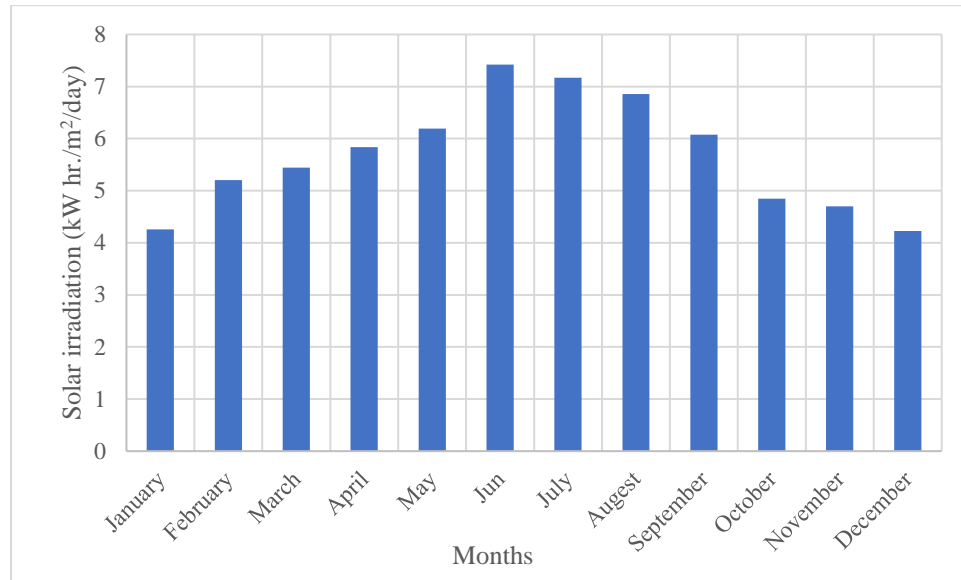


Figure 5. 1 Average monthly solar irradiation

5.2 Experimental Result

The primary objective of this section is to present the outcomes of the experimental prototype of a cooling system integrated with a photovoltaic (PV) panel. Both PV and PV/T models were utilized in the analysis of experimental performance. The study focused on the impact of ambient temperature, sunlight intensity, and cooling water flow rate. The experimental results demonstrated how the design of the water-cooling chamber influenced the electrical and thermal efficiency of the PV module. The tilt angle for the PV panel was calculated monthly using equation 3.6 for Erbil city, and the average tilt angle was used during the installation for a year.

Table 5. 1 Monthly tilt angle

Months	Tilt angle (β)
January	56.86°
February	49.02°
March	37.79°
April	25.98°
May	16.93°
Jun	13.02°
July	15.51°
August	23.56°
September	35°
October	46.76°
November	55.81°
December	58.58°
Average	36.2°

5.2.1 Ambient Temperature and Solar Radiation

Figure 5.2, displays the outside air temperature recorded over the summer months (July and August). Based on this data, the average daily temperature for the month of July begins at 40°C on July 3rd and gradually increases until it reaches its highest value of 46°C on July 18th. The temperature then starts to drop after the 18th of the month.

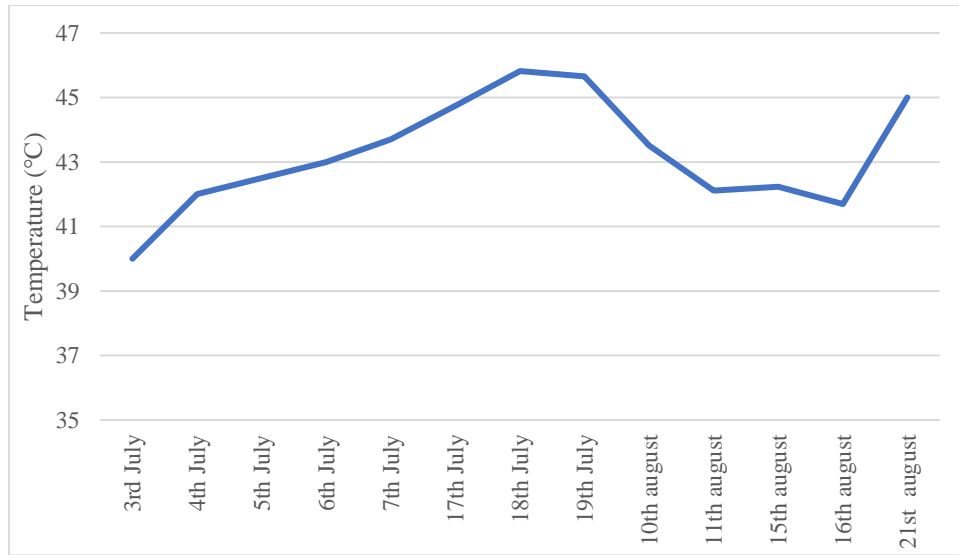


Figure 5. 2 Average daily ambient temperature (July and August).

The outdoor temperature for August begins on the 10th with a reading of 43.5°C and drops to a record low of 41.7°C on the 16th of August. On August 21st, the temperature reached 45°C, which is the highest reading recorded for this month.

The monthly average of solar irradiance for July and August is shown in Figure 5.3. The solar irradiance exposure is relatively constant throughout the month, which begins on July 3rd, when solar irradiance is 813 W/m², and end on July 19th, when it is 819 W/m². The solar irradiance value of 848 W/m² was recorded on July 4th, and this value is considered the month's highest value. In August, the records of solar irradiance showed a slight difference during the days, and the highest irradiance was observed on August 16th. This was due to the sky being clear that day.

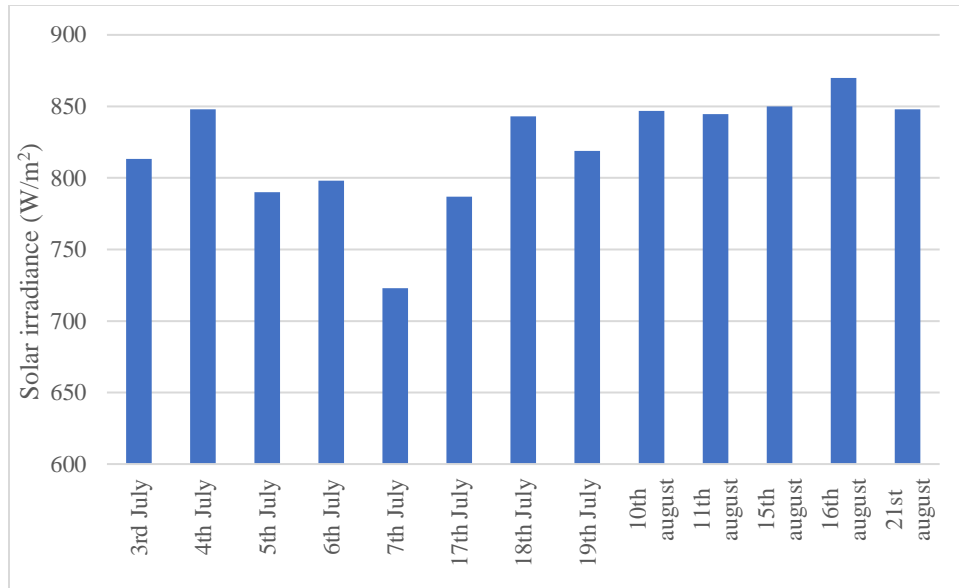


Figure 5. 3 Average daily solar radiation (July and August).

Figures 5.4 and 5.5 illustrate the solar irradiance during the day that was present on the 4th of July and the 16th of August, respectively. Figure 5.4 shows that at 8:00 AM., the daily measurements of solar irradiance began at 410 W and increased gradually until it reached the maximum value at 13:00 of 1026 W/m². Then the solar irradiance decrease to 714 W/m² at 15:00.

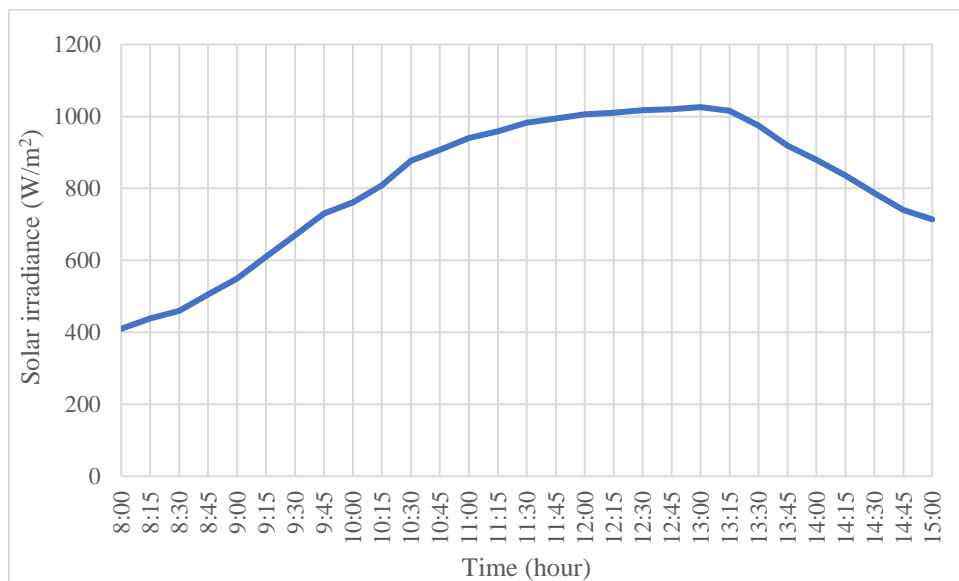


Figure 5. 4 Global Solar radiation during the day (July 4th)

The graph in Figure 5.5 shows solar irradiance starting at 8:00 in the morning with a value of 442 W/m² and progressively increasing until it reaches the maximum value of 1068 W/m² at 13:00. The sun decline to 800 W/m² at 15:00.

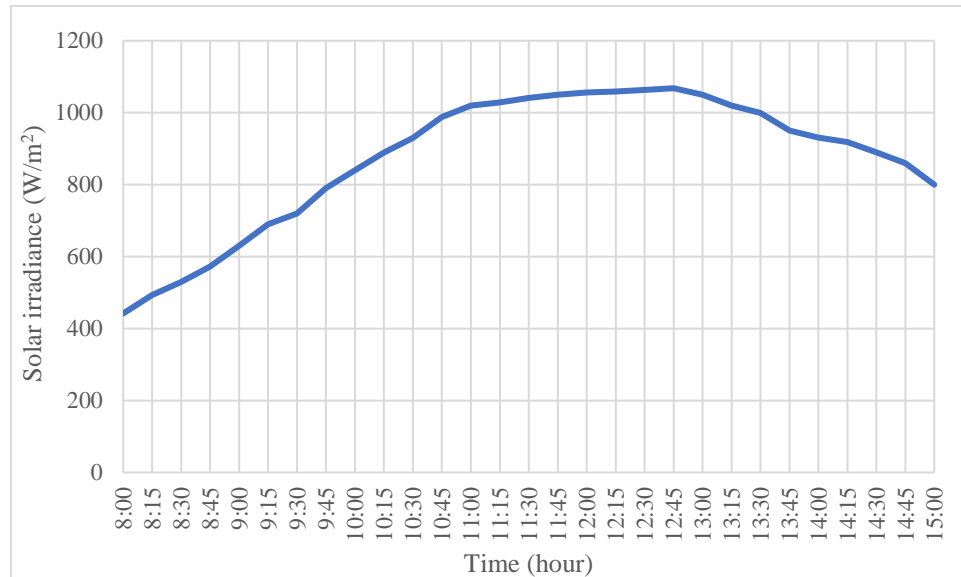


Figure 5. 5 Global Solar radiation during the day (August 16th)

The findings presented in both figures illustrate daily solar irradiance throughout July and August. The irradiation recorded its highest value at 13:00. As a result, the panel temperature increased with the increase in solar irradiance intensity, as shown in Figure 5.6 and 5.7.

5.2.2 Photovoltaic Panel's Temperature

The surface temperature of the PV panel as well as the surrounding air temperature are displayed in Figure 5.6. The surface temperature of the panel started with 48°C, and the temperature increased through the day, because the solar radiance increased

also the ambient temperature increased during the day. The highest surface temperature of 66.28°C recorded at 1:00 PM.

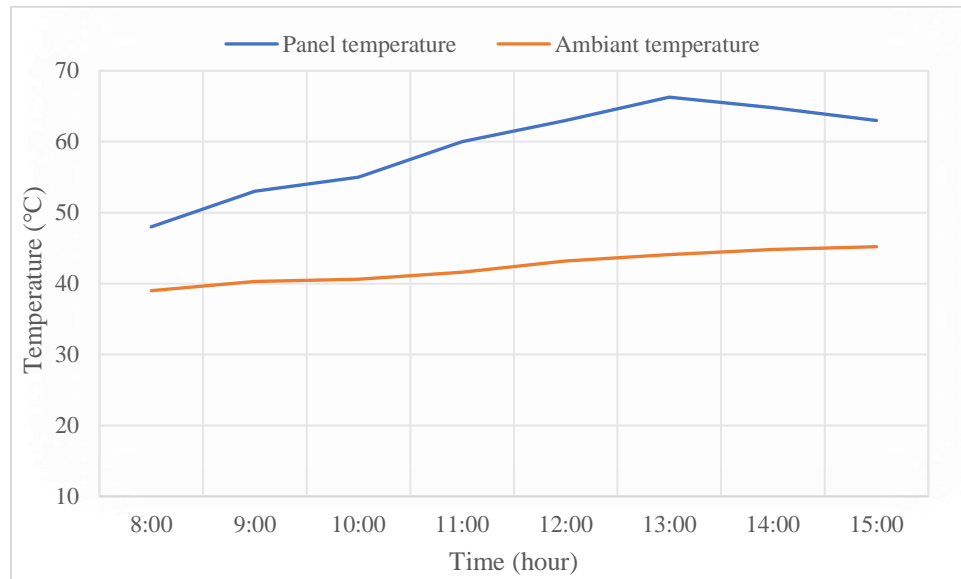


Figure 5. 6 The surface temperature of the PV panel and the ambient temperature on (July 4th).

Figure 5.7 depicts the water-cooling chamber affixed to the back of the PV panel. Water experiences the high heat transfer rate, leading to a lower back surface temperature. On July 4th, the flow rate of water into the chamber was set at 2.5 l/min. The panel surface temperature was 48°C without cooling, and dropped to 34°C with cooling due to low solar radiation and ambient temperature during that day. This resulted in a temperature reduction of 28.9%. While, in figure 5.14 the panel's surface temperature without cooling was 66°C , which reduced to 41°C with water cooling at 1 PM. This indicates that cooling can reduce the temperature by 37.8%. The drop in temperature of the PV panel boosted its output power.

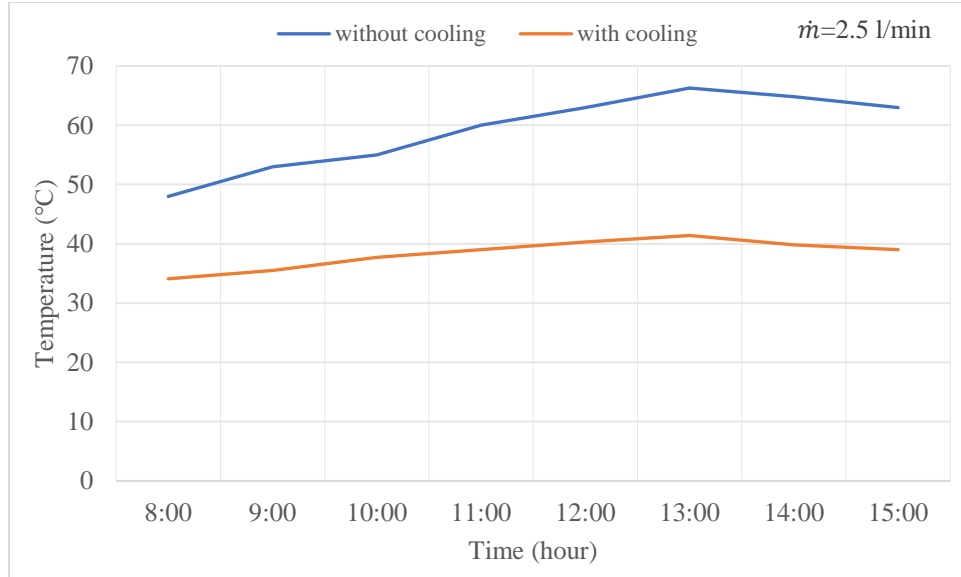


Figure 5. 7 The surface temperature of the PV panel with and without cooling on (July 4th).

When employing 3.5 l/min of water flow rate at 8:00 AM on July 3rd, the reduction temperature is 29.5%; it then rises significantly to 49.7% until 1:00 PM, as illustrated in Figure 5.8. The amount of temperature reduction is proportional to the water volume flow rate. The higher the flow rate, the higher the temperature reduction.

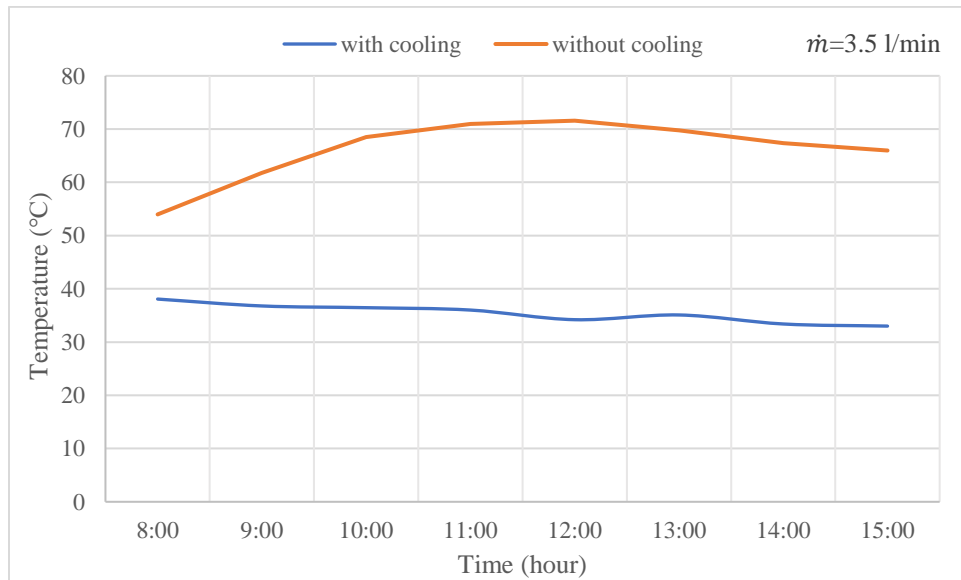


Figure 5. 8 The surface temperatures of both PV panels on (July 3rd).

In Figure 5.9, the impact of different volume flow rates on the temperature of a photovoltaic panel is demonstrated. A water cooling system with a flow rate of 3.5 l/min produced a significant reduction in the average back surface temperature of the PV panel. The average temperature drop percentages for the PV panel were 32.8%, 34.4%, 36.5%, 41.6%, and 46% for 1.5, 2, 2.5, 3, and 3.5 l/min, respectively. The study found that the temperature of the panel decreases with an increase in the water flow rate, as the heat transfer rate increases.

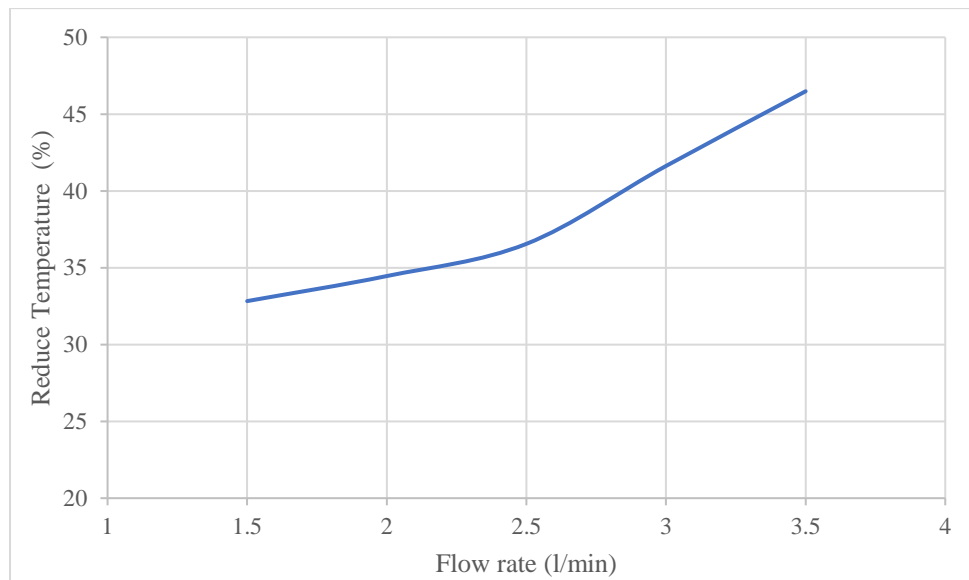


Figure 5. 9 The temperature of the collector's backside at different water volume flow rates.

Figure 5.10, the variation in cooling water temperature between the inlet and outlet is depicted. It is evident that an increase in water flow rate leads to a reduction in temperature difference. When the water flow rate is low and has the same heat rate, the volume of water passing through the chamber section per minute is smaller. Consequently, water molecules heat up faster. At the conclusion of the experiment, the highest and lowest temperatures observed for 1 and 3.5 l PM were 3.19 °C and 2.13°C, respectively.

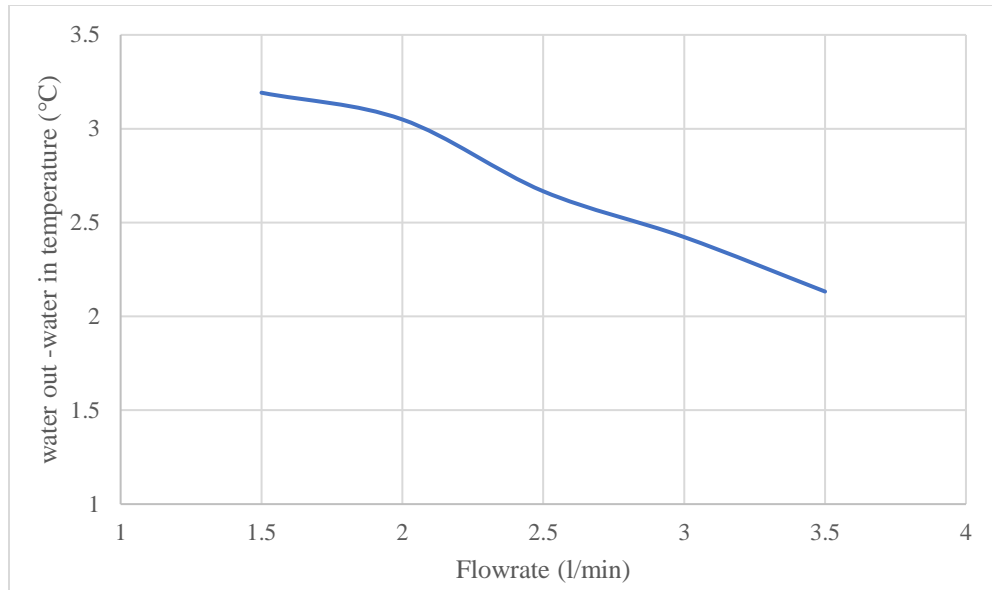


Figure 5. 10 The temperature difference between out and in of the water.

The effect that different water volume flow rates have on the amount of heat that is transferred from the panel to the water is illustrated in Figure 5.11. The heat transfer rate increased with the increase in the volume flow rate since the velocity and turbulence were fluctuating. When the volume flow rates increase, it indicates that the velocity is also higher, which in turn results in the highest heat transfer coefficient and, thus, an enhanced heat transfer rate. The minimum heat transfer rate recorded was 340.18 W at 1 PM, while the highest rate was 530 W at 3.5 l PM.

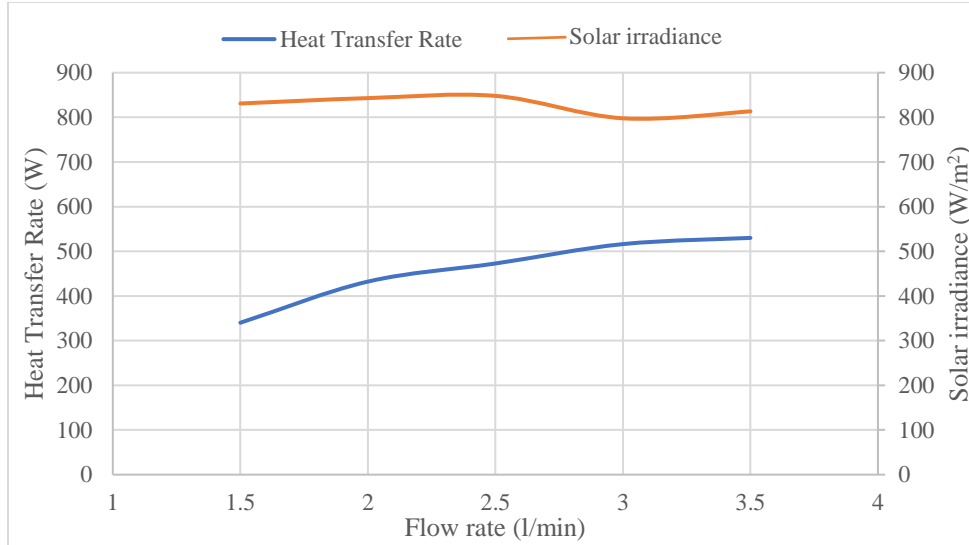


Figure 5. 11 Heat transfer rate of the cooling system and total solar irradiance.

Figure 5.12 illustrates the thermal efficiency under various volume flow rates. The study revealed that there is a direct correlation between thermal efficiency and volume flow rates. At volume flow rates of 1.5, 2, 2.5, 3, and 3.5 l/min, the thermal efficiency was 49.6%, 62.2%, 67.5%, 78%, and 79%, respectively. As water has a higher specific heat, it can absorb more heat from the PV panel, resulting in an increase in thermal efficiency.

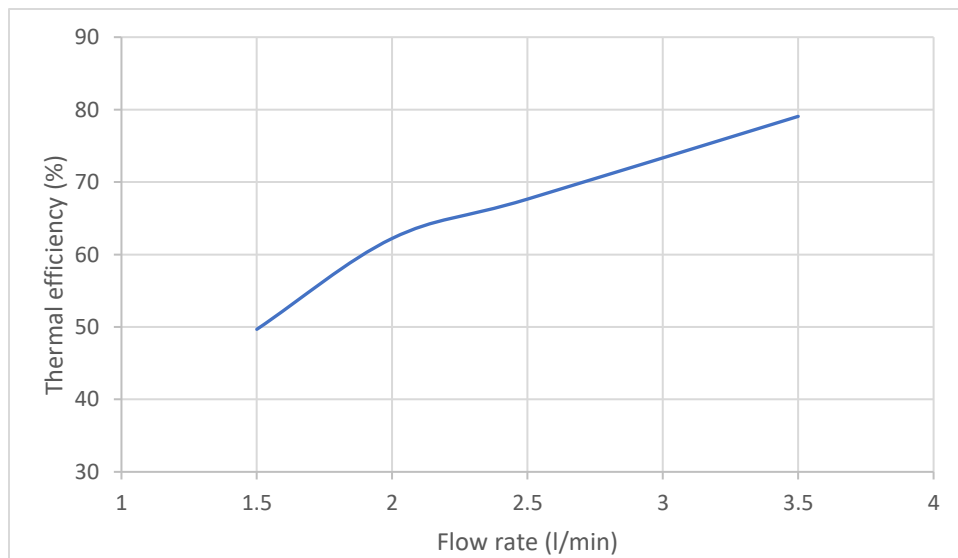


Figure 5. 12 Thermal efficiency at difference volume flow rate.

5.2.3 Performance Analysis

When the solar irradiance recorded high, the output of electrical power increased linearly. This is because the increase in sunlight causes both the current and the voltage of the PV to increase. The amount of solar irradiance and the amount of power produced are related in a straight line. As shown in Figure 5.13, both voltage and power are increased as a result of the increase in solar radiation. When the solar irradiance records 500 W/m^2 , the PV power produces 85 W of power and 22.5 V of voltage, while irradiance at 1000 W/m^2 results in the production of roughly 179.2 W of power and 23.7 V of voltage.

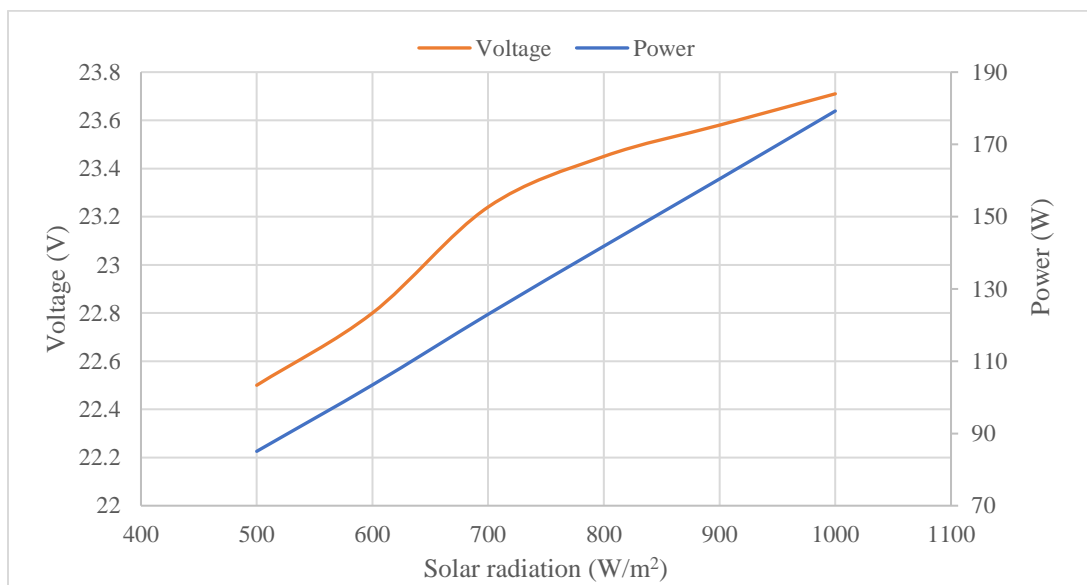


Figure 5. 13 Relation between solar irradiance with power and voltage.

The PV panel efficiency and power production are presented in the figures below. The electric power output is shown in Figure 5.14 for the selected day in July. On July 4th, the system ran with a cooling water of 2.5 l/min. The power output started in the morning at 80 watts without cooling and 100 watts with cooling. The noncooled PV panel's maximum output power was recorded at 161 W at noon. The

highest power produced by the water chamber cooling system is 188 W, while the highest power enhancement percentage is 13.7%.

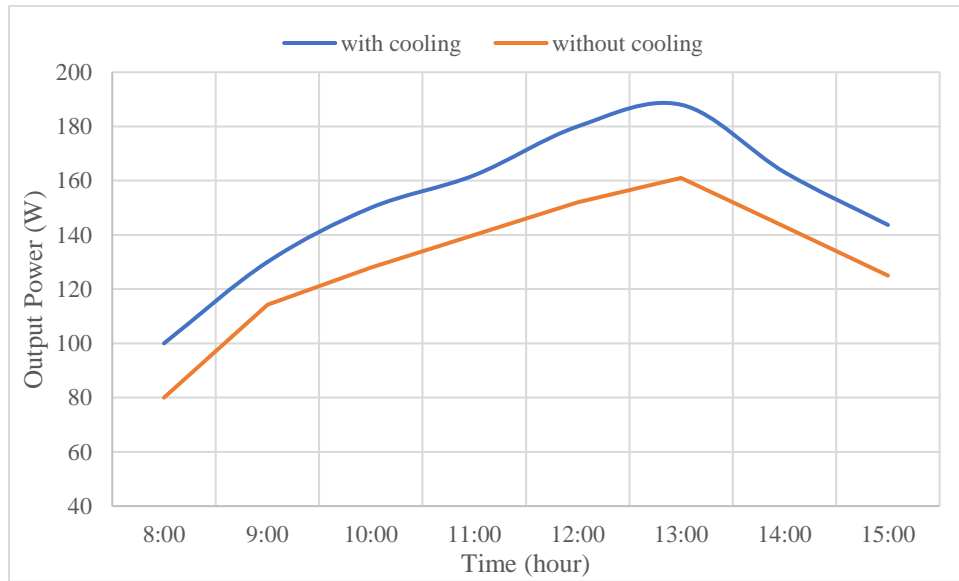


Figure 5. 14 Electrical power generated by a PV panels (July 4th)

Due to the fixed south-facing position of the panel, the amount of power produced decreased towards the end of the day when the solar irradiance was low. However, Figure 5.15 illustrates the improvement in power output with different water flow rates. The study demonstrated that an increase in the volume flow rate of water led to an increase in the output power of the cooling system. The application of flow rates of 1.5, 2, 2.5, 3, and 3.5 l/min resulted in an average increase in the amount of power produced by 10.42%, 11.87%, 13.77%, 18.09%, and 19.72%, respectively.

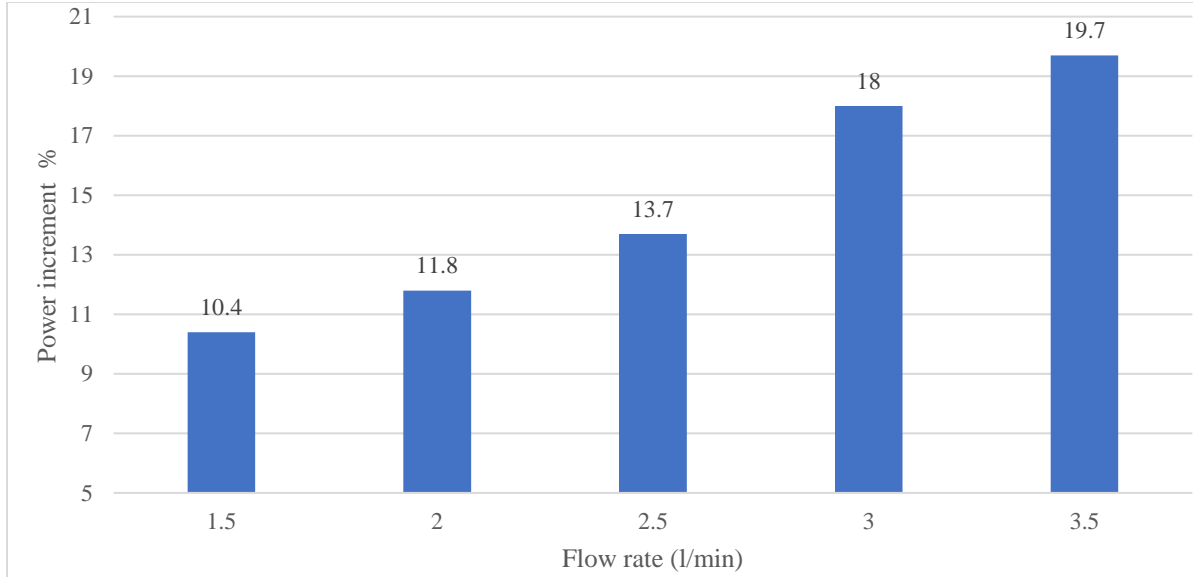


Figure 5. 15 Rate of power at a different water flow rate for July

On July 4th, the electrical efficiency was calculated and analyzed, as shown in Figure 5.16. With the increase in solar irradiance intensity, the PV panel surface temperature increases. Electrical efficiency is measured at its highest level at 8 a.m. because at this time the solar intensity is low. The minimum electrical efficiency values recorded were 19.1% and 22.3% for without cooling and with cooling, respectively. The findings revealed that the average electrical efficiency with and without the cooling system was 24.19% and 20.92%, respectively. According to the findings, the electrical efficiency of the proposed cooling system is 13.7% better than the electrical efficiency of the PV panel without cooling.

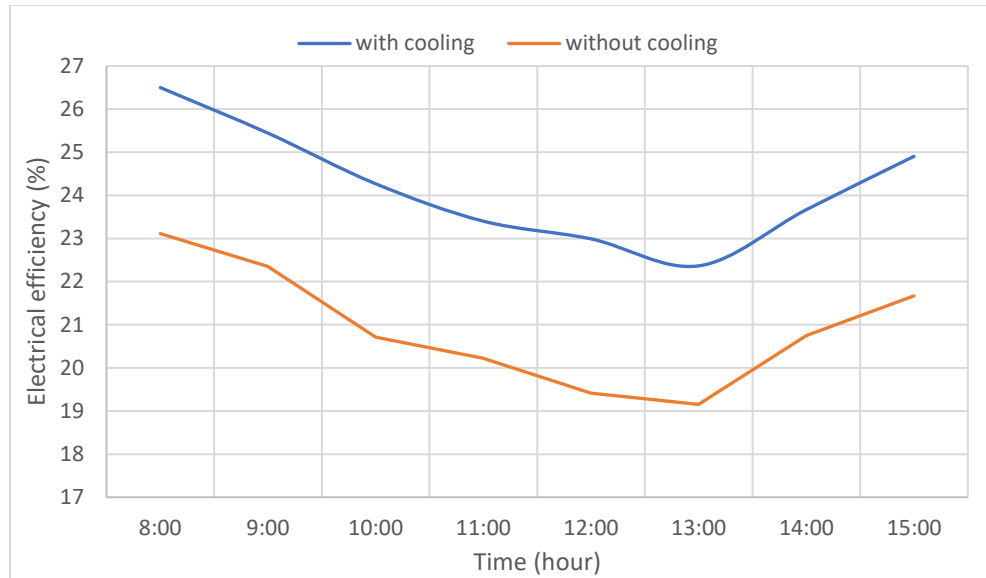


Figure 5. 16 PV panel electrical efficiency during the day on (July 4th)

The electrical efficiency of the PV panels on August 4th is demonstrated in Figure 5.17. Maximum electrical efficiency is observed in the morning and subsequently declines during midday. The average amounts of electricity without a cooling system and with a cooling system are 21.2% and 23.94%, respectively. On August 4th, the overall electrical efficiency had seen an 11.44% improvement.

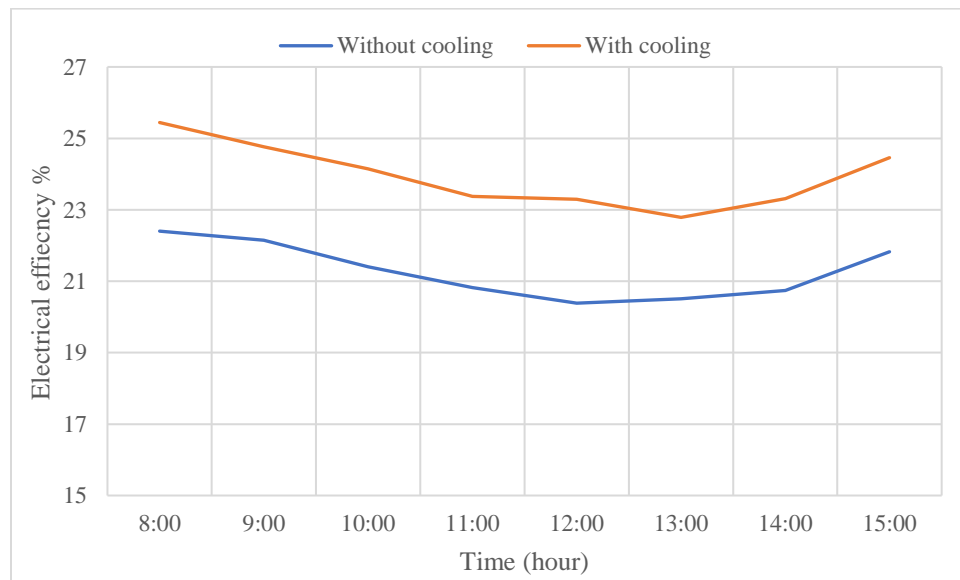


Figure 5. 17 PV panel electrical efficiency during the day on (August 16th)

In figures 5.16 and 5.17, the electrical efficiency is determined at low level. Based on eq. 3.1, the solar irradiance and electrical efficiency have an inversely proportional relationship.

5.2.4 A Comparative Study of The Results

Previous studies, such as those by (Bahaidarah et al., 2013), found that putting a water-cooling heat exchanger on the back of the cell lowered the temperature of the cell by 20%, and electrical efficiency increased by 9%. And according to (Fakouriyan et al., 2019), the experimental study's design container was direct water cooling at the backside of the photovoltaic panels. The raise in electrical efficiency was 12.3%. Another study of the PV panel was placed on the back side of the water-cooling chamber, and the electrical efficiency with and without cooling was 10% and 9.17%, respectively (Mohammed et al., 2019). (Muslim et al., 2020), studied the water-cooling chamber which was connected to the rear side of the photovoltaic panel using three different flow angles: 60, 30, and 0 at 4 l/min. There was a 17%, 13.6%, and 15.3% increase in electrical efficiency, respectively. Figure 5.18 compares the PV/T system performance achieved in this experiment to that of previous studies.

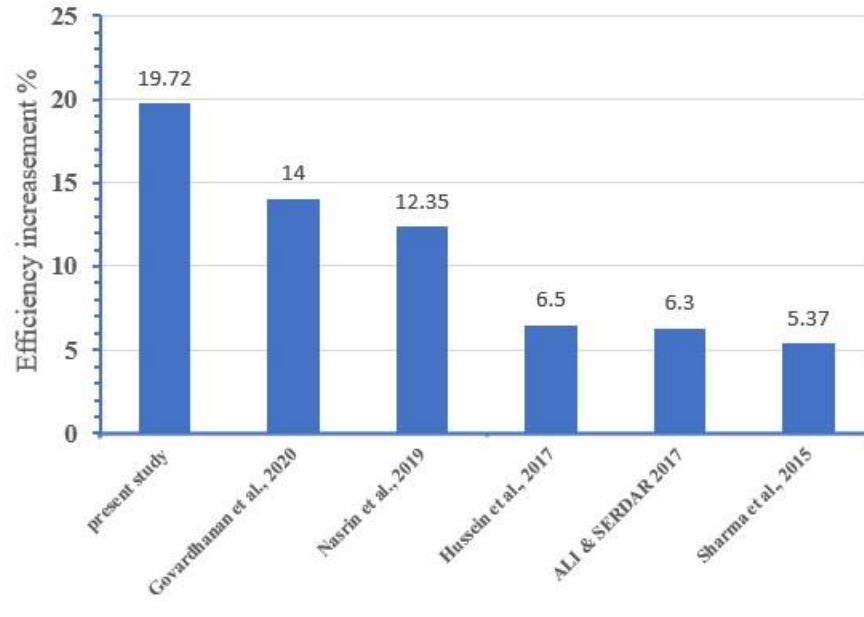


Figure 5. 18 The comparison between the current investigation and the earlier suggested designs for water cooling.

The conclusions from this study, when compared to the earlier studies mentioned above, show that the proposed strategy in this research improves a PV's performance by 19.72%. In this study, the efficiency of the module improved by using new back side water cooling chamber design while the previous studies showed less improvement in the overall efficiency

5.3 Simulation Results

5.3.1 Verification of Simulation Results with The Experimental Setup

An ANSYS simulation program was developed to analyze numerically the case study, which was implemented experimentally during the summer months. The experimental prototype of a PV system was installed in the Research Center at Erbil Polytechnic University, Erbil, Iraq. The photovoltaics, tank, and pumps are the main components of this system. In addition, the system is linked to a data logger for saving data in real-time. The average yearly tilt angle for Erbil City is 36°. Through

simulating with ANSYS-CFD, the results can show the temperature distribution on the photovoltaic panel with a water cooling chamber. The simulation boundary condition was designed based on the location of Erbil city (latitude 36.191 and longitude 44.009). Also, the simulation program set the weather conditions that were present during the experiment on July 18th as well.

The temperature of the PV cells with water a cooling chamber is demonstrated in Figure 5.19. This figure shows a comparison between the results of experiments and the CFD at different levels of solar irradiance. When the solar irradiance was 550 W/m², the cell temperature for both the experimental and ANSYS results was 35.8°C and 34.8°C, respectively. At 1000 W/m² of solar irradiance, the surface temperature of the glass was recorded as 36.9°C for the experiment and 36.3°C for the ANSYS results.

The outlet water temperature at different levels of solar irradiance is illustrated in Figure 5.20. At the solar irradiance of 730 W/m², the outlet water temperature was 35.6°C and 34.1°C for experimental and ANSYS results, respectively. Under 1000 W/m² of sunlight irradiance, the output water temperature was 37.2°C in the experiments and 37°C with ANSYS. From the results mentioned above, there is good agreement between the experiment and simulation results.

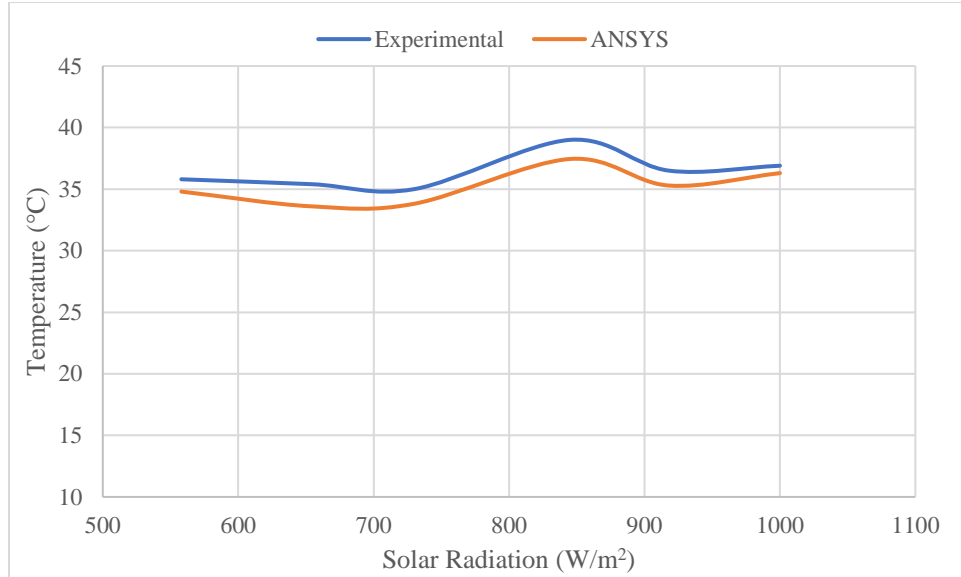


Figure 5. 19 Surface temperature at difference solar irradiance at flow rate (2 l/min).

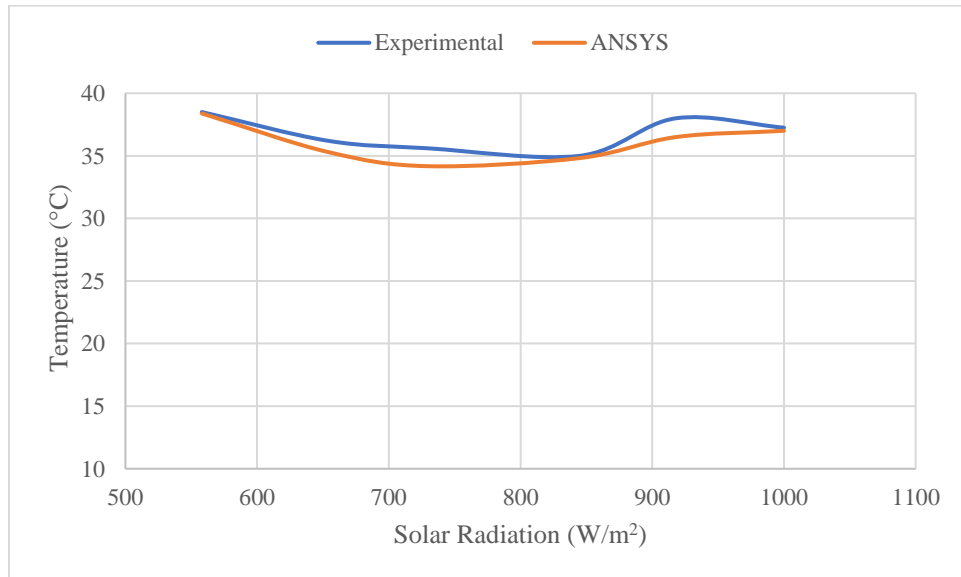


Figure 5. 20 Outlet water temperature at difference solar irradiance at flow rate (2 l/min).

5.3.2 Test for Mesh Independence

Taking data from the experimental setup as shown in Table 5.2. ANSYS Fluent 2019 R2 was used to mesh the model; depending on the number of elements and nodes, the solution's precision varies. In this section, four different studies were

verified, each with a different element size, as shown in Table 5.3. Case 1 element size is 3 mm, the glass temperature was 37.75°C, and the outlet water temperature was 37.27°C. while in case 2, the element size is 4 mm, the glass temperature was 37.79°C, and the output water temperature was 37.67°C. In Cases 3 and 4, the element sizes are 6 and 8 mm, respectively, and the glass temperatures were 37.72°C and 37.62°C, and the outlet temperatures were 37.28°C and 36.45°C. Case 2 was picked because the glass and outlet water temperatures in Case 2 were nearly identical to the experimental result.

Table 5. 2 Experimental data

Experimental data when solar irradiance is 810 W/m ² , water volume flow rate 1.5 l/min, and inlet water temperature is 34.75°C	Temperature of the Glass (°C)	Temperature of the water outlet (°C)
	38.64	37.9

Table 5. 3 Test for mesh independence.

Cases	Element size (mm)	Elements	Nodes	Temperature of the Glass (°C)	Temperature of the water outlet (°C)
1	3	792000	870972	37.75	37.27
2	4	364500	409360	37.79	37.67
3	6	144000	164619	37.72	37.28
4	8	71400	83352	37.62	36.45

5.3.3. Thermal Analysis

Figure 5.21 presents the glass surface temperature at varying solar irradiance levels. Solar irradiance and glass surfaces have a direct relationship. for the reason that when the intensity of the solar radiation is high, which causes the ambient temperature to increase and the surface temperature of the PV panel also increases.

For 600, 800, and 1000 W/m² of solar irradiance, the glass surface temperature is 36°C, 46.1°C, and 55.3°C, respectively.

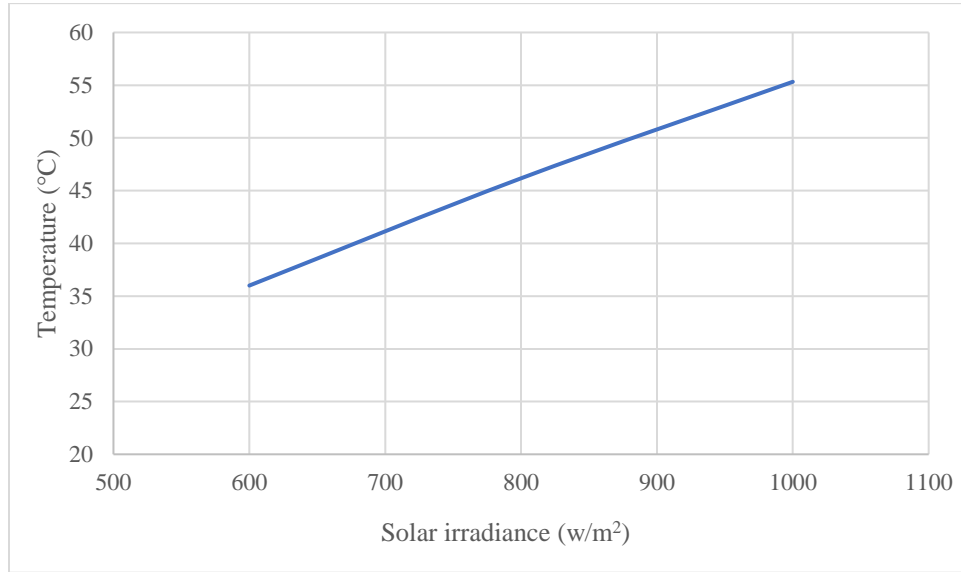


Figure 5. 21 Glass surface temperature without water cooling.

In Figure 5.22, the variation of photovoltaic panel temperature is demonstrated with different inlet cooling water temperatures and volume flow rates. The panel's temperature was measured at 34.7°C, 32.7°C, 31.9°C, 31.2°C, and 30.8°C for flow rates of 0.5, 1, 1.5, 2.5, and 3.5 l/min, respectively, when the inlet water temperature was 25°C. Moreover, the temperature of the panel surface was significantly influenced by the inlet water temperature. As the inlet water temperature decreased, the heat transfer rate increased due to the increased temperature difference between the water and the PV panel, resulting in the cooling fluid absorbing more heat from the panel. This relationship was found to be linear. Furthermore, when the volume flow rate was 2.5 l/min and the inlet water temperatures were 20°C, 25°C, and 30°C, the PV panel temperatures were 28.4°C, 31.2°C, and 34.5°C, respectively.

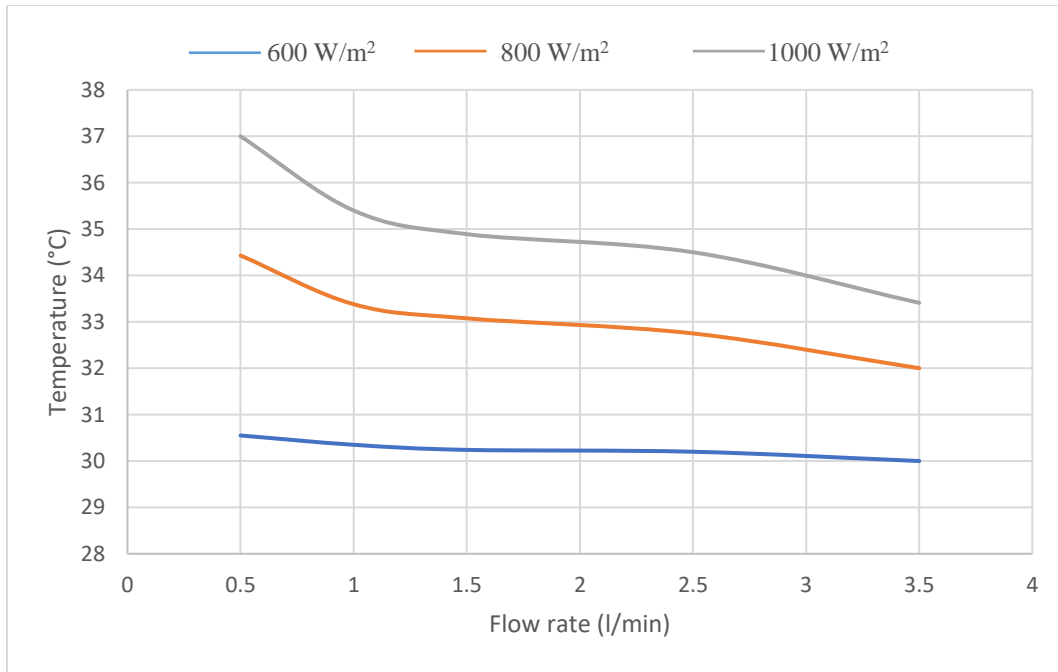


Figure 5. 22 Panel surface temperature at solar irradiance (1000 W/m²)

Figures 5.23, 5.24, and 5.25 show a comparison of the temperature of a PV panel at 20, 25, and 30°C water cooling temperatures at different solar irradiance and water flow rates. From the results, the glass temperature decreased with the increased cooling water flow rate, because of increasing in the heat transfer rate. Also, the figures demonstrate the effect of different solar irradiance on the photovoltaic panel's front surface.

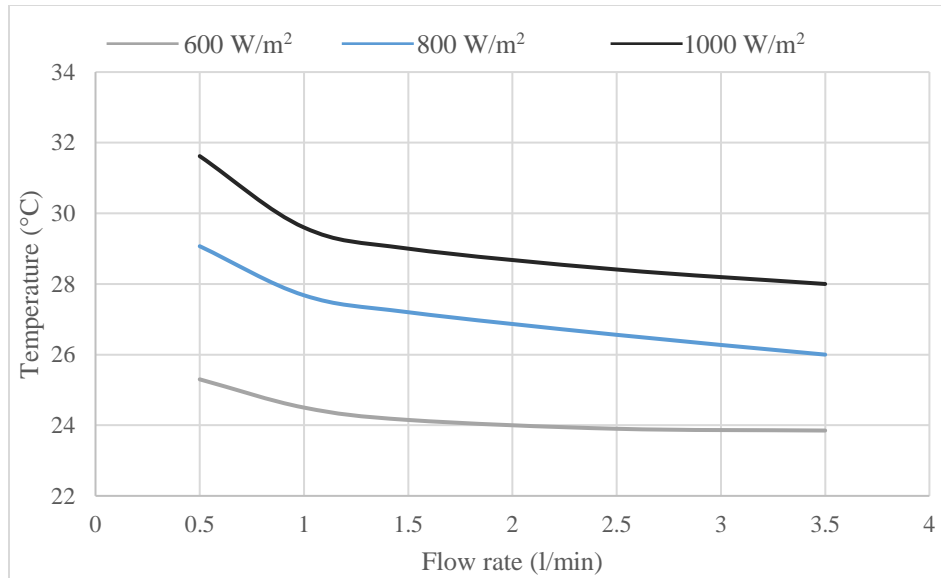


Figure 5. 23 Panel surface temperature at inlet water temperature (20°C)

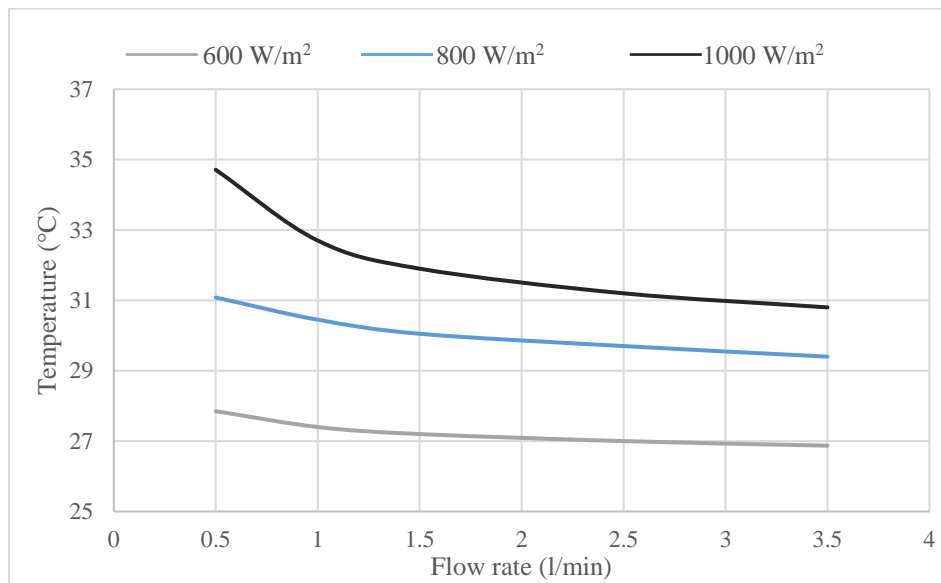


Figure 5. 24 Panel surface temperature at inlet water temperature (25°C)

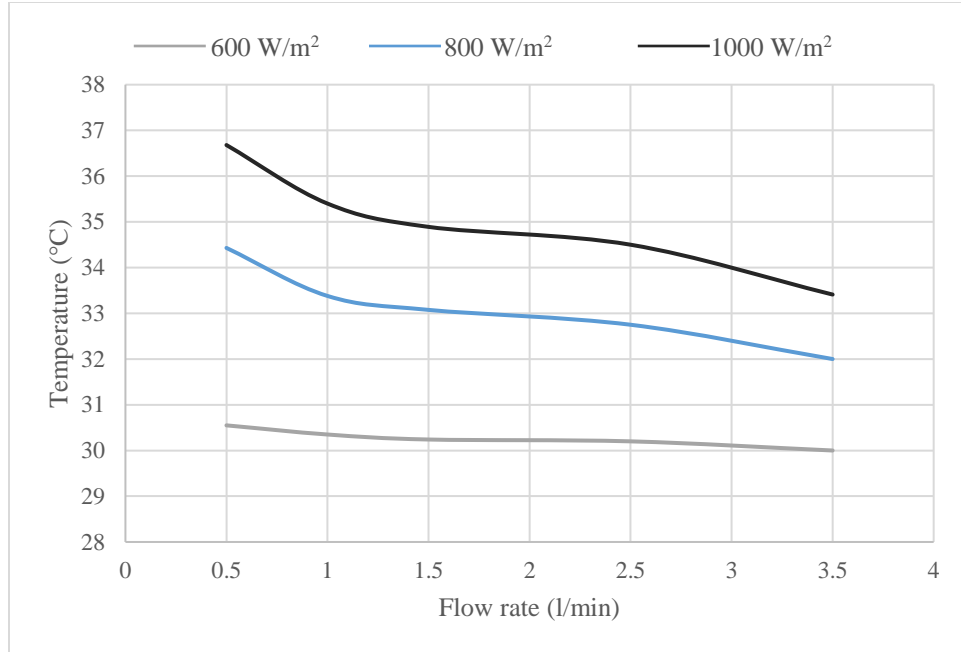


Figure 5. 25 Panel surface temperature at inlet water temperature (30°C)

Figure 5.26 describes the cooling water outlet temperature from the cooling chamber at different inlet temperatures at a nominal solar irradiance of 1000 W/m². The outlet water temperature increase with the increase in the inlet water temperature at the same flow rate. While increasing the flow rate of water cooling from 0.5 to 1.5 l/min, the outlet temperature decreases to 38.75°C and 33.8°C, respectively.

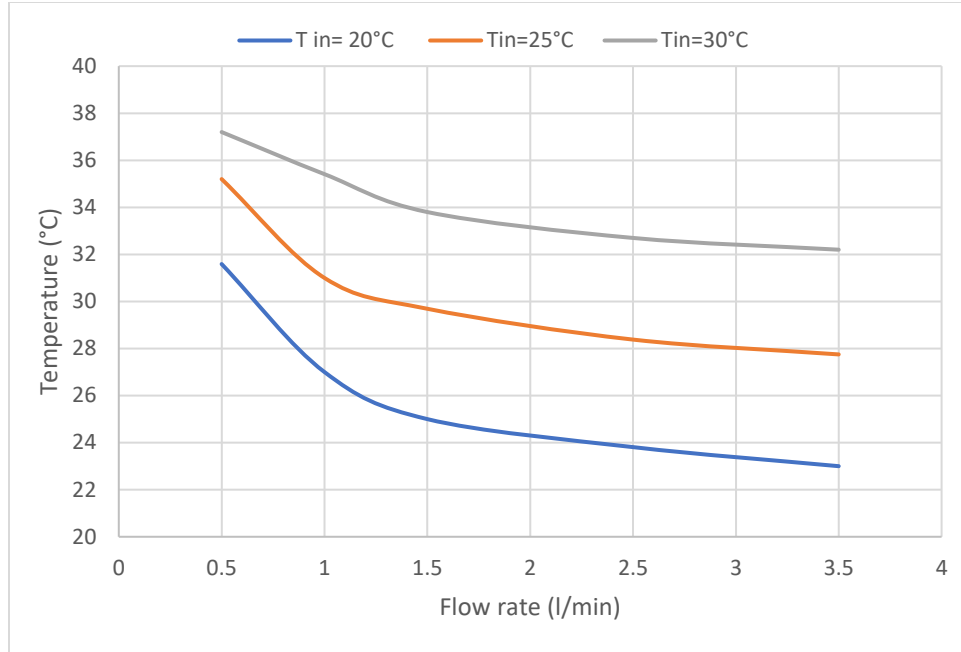


Figure 5. 26 Water outlet Temperature at solar irradiance (1000 W/m²)

While Figures 5.27, 5.28, and 5.29 illustrate the outlet water temperature at the base inlet at 20, 25, and 30°C for solar irradiance of 600, 800, and 1000 W/m². In this figure, it is shown that the outlet water temperature decreases with increasing water flow rate for each of the following solar irradiance: 600, 800, and 1000 W/m². From the figures, it can be seen that when the intensity of solar radiation is low, the outlet temperature changes little with increasing water flow rate because the temperature difference between the PV panel and water inlet is small. And in these figures, we see the reverse proportional relation between outlet temperature and water flow rate, because an increase in water flow rate for the same heat source will affect on the temperature difference between the outlet and inlet water temperature.

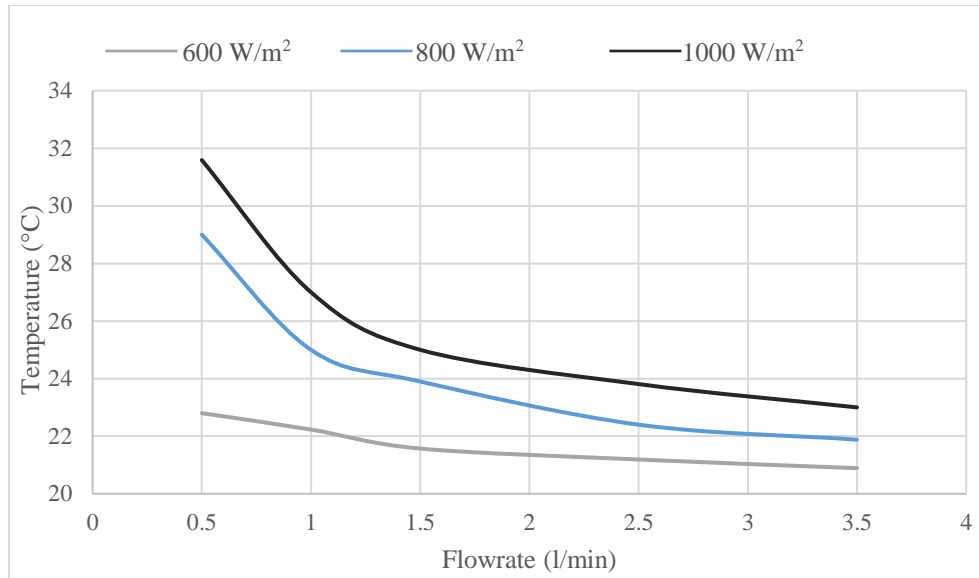


Figure 5. 27 Outlet water temperature at inlet water temperature (20°C)

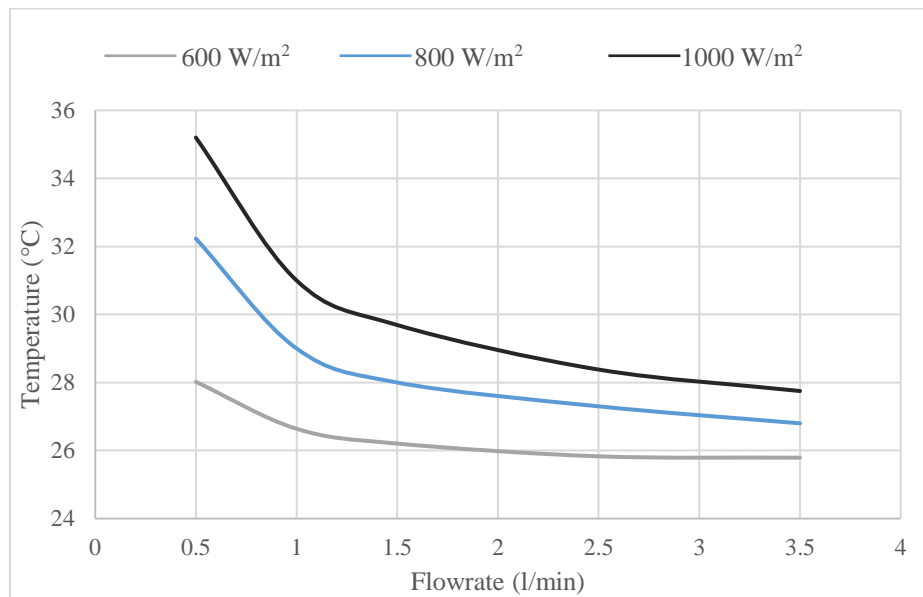


Figure 5. 28 Outlet water temperature at inlet water temperature (25°C)

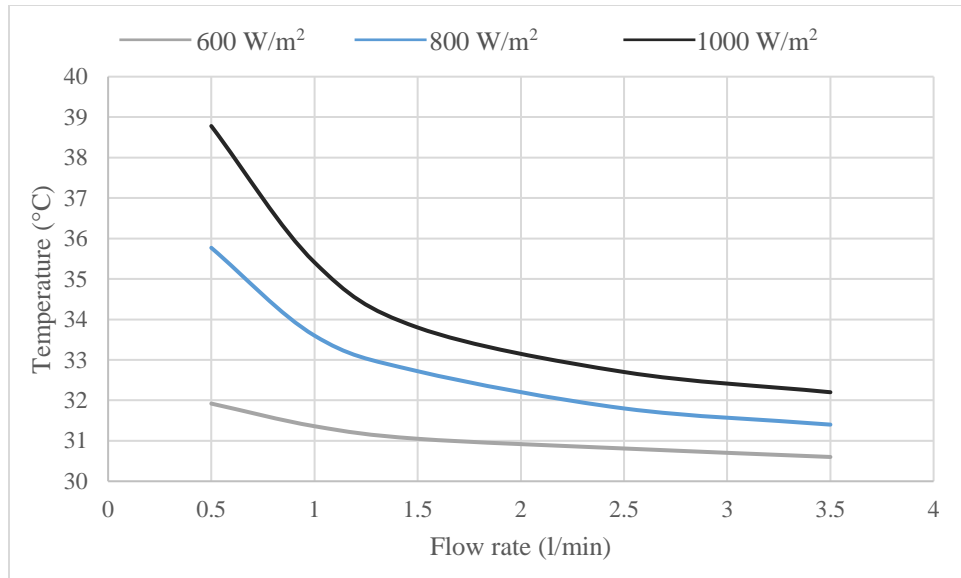


Figure 5. 29 Outlet water temperature at inlet water temperature (30°C)

Figure 5.30 relates the heat transfer rate to the water flow rate at a variable inlet water temperature. As noted, the solar irradiance is 1000 W/m², and the maximum heat transfer rate appears at the inlet water temperature of 20°C. Meanwhile, the relationship between volume flow rate and heat transfer rate is direct at different inlet water temperatures. When the water flow rate is increased, the water velocity increases, resulting in an increase in the heat transfer rate.

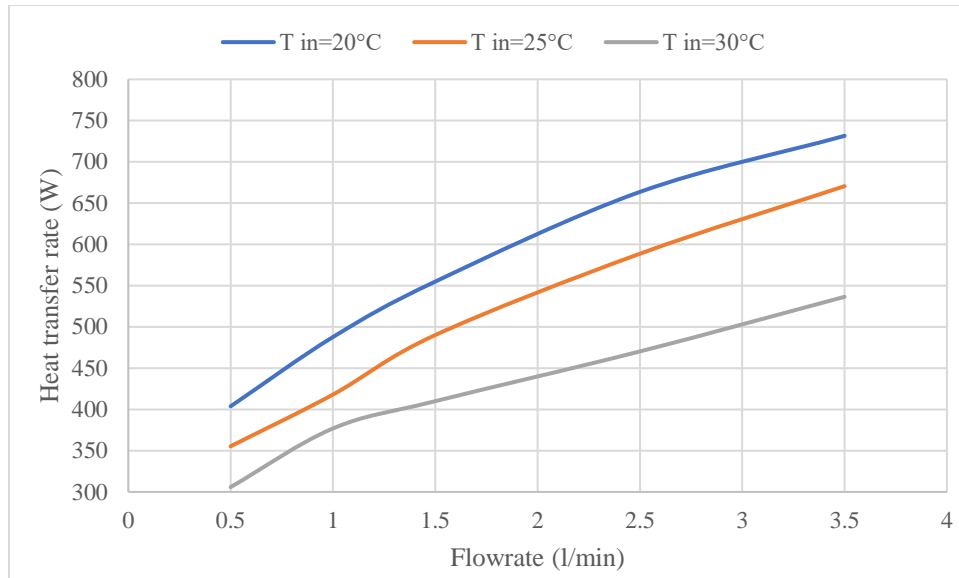


Figure 5. 30 Heat transfer rate at solar irradiance (1000 W/m^2)

Figures 5.31, 5.32, and 5.33 show that the water heat transfer rate increases with both increasing solar irradiance and water volume flow rate at different inlet water temperatures. According to the findings, the rate of heat transfer is directly proportional to the rate of solar irradiance and the rate of water volume flow. In other words, when the temperature differences between the surface panel and the inlet water temperature increase, more heat transfer will achieve. And the surface temperature increased due to an increase in solar irradiance.

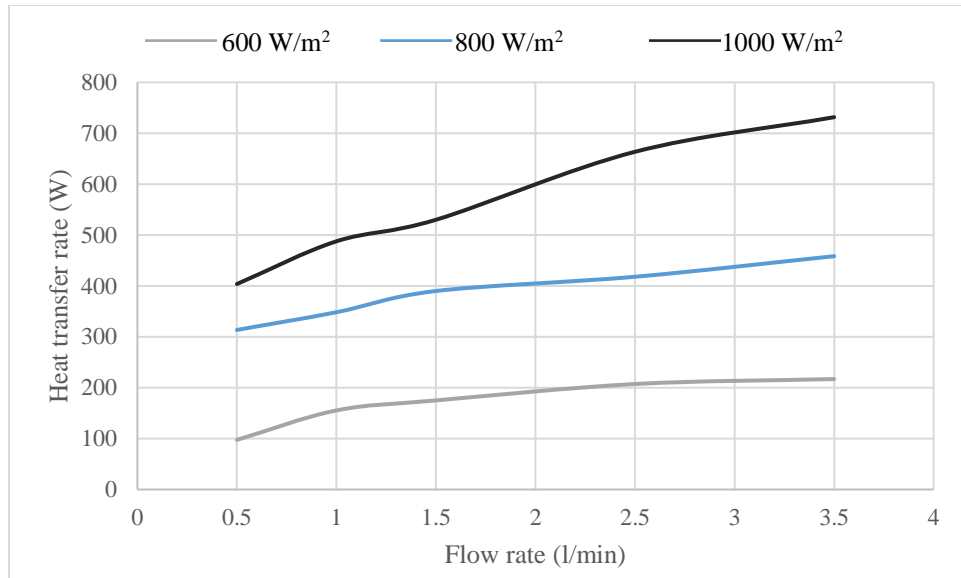


Figure 5. 31 Heat transfer rate at inlet water temperature (20°C)

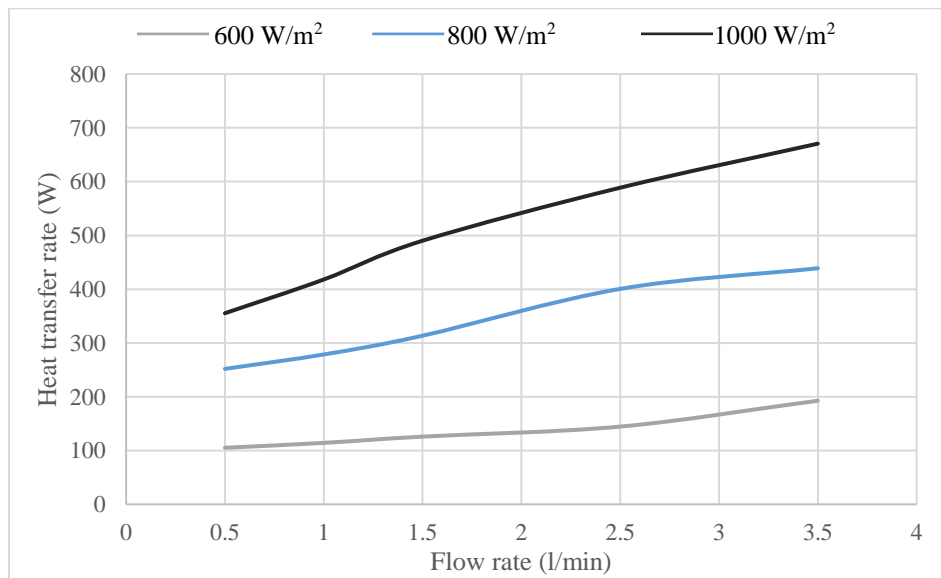


Figure 5. 32 Heat transfer rate at inlet water temperature (25°C)

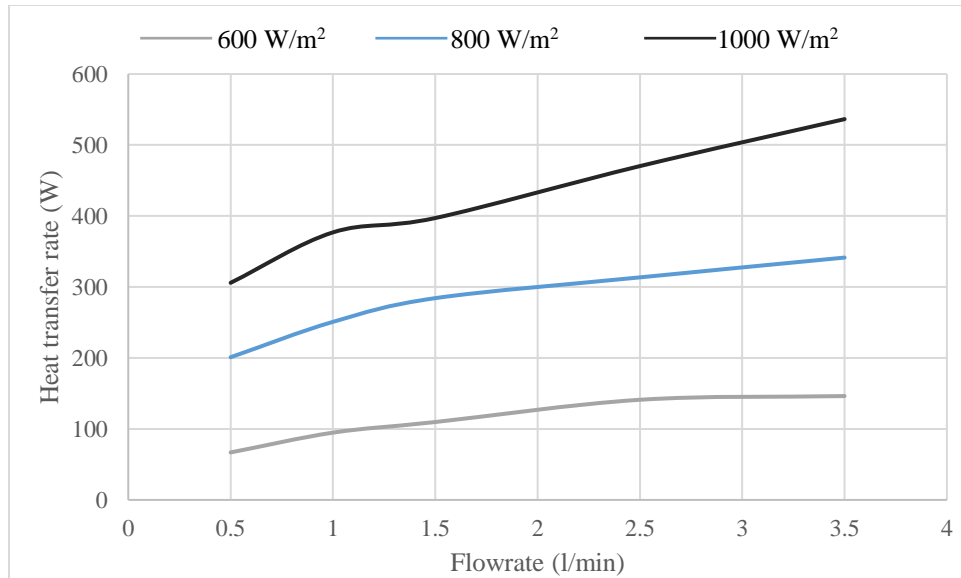


Figure 5. 33 Heat transfer rate at inlet water temperature (30°C)

Figure 5.34 explains thermal efficiency with different volume flow rates and water inlet temperatures. Thermal efficiency varies in direct proportion to the rate of water flow. As the inlet water temperature increases, the efficiency decreases.

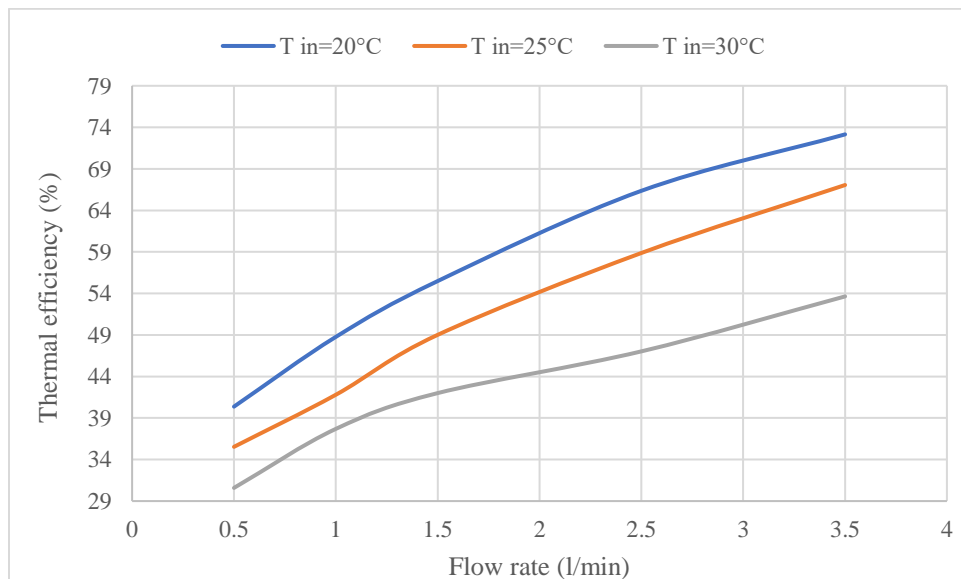


Figure 5. 34 Thermal efficiency at solar irradiance (1000 W/m²)

5.3.4 Performance Analysis

The electric efficiency is shown in Figure 5.35 with variable inlet water temperature and volume flow rate at 1000 W/m^2 solar irradiance. The relationship between electrical efficiency and water flow rate is direct. While using minimum water inlet temperature, the electrical efficiency rises because minimum water inlet temperature causes the panel's temperature to be reduced.

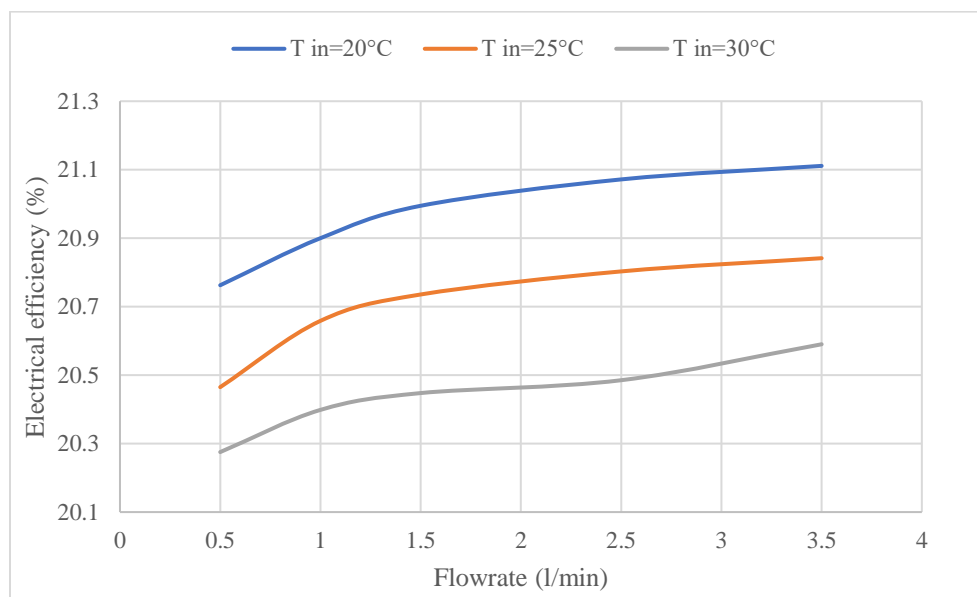


Figure 5. 35 Electrical efficiency at solar irradiance (1000 W/m^2)

For different water inlet temperatures, Figure 5.36 depicts electrical efficiency without and with cooling at a 1.5 l/min volume flow rate. As can be seen, the amount of solar irradiance is increasing at the same time that the efficiency of electricity is declining. As solar irradiance rose, the temperature of the module cells rose, which made the electrical efficiency of the module decrease.

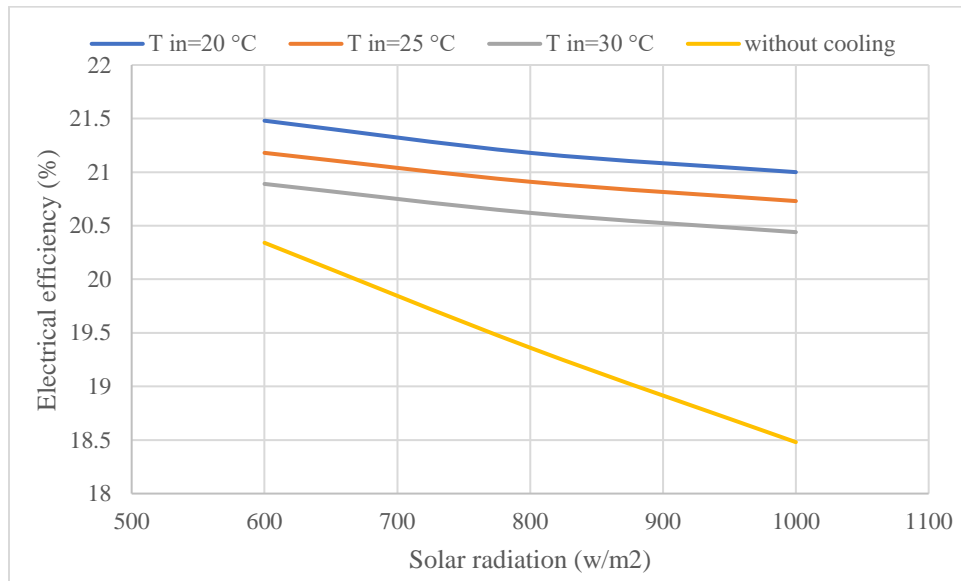


Figure 5. 36 Electrical efficiency with cooling and without cooling.

CHAPTER SIX

CONCLUSION, RECOMMENDATIONS

6.1 Introduction

The world today is becoming more interested in using renewable energy technologies because of the energy crisis and the problems that come with using fossil fuels. During the upcoming years, there will be an increase in the power demand, making it necessary to find alternative renewable energy resources by installing photovoltaic panels.

The surface temperature of the PV panel rises in the summer, which reduces its efficiency. To eliminate this problem, a cooling system was developed and installed. In this study, a monocrystalline silicon PV panel was used for noncooled PV and modified cooled PV. Both panels were tested and compared.

An experimental study under outdoor conditions in Erbil city and a simulated (ANSYS) program were used to improve the solar PV system.

This chapter is a summary of the most important findings from the study. Using both experiments and simulations (ANSYS), a water cooling system for the PV panel was made.

6.2 Conclusion

The system's evaluation results demonstrate good agreement among experimental and theoretical findings. Based on the findings of using proposed water chamber cooling for PV panels, the following points are concluded:

1. Installing a photovoltaic (PV) panel with a tilt angle of 36° , based on calculation, the average tilt angle is 36° .
2. The temperature of the PV panel rises in the summer due to higher solar intensity and ambient temperature, which decreases the panel's efficiency. When a water cooling chamber with a different flow rate is used to cool the photovoltaic (PV) panels, the efficiency enhanced and increased.
3. Applying different volume flow rate on the back side of the PV panel's allows for more heat to be removed from the panel.
4. Using different volume flow rates of 1.5, 2, 2.5, 3, and 3.5 l/min resulted in a reduction in PV panel temperature of 32.8%, 34.4%, 36.5%, 41.6%, and 46%, respectively.
5. The water inlet temperature has an effect on the reduce PV panel's temperature. Based on the ANSYS result, the cell temperature recorded 29°C , 31.9°C , and 34.89°C when the inlet water temperatures are 20°C , 25°C , and 30°C , respectively, with a volume flow rate of 1.5 l/min.
6. The outlet water temperature increased with the increasing in the inlet water temperature at the same flow rate. Also, by increasing the amount of cooling water flow rate through the system from 0.5 to 1.5 l/min, the outlet temperature dropped from 35.2°C to 27.7°C .

7. Once the temperature of the photovoltaic panel is low, the electrical efficiency of the PV panels increases.
8. The average amount of power generated increases by 10.42%, 11.87%, 13.77%, 18.09%, and 19.72% with flow rates of 1.5, 2, 2.5, 3, and 3.5 l/min, respectively.
9. The volume flow rate temperature and the inlet water temperature are direct proportional with the rate of heat transfer and the thermal efficiency. When the volume flow rates increase, the velocities also rise, which means that the heat transfer coefficient is at its highest. As a result, the heat transfer rate increased.
10. The highest heat transfer rate and thermal efficiency are 530 W and 79%, respectively at 3.5 l/min.
11. The amount of electricity produced is directly related to the amount of sunlight that hits the PV panels. The output power was increased from 80W to 179W when the solar irradiance was changed from 500W/m² to 1000W/m².
12. Finally, the relationship is linear between the inlet water temperature and electrical efficiency as shown in the results.

6.3 Recommendation

Several recommendations may be suggested in this study for the future work in this field, especially the PV panel performance, which has become the main objective of the future of the power production. The following recommendations are considered

- 1- Using different cooling fluid to enhance the heat transfer rate and to reduce the power consumption by pumping.
- 2- Develop different style of cooling water chamber through different designs of baffles.

- 3- Modified the backside water chamber material that is used with the PV panel.
- 4- The water cooling system using combine (front and back) side.

REFERENCES

- ABASS, K. I., AL-WAELI, A. & AL-ASADI, A. The use of Water Cooling Photovoltaic Thermal (PV/T) System in Domestic Heating Water.
- ABU-RAHMEH, T. M. J. J. O. P. & ENGINEERING, E. 2017. Efficiency of Photovoltaic Modules Using Different Cooling Methods: A Comparative Study. 5, 32.
- AGYEKUM, E. B., PRAVEENKUMAR, S., ALWAN, N. T., VELKIN, V. I., SHCHEKLEIN, S. E. & YAQOOB, S. J. J. I. 2021a. Experimental investigation of the effect of a combination of active and passive cooling mechanism on the thermal characteristics and efficiency of solar PV module. 6, 63.
- AGYEKUM, E. B., PRAVEENKUMAR, S., ALWAN, N. T., VELKIN, V. I. & SHCHEKLEIN, S. E. J. H. 2021b. Effect of dual surface cooling of solar photovoltaic panel on the efficiency of the module: Experimental investigation. 7, e07920.
- AHMAD, F. F., GHENAI, C., HAMID, A. K., REJEB, O. & BETTAYEB, M. J. C. S. I. T. E. 2021. Performance enhancement and infra-red (IR) thermography of solar photovoltaic panel using back cooling from the waste air of building centralized air conditioning system. 24, 100840.
- AHMED, W. K., SALAM, A. Q., MAHDIY, M. T. & CHAICHAN, M. T. J. J. O. T. E. ENVIRONMENTAL IMPACT OF USING GENERATORS IN THE UNIVERSITY OF TECHNOLOGY IN BAGHDAD, IRAQ. 6, 272-281.
- ALDIHANI, A. 2017. Enhancing the performance of PV system in dusty environment. University of Birmingham.
- ALI, R. & CELIK, S. J. I. P. C. B. E. E. 2017. Effect of Cooling on Solar Panel Performance Rehan. 100, 118-123.
- AMELIA, A., IRWAN, Y., IRWANTO, M., LEOW, W., GOMESH, N., SAFWATI, I., ANUAR, M. J. I. J. O. E. & ENGINEERING, C. 2016. Cooling on photovoltaic panel using forced air convection induced by DC fan. 6, 526.
- ARIBISALA, H. A. 2013. Improving the efficiency of solar photovoltaic power system, University of Rhode Island.
- ARUN, M. J. I. J. O. S. D. & RES 2019. Types of solar cells and its applications. 4, 260-267.

AYADI, O., SHADID, R., BANI-ABDULLAH, A., ALRBAI, M., ABU-MUALLA, M. & BALAH, N. J. E. R. 2022. Experimental comparison between Monocrystalline, Polycrystalline, and Thin-film solar systems under sunny climatic conditions. 8, 218-230.

BAHAIDARAH, H., SUBHAN, A., GANDHIDASAN, P. & REHMAN, S. J. E. 2013. Performance evaluation of a PV (photovoltaic) module by back surface water cooling for hot climatic conditions. 59, 445-453.

BAHAIDARAH, H. M., BALOCH, A. A., GANDHIDASAN, P. J. R. & REVIEWS, S. E. 2016. Uniform cooling of photovoltaic panels: A review. 57, 1520-1544.

BALOCH, A. A., BAHAIDARAH, H. M. & GANDHIDASAN, P. An experimental study of the effect of converging channel heat exchanger on PV system. 2015 IEEE 42nd Photovoltaic Specialist Conference (PVSC), 2015. IEEE, 1-4.

BARANWAL, N. K. & SINGHAL, M. K. 2021. Modeling and Simulation of a Spiral Type Hybrid Photovoltaic Thermal (PV/T) Water Collector Using ANSYS. Advances in Clean Energy Technologies. Springer.

BASHIR, M. A., ALI, H. M., AMBER, K. P., BASHIR, M. W., ALI, H., IMRAN, S. & KAMRAN, M. S. J. T. S. 2018. Performance investigation of photovoltaic modules by back surface water cooling. 22, 2401-2411.

BAYOD-RÚJULA, A. A. 2019. Solar photovoltaics (PV). Solar Hydrogen Production. Elsevier.

BELL, S. A. 2001. A beginner's guide to uncertainty of measurement.

BEVILACQUA, P., BRUNO, R. & ARCURI, N. J. E. 2020. Comparing the performances of different cooling strategies to increase photovoltaic electric performance in different meteorological conditions. 195, 116950.

CHIN, C. S., GAO, Z., HAN, M. & ZHANG, C. J. I. R. P. G. 2020. Enhancing performance of photovoltaic panel by cold plate design with guided channels. 14, 1606-1617.

DASH, P., GUPTA, N. J. I. J. O. E. R. & APPLICATIONS 2015. Effect of temperature on power output from different commercially available photovoltaic modules. 5, 148-151.

DIECK, R. H. J. T. M., INSTRUMENTATION & SENSOR HANDBOOK, I. P., SPRINGER 1999. Measurement accuracy.

DUFFIE, J. A. & BECKMAN, W. A. 1980. Solar engineering of thermal processes, Wiley New York.

- EBRAHIMI, M., RAHIMI, M., RAHIMI, A. J. I. C. I. H. & TRANSFER, M. 2015. An experimental study on using natural vaporization for cooling of a photovoltaic solar cell. 65, 22-30.
- ELMINSHAWY, N. A., EL-GHANDOUR, M., ELHENAWY, Y., BASSYOUNI, M., EL-DAMHOGI, D. & ADDAS, M. F. J. S. E. 2019. Experimental investigation of a V-trough PV concentrator integrated with a buried water heat exchanger cooling system. 193, 706-714.
- FAKOURIYAN, S., SABOOHI, Y. & FATHI, A. J. R. E. 2019. Experimental analysis of a cooling system effect on photovoltaic panels' efficiency and its preheating water production. 134, 1362-1368.
- GOMAA, M. R., AHMED, M. & REZK, H. J. E. R. 2022. Temperature distribution modeling of PV and cooling water PV/T collectors through thin and thick cooling cross-fined channel box. 8, 1144-1153.
- GOMAA, M. R., HAMMAD, W., AL-DHAIFALLAH, M. & REZK, H. J. S. E. 2020. Performance enhancement of grid-tied PV system through proposed design cooling techniques: An experimental study and comparative analysis. 211, 1110-1127.
- GOVARDHANAN, M., KUMARAGURUPARAN, G., KAMESWARI, M., SARAVANAN, R., VIVAR, M. & SRITHAR, K. J. I. J. O. P. 2020. Photovoltaic module with uniform water flow on top surface. 2020.
- HACHICHA, A. A., GHENAI, C., HAMID, A. K. J. I. J. O. E. & ENGINEERING, P. 2015. Enhancing the performance of a photovoltaic module using different cooling methods. 9, 1106-1109.
- HADIPOUR, A., ZARGARABADI, M. R. & RASHIDI, S. J. R. E. 2021. An efficient pulsed-spray water cooling system for photovoltaic panels: Experimental study and cost analysis. 164, 867-875.
- HASAN, H. A., SOPIAN, K., JAAZ, A. H. & AL-SHAMANI, A. N. J. S. E. 2017a. Experimental investigation of jet array nanofluids impingement in photovoltaic/thermal collector. 144, 321-334.
- HASAN, I., FAFRAJ, S., KADEM, A. J. E. & JOURNAL, T. 2017b. Enhancing Photoelectric Conversion Efficiency of Photovoltaic Panel Using Cooled Water by Evaporation. 35.
- HASHIM, E. T. & ABBOOD, A. A. J. J. O. E. 2016. Temperature effect on power drop of different photovoltaic modules. 22, 129-143.

HIDAYANTI, F. J. I. J. 2020. The effect of monocrystalline and polycrystalline material structure on solar cell performance. 8.

HJERRILD, N. E., MESGARI, S., CRISOSTOMO, F., SCOTT, J. A., AMAL, R., TAYLOR, R. A. J. S. E. M. & CELLS, S. 2016. Hybrid PV/T enhancement using selectively absorbing Ag–SiO₂/carbon nanofluids. 147, 281-287.

HOSSAIN, M., PANDEY, A., SELVARAJ, J., ABD RAHIM, N., RIVAI, A. & TYAGI, V. J. A. T. E. 2019. Thermal performance analysis of parallel serpentine flow based photovoltaic/thermal (PV/T) system under composite climate of Malaysia. 153, 861-871.

HUSSEIN, H. A., NUMAN, A. H. & ABDULRAHMAN, R. A. J. I. J. O. P. 2017. Improving the hybrid photovoltaic/thermal system performance using water-cooling technique and Zn-H₂O nanofluid. 2017.

INDARTONO, Y., PRAKOSO, S., SUWONO, A., ZAINI, I. & FERNALDI, B. Simulation and experimental study on effect of phase change material thickness to reduce temperature of photovoltaic panel. IOP conference series: materials science and engineering, 2015. IOP Publishing, 012049.

IRWAN, Y., LEOW, W., IRWANTO, M., AMELIA, A., GOMESH, N. & SAFWATI, I. J. E. P. 2015. Indoor test performance of PV panel through water cooling method. 79, 604-611.

JAILANY, A., EL-AL, A. & RASHWAN, M. J. M. J. O. A. E. 2016. EFFECT OF WATER COOLING ON PHOTOVOLTAIC PERFORMANCE. 33, 257-268.

JUMRUSPRASERT, P., SMITH, G. & KIRKUP, L. Comparing the efficiency of fixed solar cell panels in a tropical location. Proceedings of ISES World Congress 2007 (Vol. I–Vol. V) Solar Energy and Human Settlement, 2009. Springer, 1478-1483.

KALOGIROU, S. A. 2013. Solar energy engineering: processes and systems, Academic press.

KUMAR, P. & DUBEY, R. J. I. J. E. R. T. 2018. Efficiency Improvement of Photovoltaic Panels by Design Improvement of Cooling System using Back Water Cooling Tubes. 7, 74-77.

LEARY, P. 2019. Design & Evaluation of Cooling Systems for Photovoltaic Modules.

MAZÓN-HERNÁNDEZ, R., GARCÍA-CASCALES, J. R., VERA-GARCÍA, F., KÁISER, A. & ZAMORA, B. J. I. J. O. P. 2013. Improving the electrical parameters of a photovoltaic panel by means of an induced or forced air stream. 2013.

MEHROTRA, S., RAWAT, P., DEBBARMA, M., SUDHAKAR, K. J. I. J. O. S., ENVIRONMENT & TECHNOLOGY 2014. Performance of a solar panel with water immersion cooling technique. 3, 1161-1172.

MICHAEL, J. J., SELVARASAN, I. & LOGANATHAN, S. Simulation of the temperature distribution inside a solar photovoltaic thermal collector. 2015. 3rd Southern African Solar Energy Conference, South Africa, 11-13 May, 2015.

MIRZAEI, M. & MOHIABADI, M. Z. J. E. F. S. D. 2017. A comparative analysis of long-term field test of monocrystalline and polycrystalline PV power generation in semi-arid climate conditions. 38, 93-101.

MISHA, S., ABDULLAH, A. L., TAMALDIN, N., ROSLI, M. & SACHIT, F. J. E. R. 2020. Simulation CFD and experimental investigation of PVT water system under natural Malaysian weather conditions. 6, 28-44.

MOAVENI, S. J. J. O. S. E. 2008. Teaching Engineering Fundamentals Using Fundamental Dimensions: An Innovative Approach. 8.

MOHAMMED, F. M., MOHAMMED, J. A.-K. & NOURI, R. A. J. A.-K. E. J. 2018. Efficiency Enhancement of a Dual-axis Solar PV Panel Tracker Using Water-Flow Double Glazing Technique. 14, 32-47.

MOHAMMED, F. M., MOHAMMED, J. A.-K. & SANAD, M. A.-S. J. A.-N. J. F. E. S. 2019. Performance Enhancement of Photovoltaic Panel Using Double-sides Water Glazing Chambers Cooling Technique. 22, 22-30.

MUSLIM, N. H., GHADHBAN, S. A. & HILAL, K. J. I. J. O. R. E. R. 2020. Enhancement of solar photovoltaic module performance by using a water-cooling chamber for climatic conditions of Iraq. 10, 1103-1110.

NASRIN, R., HASANUZZAMAN, M. & RAHIM, N. A. J. I. J. O. E. R. 2018. Effect of high irradiation and cooling on power, energy and performance of a PVT system.

NASRIN, R., HASANUZZAMAN, M., RAHIM, N. A. J. I. J. O. N. M. F. H. & FLOW, F. 2019. Effect of nanofluids on heat transfer and cooling system of the photovoltaic/thermal performance.

NIŽETIĆ, S., GRUBIŠIĆ-ČABO, F., MARINIĆ-KRAGIĆ, I. & PAPADOPOULOS, A. M. J. E. 2016. Experimental and numerical investigation of a backside convective cooling mechanism on photovoltaic panels. 111, 211-225.

PATEL, M. R. & BEIK, O. 2021. Wind and solar power systems: design, analysis, and operation, CRC press.

PENG, Z., HERFATMANESH, M. R., LIU, Y. J. E. C. & MANAGEMENT 2017. Cooled solar PV panels for output energy efficiency optimisation. 150, 949-955.

PRECUP, R., KAMAL, T. & HASSAN, S. Z. J. S. S. 2019. Solar photovoltaic power plants.

RAHMAN, M., HASANUZZAMAN, M., RAHIM, N. A. J. E. C. & MANAGEMENT 2015. Effects of various parameters on PV-module power and efficiency. 103, 348-358.

RAKINO, S. A., SUHERMAN, S., HASAN, S. & RAMBE, A. A Passive Cooling System for Increasing Efficiency of Solar Panel Output. Journal of Physics: Conference Series, 2019. IOP Publishing, 012017.

RAVAL, H. D., MAITI, S., MITTAL, A. J. J. O. R. & ENERGY, S. 2014. Computational fluid dynamics analysis and experimental validation of improvement in overall energy efficiency of a solar photovoltaic panel by thermal energy recovery. 6, 033138.

RUOPING, Y., XIAOHUI, Y., FUWEI, L. & HUAJUN, W. J. R. E. 2020. Study of operation performance for a solar photovoltaic system assisted cooling by ground heat exchangers in arid climate, China. 155, 102-110.

SAINTHIYA, H., BENIWAL, N. S. J. E. S., PART A: RECOVERY, UTILIZATION, & EFFECTS, E. 2020. Comparative analysis of electrical performance parameters under combined water cooling technique of photovoltaic module: An experimental investigation. 42, 1902-1913.

SHARAF, M., YOUSEF, M. S., HUZAYYIN, A. S. J. E. S. & RESEARCH, P. 2022. Review of cooling techniques used to enhance the efficiency of photovoltaic power systems. 1-29.

SHARMA, M., BANSAL, K. & BUDDHI, D. J. P. C. S. 2015. Real time data acquisition system for performance analysis of modified pv module and derivation of cooling coefficients of electrical parameters. 48, 582-588.

SHIRAHATA, Y., OKU, T., FUKUNISHI, S., KOHNO, K. J. M. S. & APPLICATIONS 2017. Fabrication of perovskite-type photovoltaic devices with polysilane hole transport layers. 8, 209-222.

SMETS, A. H., JÄGER, K., ISABELLA, O., SWAAIJ, R. A. & ZEMAN, M. 2015. Solar Energy: The physics and engineering of photovoltaic conversion, technologies and systems, UIT Cambridge.

SUGIANTO, S. J. I. J. P. 2020. Comparative analysis of solar cell efficiency between monocrystalline and polycrystalline. 7, 92-100.

SULTAN, T. N., FARHAN, M. S. & ALRIKABI, H. T. S. Using Cooling System for Increasing the Efficiency of Solar Cell. *Journal of Physics: Conference Series*, 2021. IOP Publishing, 012129.

SYAFIQA, Z., AMIN, N., IRWAN, Y., MAJID, M. & AZIZ, E. N. Simulation study of air and water cooled photovoltaic panel using ANSYS. *Journal of Physics: Conference Series*, 2017a. IOP Publishing, 012074.

SYAFIQA, Z., AMIN, N., IRWAN, Y., SHOBRY, M. & MAJID, M. Analysis of photovoltaic with water pump cooling by using ANSYS. *Journal of Physics: Conference Series*, 2017b. IOP Publishing, 012083.

WANG, C. & LU, Y. 2016. Solar Photovoltaic.

XU, Y., XUAN, Y., YANG, L. J. E. C. & MANAGEMENT 2015. Full-spectrum photon management of solar cell structures for photovoltaic–thermoelectric hybrid systems. 103, 533-541.

YAN, J. & SAUNDERS, B. R. J. R. A. 2014. Third-generation solar cells: a review and comparison of polymer: fullerene, hybrid polymer and perovskite solar cells. 4, 43286-43314.

APPENDIX A

Monthly Solar Radiation

The monthly solar radiation calculation in Erbil on July 3rd.

n=184 for July 3rd

$$\delta = 23.42 * \sin \frac{360*(284+n)}{365} \quad \text{A.1}$$

$$\delta = 23.42 * \sin \frac{360 * (284 + 184)}{365}$$

$$\delta = 22.94^\circ$$

$$\beta = |\phi - \delta| \quad \text{A.2}$$

while Erbil's latitude (ϕ) is = 36.19°

$$\beta = |36.19 - 22.94|$$

$$\beta = 13.24^\circ$$

- Horizontal radiation (\bar{H})

$$\bar{K}_T = \frac{\bar{H}}{\bar{H}_0} \quad \text{A.3}$$

$$\bar{H}_0 = \frac{24 * 3600}{\pi} * G_{sc} * \left(1 + 0.033 * \cos \frac{360 n}{365} \right) * (\cos \phi \cos \delta \sin w_s + \frac{\pi w_s}{180} \sin \phi \sin \delta)$$

A.4

$$\cos w_s = -\tan\phi * \tan\delta \quad \text{A.5}$$

$$\cos w_s = -\tan (36.19) * \tan (22.94)$$

$$\cos w_s = 108.03^\circ$$

$$\begin{aligned} \bar{H}_0 = & \frac{24 * 3600}{\pi} * 1367 * \left(1 + 0.033 * \cos \frac{360 * 184}{365} \right) \\ & * [(\cos(36.19) \cos(22.94) \sin(108.03) \\ & + \frac{\pi * 108.03}{180} \sin(36.19) \sin(22.94)] \end{aligned}$$

$$\bar{H}_0 = 41.46 \text{ MJ/m}^2$$

$$0.65 = \frac{\bar{H}}{41.46}$$

$$\bar{H} = 26.949 \text{ MJ/m}^2$$

- Diffused radiation (\bar{H}_b)

$$\bar{H}_b = \bar{H} - \bar{H}_d \quad \text{A.6}$$

$$\frac{\bar{H}_d}{\bar{H}} = 1.311 - 3.022 \bar{K}_T + 3.427 \bar{K}_T^2 - 1.821 \bar{K}_T^3 \quad \text{A.7}$$

$$\frac{\bar{H}_d}{26.949} = 1.311 - (3.022 * 0.65) + (3.427 * (0.65)^2) - (1.821 * (0.65)^3)$$

$$\bar{H}_d = 7.936 \text{ MJ/m}^2$$

$$\bar{H}_b = 26.949 - 7.936$$

$$\bar{H}_b = 19.013 \text{ MJ/m}^2$$

- Incident radiation (\bar{H}_T)

$$\bar{H}_T = \bar{H}_b * \bar{R}_b + \bar{H}_d \left(\frac{1+\cos\beta}{2} \right) + \bar{H} \rho_g \left(\frac{1-\cos\beta}{2} \right) \quad A.8$$

$$\bar{R}_b = \frac{\cos(\emptyset-\beta)\cos\delta \sin\omega_s + \left(\frac{\pi}{180}\right) \omega_s \sin(\emptyset-\beta) \sin\delta}{\cos\emptyset\cos\delta \sin\omega_s + \left(\frac{\pi}{180}\right) \omega_s \sin\emptyset \sin\delta} \quad A.9$$

$$\omega_s = \cos^{-1} (-\tan(\emptyset - \beta) \tan\delta) \quad A.10$$

$$\omega_s = \cos^{-1} (-\tan(36.19 - 13.24) \tan (22.94))$$

$$\omega_s = 100.32^\circ$$

$$\bar{R}_b = \frac{[\cos(36.19-13.24)*\cos(22.94)*\sin(100.32)] + \left[\left(\frac{\pi}{180}\right) 100.32 * \sin(36.19-13.24)*\sin(22.94)\right]}{[\cos(36.19)*\cos(22.94)*\sin(108.03)] + \left[\left(\frac{\pi}{180}\right) * 108.03 * \sin(36.19)*\sin(22.94)\right]}$$

$$\bar{R}_b = 0.9647$$

$$\bar{H}_T = (19.013 * 0.9647) + \left[7.936 * \left(\frac{1+\cos(13.24)}{2} \right) \right] + [26.949 * 0.2 * \left(\frac{1-\cos(13.24)}{2} \right)]$$

$$\bar{H}_T = 26.244 \text{ MJ/m}^2 = 7.29 \text{ kw h./m}^2/\text{day}$$

APPENDIX B

UNCERTAINTY AND CALIBRATION ANALYSIS

There was uncertainty and calibration analysis for each instrument used to measure volume flow rate, water and ambient temperatures, and so on.

Table B. 1 Example to determine the uncertainty of water volume flow rate.

Water Flow meter (l/min)	$x_i - \bar{x}$	$(x_i - \bar{x})^2$
x_i		
2.24	-0.26	0.0676
2.58	0.08	0.0064
2.52	0.02	0.0004
2.53	0.03	0.0009
2.54	0.04	0.0016
2.48	-0.02	0.0004
2.46	-0.04	0.0016
2.46	-0.04	0.0016
2.54	0.04	0.0016
2.57	0.07	0.0049

(\bar{x})	2.5
Number of reading (n)	10

The uncertainty of water volume flow rate determined by this equation:

$$\text{Uncertainty (u)} = \sqrt{\frac{\sum_{i=1}^n (x_i - \bar{x})^2}{n * (n-1)}} \quad \text{B.1}$$

$$\text{Uncertainty (u)} = \sqrt{\frac{0.087}{10 * (10 - 1)}}$$

$$\text{Uncertainty (u)} = \pm 0.03$$



Figure B. 1 Calibration the K-type thermocouple



Figure B. 2 Calibration of the DBTU1300 solar power meter

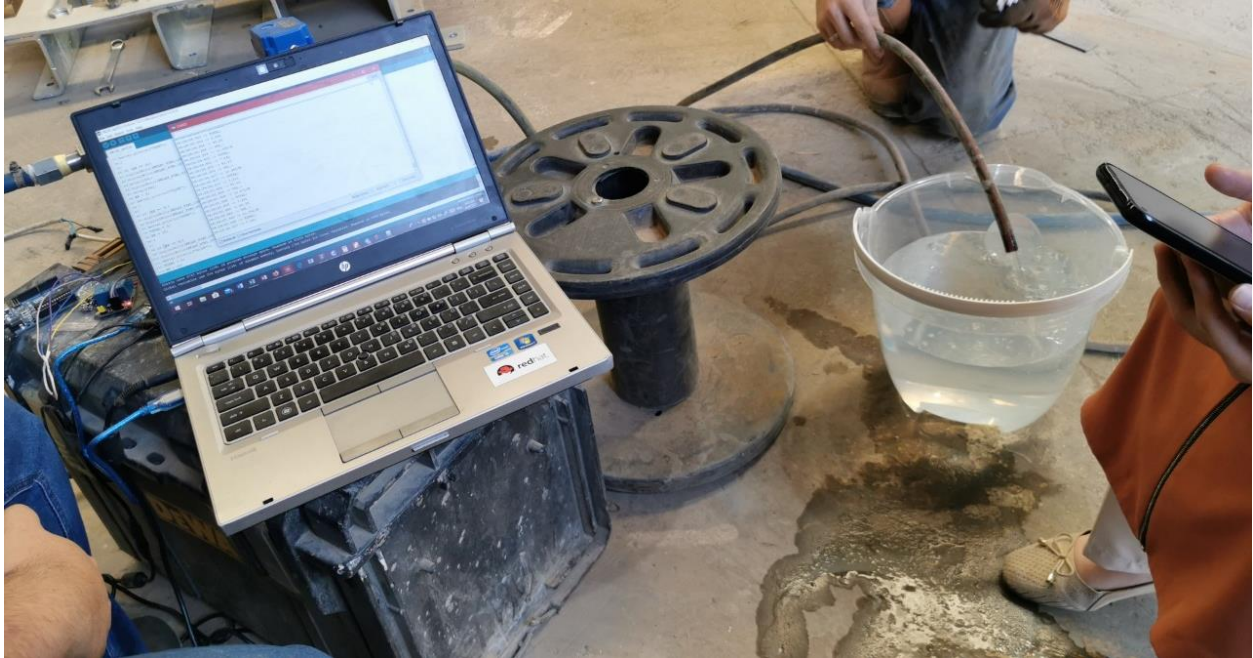


Figure B. 3 Calibration of the volume flow rate

APPENDIX C

ANSYS RESULTS

There are the figures of the ANSYS simulation result for the PV panel surface.

The PV panel's surface at solar irradiance is 600 W/m^2 , and the water inlet temperature is 20°C with a volume flow rate of 1 l/min .

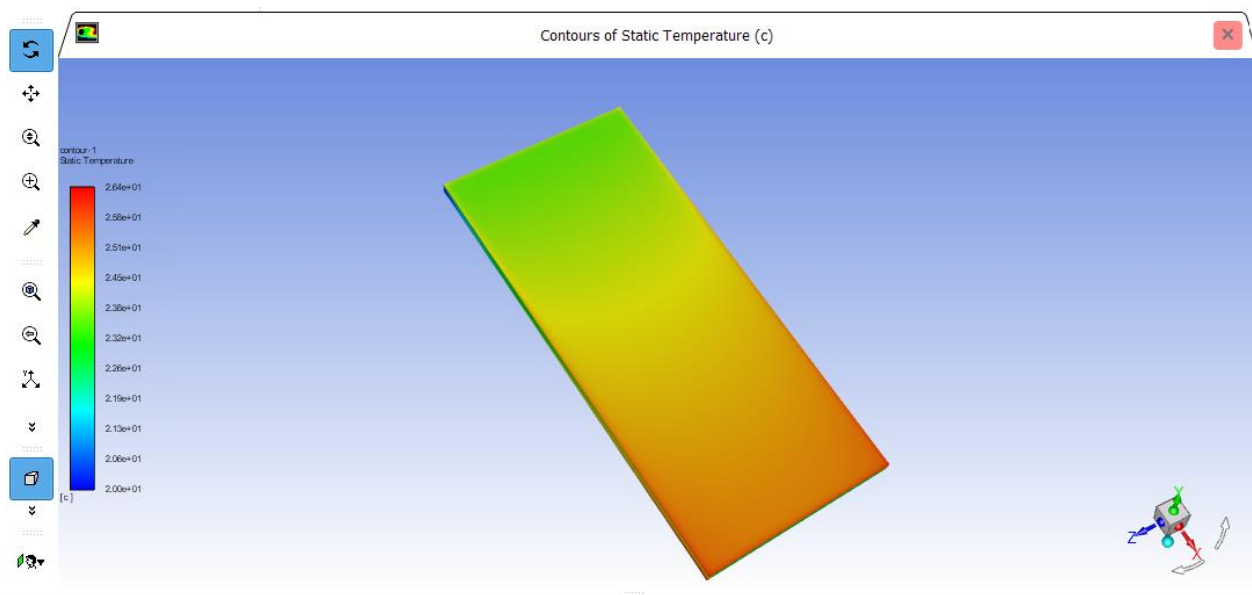


Figure C. 1 Surface of PV panel temperature

The PV panel's surface at solar irradiance is 800 W/m^2 , and the water inlet temperature is 20°C with a volume flow rate of 1 l/min .

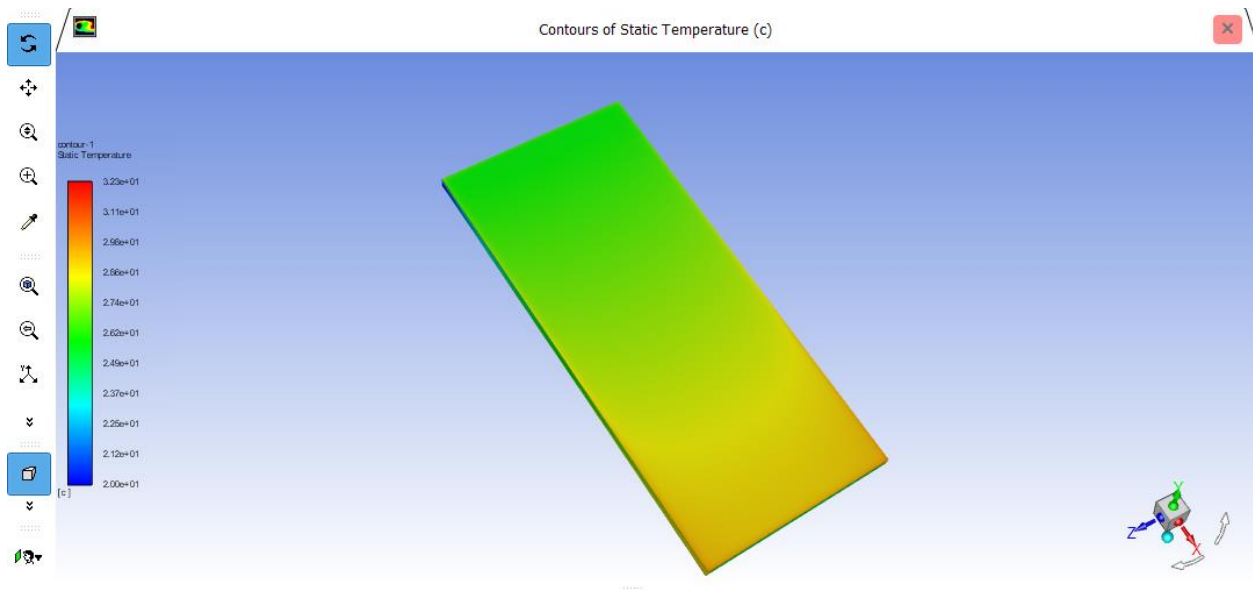


Figure C. 2 Surface of PV panel temperature

The PV panel's surface at solar irradiance is 800 W/m^2 , and the water inlet temperature is $20 \text{ }^{\circ}\text{C}$ with a volume flow rate of 1 l/min .

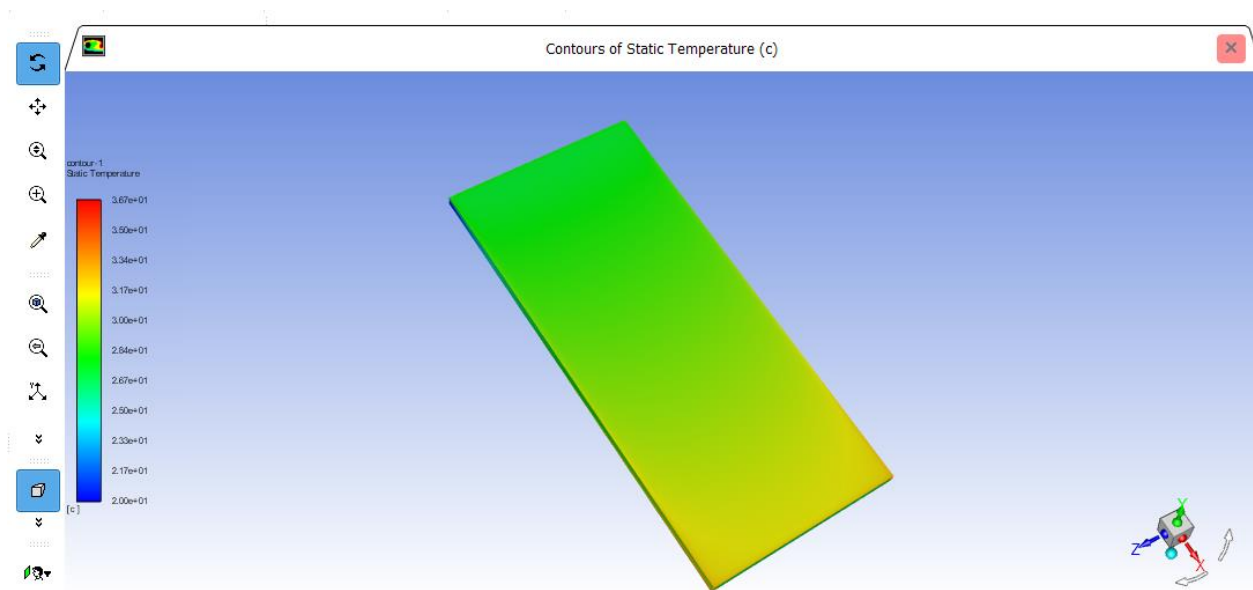


Figure C. 3 Surface of PV panel temperature

LIST OF PUBLICATIONS

1. Published of the paper" Experimental Study of PV Panel Performance using Backside Water Cooling Chamber."



WESSEX INSTITUTE

Ashurst Lodge, Ashurst, Southampton, SO40 7AA, UK
Tel: 44 (0) 238 029 3223 Fax: 44 (0) 238 029 2853 Email: wit@wessex.ac.uk Web: www.wessex.ac.uk

Alexander Carlos Brebbia, Chairman

9 February 2023

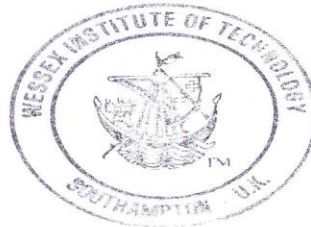
To Whom It May Concern

Dear Sirs

I confirm that the paper "Experimental Study of PV Panel Performance using Backside Water Cooling Chamber" by Ilaf N Rasool & Ranj S Abdullah, has been reviewed and accepted for publication in our International Journal of Energy Production and Management.

Yours faithfully

Mrs Jane E Chantler
Academic Coordinator



پوخته

يەككىك لە گەورەترین كىشەكانى جيهان كه لەم رۆژانەدا دەژين، پيسبوونى ژينگهيه كه بههۆى زياڤەرۆيى له بهكارهينانى وزەدا دروست دەبێت. كاتيك سووتەمەنى بەردىنى دەسووتنرێت بۆ بەرهمههينانى وزە، CO2 دەرەدەن كه سەرچاوهيهكى سەرەكى پيسبوونى هەوايه. وزەى خۆر توانای ئەوەى هەيه كه جىگهى سووتەمەنى بەردىنى بگرتەوه وەك سەرچاوهيهكى بەدیل بۆ وزەى نوێبوووه.

سيستەمى فۆتوفۆلتايكى خۆر يەككىكه له جۆرەكانى سيستەمى خۆر كه توانای گۆرینی تيشكى خۆرى هەيه بۆ وزەى كارەبايى. يەككىك لە كىشەكانى فۆتوفۆلتايك ئەوەيه كه پلهى گەرمى خانەكانى بەرز دەبێتەوه به تايبەت له وەرزی هاویندا كاتيك پلهى گەرمى دەرووبەر تا 50 پلهى سەدى بەرز دەبێتەوه. لەگەڵ بەرزبوونەوى پلهى گەرمى خانەكانى فۆتوفۆلتايك، هەردوو هێزى دەرچوون و كارايى كارەبايى كەم دەبنەوه.

به مەبەستى باشتەركردنى كارايى گشتى له هەمان كاتدا درێژكردنەوى تەمەنى فۆتوفۆلتايك، ئەم توێژینەوهيه پيشنيارى دابەزاندنى پلهى گەرمى خانە فۆتوفۆلتايك دەكات به بهكارهينانى ئاو وەك شلەيهكى ساردكەرەوه. پانێلێ خۆرى پيشنياركراوى له رىگهى هەردوو ليكۆلێنەوى تاقىكارى و بهكارهينانى رىگهى سۆفتویرى ANSYS Fluent نیشاندرأ. ئەو مۆډيولهى فۆتوفۆلتايك كه ديزاين كراوه ژوورێكى ساردكەرەوى ئاوى هەيه به مەبەستى دابینكردنى ساردكردنەوه له ژێر بارودۆخى شارى هەولێر. سيستەمى ساردكردنەوى ئاو بۆ بەشى پشتهوى پانێلێ فۆتوفۆلتايك بهكارهيندرا. ژوورى ساردكەرەوى ئاو دەتوانێت گەرمى له پانێلێ فۆتوفۆلتايكەوه هەلبمژێت. سيستەمى ساردكردنەوى پانێلێ خۆر خولێكى داخراوه، و ئاوى ساردكەرەوه بەركەوتەى به بەشى پشتهوى فۆتوفۆلتايك هەيه به رێژەى شىلاندى جياواز.

بەپێى ليكۆلێنەوى تاقىكارى، زۆرترین رێژەى شىلاندى ئاو 3.5 ل/دەقه رێژەى گواستەوهى گەرمى گونجاو دەدات. له كۆتايیدا ئەنجامەكان سەلماندیان كه كارايى كارەبايى بەم رێژەيهى خوارەوه زياڤى كردووه به رێژەى 10.42%، 11.87%، 13.77%، 18.09%، و 19.72% كاتيك رێژەى شىلاندى بارستەى ئاو 1.5، 2، 2.5، 3، و 3.5 ل/دەقه بوو جىبهجى كراوه. له هەمان كاتدا كارايى گەرمى فۆتوفۆلتايك 49.7% يە لەگەڵ رێژەى لێشأوى ئاو 1.5 ل/دەقه. و، كارايى گەرمى 79.2% تۆمار دەكات كاتيك سيستەمەكه به رێژەى لێشأوى 3.5 ل/دەقه كار دەكات.



دیراسەتییکی ژمارەیی و کرداری بۆ پانیلی فۆتۆفۆلتایکی خۆر بە بەکارهێنانی ژووری ساردکردنەوهی ئاوی لای پشتهوه

نامەپێکە

پیشکەشی ئێنجۆمەنی کۆلیژی تەکنیکی ئەندازیاری هەولێر کراوە لە زانکۆی پۆلیتەکنیکی هەولێر وەک
بەشیکی جێبەجێکردنی مەرجەکان بۆ بەدەست هێنانی پرونامەی ماستەر لە ئەندازیاری میکانیک و وزە

لە لایەن

ایلاف نوزاد رسول

(بەکالۆریۆس لە ئەندازیاری ساردکردنەوهی هەواسازی، ٢٠١٤)

بە سەرپرشتیاری

پ. ی. د. رەنج سیروان عبدالله

هەولێر - کوردستان

ئازار ٢٠٢٣